FINAL TECHNICAL REPORT

March 27, 2017 – Sept 30, 2021

CB10412 - Bulk CWA Destruction

Submitted by:

Mark K Kinnan
Chemical and Biological Systems
Sandia National Laboratories
P.O. Box 5800
Albuquerque, New Mexico 87185-MS0734
Telephone: (505) 284-6903
Email: mkkinna@sandia.gov

Submitted to:

Glenn E Lawson
8725 John J. Kingman Road Stop 6201
Fort Belvoir, Virginia 22060-6201
Telephone: (703) 767-3311
Email: glenn.e.lawson8.civ@mail.mil

Oct 15, 2021

Contract Number: Sandia Project # 204453; IAA DTRA # 1002729601
Capability Area/Thrust Area: Protection & Hazard Mitigation

Contents

2. PROJECT AND REPORT OVERVIEW

The authors of this report include: Mark K Kinnan [1], Patrick D Burton [1], Jeff Greathouse [1], Chad Priest [1] Calen Leverant [1], Thomas Fisher [1], Susan Rempe [1], Todd M Alam [1], David J McGarvey [2], Bill Creasy [3]. [1] Sandia, [2] CCDC-CBC, [3] Leidos.

a. The objective of this project was to eliminate and/or render bulk agent unusable by a threat entity via neutralization and/or polymerization of the bulk agent using minimal quantities of additives.

b. Executive Summary

   a. We proposed the in situ neutralization and polymerization of bulk chemical agents (CAs) by performing reactions in the existing CA storage container via wet chemical approaches using minimal quantities of chemical based materials. This approach does not require sophisticated equipment, fuel to power generators, electricity to power equipment, or large quantities of decontaminating materials. By utilizing the CA storage container as the batch reactor, the amount of logistical resources can be significantly reduced. Fewer personnel are required since no sophisticated equipment needs to be set up, configured, or operated. Employing the CA storage container as the batch reactor enables the capability to add materials to multiple containers in a short period of time as opposed to processing one container at a time for typical batch reactor approaches. In scenarios where a quick response is required, the material can be added to all the CA containers and left to react on its own without intervention. Any attempt to filter the CA plus material solution will increase the rate of reaction due to increased agitation of the solution.

c. Summary of key accomplishments/findings over the reporting period.

   1. Accomplishments

      a. Experimental Lithium Nitride (Li_3N) plus water (H_2O)

         a) Optimized $Li_3N + H_2O$ reaction combination for optimal performance on neat agent solutions. It was determined that 3 moles of H_2O are required per 1 mole of Li_3N.

         b) Using 21% by volume additive of Li_3N and H_2O in a small-scale reaction, approximately 50% of the GB was neutralized in 10 minutes with gelling occurring within 6 hours.

         c) CAs (GB, GD, VX) and precursors (QL and DF) were reactive with $Li_3N + H_2O$. They could be decontaminated. The reaction mixtures of GB, GD, and VX formed viscous gels that had different physical properties compared to neat agent.

            1. QL and DF reacted well with just water, without additional reagent. DF may also react with glass, but further studies are needed.

2. HD was the most difficult agent to react. Some solids were formed in some cases, but no reaction products were ever observed.

d) Li_3N can be reacted with other hydroxyl containing chemicals like methanol or propylene glycol.

1. Preliminary results indicated organic solvents may be more effective than water.

e) Tablets ½" and ¼" in diameter were manufactured at Sandia and provided to U.S. Army Combat Capabilities Development Command Chemical Biological Center (CBC) for all tablet based testing of the 10, 100, and 1000 mL reactions.

f) 100 mL reactions of neat (pure) GB, GD, VX, QL, and DF were performed using the Li_3N chemistry.

1. A robotic arm was used to deliver reagents to the neat agents inside a blast chamber as a safety measure.

2. A video was created at CBC and edited at Sandia and provided to DTRA showing the 100 mL VX and QL reactions. Material for videos of other reactions were recorded but not edited into a final video format.

3. Extensive analyses of the 100 mL VX reaction reveals predominately VX acid (ethyl methyl-phosphonic acid) and VX disulfide [bis(2-diisopropylaminoethyl) disulfide] products. These products are expected from alkaline hydrolysis of VX. Analysis of products of the other reactions also indicated an alkaline hydrolysis reaction was taking place.

g) 1000 mL reaction of neat DMMP was performed using the Li_3N chemistry to develop safe and effective reaction conditions.

h) 1 L GB reaction is funded but was delayed. Results will be reported in a technical report.

b. Experimental Lithium Aluminum Hydride ($LiAlH_4$)

a) $LiAlH_4$ reacts so fast against organophosphates that the reaction is nearly complete by the time the first NMR spectra could be acquired.

b) Identified primary phosphate product for the reaction of organophosphates with $LiAlH_4$. It was determined that methyl phosphine is the resulting organophosphate product from the reaction.

c) Reactions of GB, GD, and VX with $LiAlH_4$ were less likely to go to completion with small amount of the reagent. A volatile product was produced, but the reaction consumed a high molar amount of the reagent. A viscous paste was formed with the residue from the $LiAlH_4$ that absorbed GB, GD, VX, QL, and HD.

d) Using a Press and Die, pellets of $LiAlH_4$ were successfully fabricated and tested with neat agent.

c. Other Experimental Results to Note

a) After 8 days of reaction, the amount of residual GB was 7% for both $LiBH_4$ and $NaBH_4$ reactions.

d. Computational Modeling

a) Determined that our chosen force field parameters for GB and VX are appropriate for further analyses. Molecular dynamics (MD) simulations of pure liquids and potential reaction mixtures are needed to evaluate the transport properties of these fluid mixtures. The kinetics of fluid mixing will significantly affect reaction rates.

b) Completed AIMD simulations to obtain structural properties of bulk fluids. These simulations serve as the "gold standard" for assessing empirical (force field) models for classical MD simulations, which are needed to access the large system sizes and simulation times needed to calculate fluid transport properties.

c) Determined favorable reaction pathways for hydrolysis and ammonolysis of GB and VX using quantum methods. These results helped in the interpretation of experimental results and suggested new reaction schemes.

d) Developed web interface to determine reaction favorability of reactions based on Gibbs Free Energy. This tool is based on a freely available artificial neural net model that uses machine learning to predict molecular geometries and energies with quantum-level accuracy. The understanding developed under this project enabled the accurate prediction of reaction favorability (as validated by experimental results) at a fraction of the computing time required for quantum methods.

2. Manuscripts, Published and/or Peer Reviewed Papers:

a. McGarvey, D., W. Creasy, and M. Kinnan, "Characterization of Solid Reaction Products from the Reaction of VX with Li_3N+H_2O for the Tactical Disablement Project," CCDC CBC Technical Report CCDC CBC-TR-1635, Feb. 2020, Aberdeen Proving Ground, MD.

a) https://apps.dtic.mil/sti/pdfs/AD1091850.pdf

b. McGarvey, D.; W. Creasy, and M. Kinnan, "Reaction of GB with Li_3N+H_2O for the Tactical Disablement Project," CCDC CBC Technical Report CCDC CBC-TR-1720, Dec. 2020, Aberdeen Proving Ground, MD.

a) https://apps.dtic.mil/sti/pdfs/AD1118232.pdf

c. McGarvey, D.; W. Creasy, and M. Kinnan, "DF Reaction with $Li_3N + H_2O$ for the Tactical Disablement Project," CCDC CBC Technical report CCDC CBC-TR-1721, Dec. 2020, Aberdeen Proving Ground, MD.

a) https://apps.dtic.mil/sti/pdfs/AD1118235.pdf

d. McGarvey, D.; W. Creasy, and M. Kinnan, "Reaction of QL with $Li_3N + H_2O$ for the Tactical Disablement Project," CCDC CBC Technical report CCDC CBC-TR-1722, Dec. 2020, Aberdeen Proving Ground, MD.

a) https://apps.dtic.mil/sti/pdfs/AD1118236.pdf

e. McGarvey, D.; W. Creasy, and M. Kinnan, "Reaction of GD with Li_3N+H_2O for the Tactical Disablement Project," CCDC CBC Technical Report, Mar. 2021, Aberdeen Proving Ground, MD.

a) Link not available before report finalized.

f. C.J. Leverant, C.W. Priest, J.A. Greathouse, M.K. Kinnan, and S.B. Rempe. Quantum Calculations of VX Ammonolysis and Hydrolysis Pathways via Hydrated Lithium Nitride. International Journal of Molecular Sciences 2021, 22, 08653.

a) https://doi.org/10.3390/ijms22168653

g. C.W. Priest, J.A. Greathouse, M.K. Kinnan, P.D. Burton, and S.B. Rempe. *Ab initio* and force field molecular dynamics study of bulk organophosphorus and organochlorine liquid structures. Journal of Chemical Physics 2021, 154, 084503.

a) https://doi.org/10.1063/5.0033426

h. McGarvey, D.; W. Creasy, R. Knoebel, and M. Kinnan, "Reaction of Large Volume GB with Li_3N+H_2O and Studies of Complex Reaction Parameters for the Tactical Disablement Project" CCDC CBC Technical Report, Aberdeen Proving Ground, MD, in preparation.

i. McGarvey, D.; W. Creasy, R. Knoebel, and M. Kinnan, "Reaction of HD with Li3N+H2O for the Tactical Disablement Project," CCDC CBC Technical Report, Aberdeen Proving Ground, MD, in preparation.

3. Conferences:

a. Poster: Mark K Kinnan, David J McGarvey, Todd M Alam, William R Creasy. Chemical Based Neutralization of Neat Chemical Warfare Agents. 2017 Chemical and Biological Defense Science & Technology (CBD S&T) Conference.

b. Poster: David McGarvey, William Creasy, Mark Kinnan, and Todd M. Alam, "Testing of Potential Decontaminants for CW Agents Target-Defeat Applications," poster presentation at the 2017 Chemical and Biological Defense Science and Technology Conference, Nov. 28-30, 2017, Long Beach, CA.

c. Poster: Mark K Kinnan, David J McGarvey, Todd M Alam, Patrick D Burton, Bill Creasy, Jeffery A. Greathouse, Chad Priest, Susan L. Rempe. Tactical Disablement of Neat Chemical Weapons. 2019 Chemical and Biological Defense Science & Technology (CBD S&T) Conference

d. William Creasy, David McGarvey, Mark Kinnan, and Todd M. Alam, "Decontaminants for CW Agents for Tactical Disablement," 2019 Gordon Research Conference on Chemical and Biological Terrorism Defense, March 3-8, 2019 at Ventura, CA.

e. William Creasy, David McGarvey, Mark Kinnan, and Todd M. Alam, "Decontaminants for CW Agents for Tactical Disablement," CCDC CBC Coffee with Colleagues, Aberdeen Proving Ground Edgewood Area, May 1, 2019.

f. D. J. McGarvey, W. R. Creasy, and M. K. Kinnan, "Tactical Disablement Reactions for Chemical Weapons Destruction at Medium (100 mL) Scale," oral presentation at the 2019 Chemical Biological Defense Science and Technology Conference, Cincinnati, OH, Nov. 18-21, 2019.

g. McGarvey, D.; W. Creasy, R. Knoebel, "Solid and Liquid NMR Analysis of Chemical Agent Reaction Masses," Practical Applications of NMR in Industry Conference, October 17-20, 2021, Nashville, TN.

4. Patents:

   a. None. The legal office at Sandia has determined that patenting of the Li_3N+H_2O cannot be patented as it was disclosed during the 2017 DTRA Conference and is beyond the 1 year limitation.

3. PROJECT BACKGROUND

A variety of reagents were tested against chemical agents (GB, GD, VX, and HD) and precursors (QL and DF) for potential use in the field. After the exploratory phase of testing the various reagents, one chemistry was down-selected for scaled up reactions. The selected chemistry is a binary reaction comprising lithium nitride (Li_3N) and water reacted together directly in the chemical agent or precursor.

Reactions at small scale (1 and 10 mL) worked exceptionally well for organophosphate based agents (GB, GD, VX, QL, and DF) using the $Li_3N + H_2O$ chemistry. Using 21% by volume additive of Li_3N and H_2O, approximately 50% of the GB in the reaction was neutralized in 10 minutes with gelling occurring within 6 hours. The successes of the reactions led to the next phase of scaling the reactions to larger volumes.

Scaling of the reactions from 10 mL up to 100 mL resulted in unexpected challenges in regards to mixing of the reagents in the neat agent. For these scaled up reactions, the Li_3N was pressed into tablets. The use of pressed tablets of Li_3N is advantageous over powder for safety and logistical reasons. The tablets were added first and sank to the bottom of the neat agent as expected. Upon the addition of water, the water remained as a discreet layer on the top of the agent as a result of the lower density of water compared to the agent. Over the course of several hours, the water would diffuse into the agent. No immediate reaction was typically observed upon adding the tablets and water to the agent. Within a day or two, a reaction can be observed as changes in the tablets and a viscous semisolid / gel-like material or solid precipitate in the neat agent.

The use of $Li_3N + H_2O$ for destruction of neat agents is effective but the transition to implementation in the field has been challenging. Experiments into the decreased reactivity as

the reaction volumes were scaled indicated that the tablets became passivated by the chemical agent (CA) or precursor immediately upon exposure. The added water is not able to directly react with the tablet due to the passivating layer protecting the tablet as well as poor mixing with the CA or precursor solution. A few different approaches were tested to increase the contact of an aqueous solution with the tablets at the bottom of the reaction vessels. Concentrated solutions of sodium chloride, potassium hydroxide, and potassium carbonate were used in place of the water. Due to the higher density of these solutions, they sank to the bottom of the solution and were in direct contact with the tablets. The improvements in reactivity were limited, though. It was not clear that the extra logistical burden of the extra reagent would be worth the small improvement in performance.

A safe procedure was developed for reactions of GB up to 1 L in volume. One GB reaction and several DMMP reactions at that scale were done.

Extensive MD simulations of bulk liquids for two classes of chemical agents were performed at the classical (FF) and quantum (DFT) levels of theory. This is the first time that a set of DFT simulations has been performed on either class of compounds. These DFT simulations and analysis of liquid structures can be used as a benchmark to develop and validate FF models for these compounds. In contrast, most prior works that validate classical force fields limit comparisons with gas phase and thermodynamic data. For example, in the case of the organic liquids studied here, prior works evaluated force fields by comparisons with thermodynamic data. In this work, we demonstrated the benchmarking for a subset of organic liquids, instead of traditional solvents such as water. Finally, we included in our FF validation a thorough comparison of dihedral angles in these compounds. Dihedral parameters are not typically derived for specific molecules, but our analysis indicates that these parameters can significantly affect intermolecular properties in pure liquids. Our approach is generally applicable for validating FFs for other liquids in bulk environments and at interfaces.

To provide molecular-level insight into potential reactions involved in this process, we studied the neutralization of the CA VX by neutral hydrolysis, alkaline hydrolysis, and ammonolysis using ab initio and DFT methods. Our calculations show alkaline hydrolysis as the most favorable mechanism, with a ≈10 kcal/mol preference for the P-S over the P-O cleavage for all methods. In aqueous solutions at the Hartree–Fock (HF) level of theory, we observe a slightly favorable ΔG for the P-S bond, but not the P-O bond, for both ammonolysis and neutral hydrolysis. This suggests that, over long periods of time, either water or NH_3 can react with VX to produce exclusively non-toxic products. Finally, we studied further reactivity of the VX reaction products to determine the full reaction pathway. Those results were found to be in good agreement with, and complementary to, experimental studies. Many experimental products can be formed by multiple different reaction pathways, making it difficult to verify the reaction pathway from experiments alone.

4. PROGRESS MADE DURING THE Project

Task 1: Elimination of HD Using Alkylaluminum Sesquihalide Chemistry

Subtask 1.1: Develop Methods to Prevent Aluminum Passivation

Approximately 300 vial-based reactions were performed using CEES and BCEE to design a chemistry for destruction of neat HD. After extensive research, a magnesium based chemistry was developed that demonstrated gelation and neutralization of CEES and BCEE. It was found that magnesium powder and magnesium-aluminum alloy powder in combination with iodine and tetrahydrofuran initiates a reaction that results in the slow (*hours to days*) solidification of the neat simulant. The addition of copper(II) chloride ($CuCl_2$) enhanced the reaction mostly likely through Kumada coupling.[1]

Subtask 1.2: Synthesize Alkylaluminium Chlorides from CEES/CEPS

Visual observations of the magnesium based reactions on CEES and BCEE repeatedly showed varying degrees of solidification of the neat simulants. The inconsistency of the reactions was attributed to lack of stirring of the reactions resulting in the metal powders falling out of solution. Slow stirring of the reactions to keep the metal powders suspended in solution was key to reproducibility of the reactions. Smaller particle sizes (e.g., 325 mesh) were easier to keep suspending in solution. Using metal chunks instead of powders was not very effective in achieving solidified reactions. The reactions appeared to take place on the metal surface creating a layer of solid material surrounding the metal chunks effectively quenching the reaction. $CuCl_2$ was introduced into the reactions via saturated solutions in THF. Pictures of one milliliter reactions using the magnesium based chemistry for CEES and BCEE are shown in Figure 1. The reactions circled in green yield highly viscous or solid solutions and were the identified reaction combinations for testing on HD at the U.S. Army Combat Capabilities Development Command Chemical Biological Center (CBC).

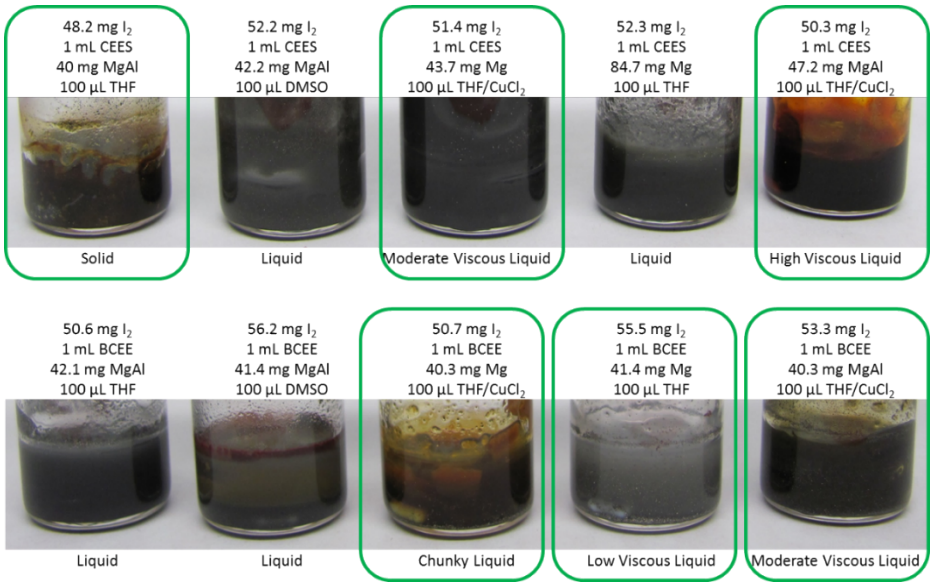

Figure 1. Pictures of reactions of CEES (top row) and BCEE (bottom row).

Selected reactions were analyzed via solid state ^{13}C MAS NMR and are outlined in Table 1. These reactions were slowly stirred and heated (30°C/86°F) in order to drive the reaction to near completion for analysis of the reaction products. Figure 2 depicts ^{13}C MAS NMR spectra of the solid reaction products for CEES (top, 044A and 044E) and BCEE (bottom, 044H and 044J).

Table 1. Outline of reactions used for NMR analysis of solid reaction products.

RXN ID	Simulant	Corroder	Metal	Catalyst
044A	CEES	I_2	MgAl (small)	THF
044E	CEES	I_2	MgAl (small)	THF/$CuCl_2$
044H	BCEE	I_2	Mg	THF/$CuCl_2$
044J	BCEE	I_2	MgAl	THF/$CuCl_2$

^{13}C MAS NMR analysis of the solid product formed for the reaction with CEES revealed the disappearance of the chloro-ethyl group indicative of neutralization of CEES. For the 044A and 044E there is a significant loss of the CEES, most notable is the reduction of the (a') and (b') resonances. Numerous other carbon species are produced in this reaction, with the observed chemical shift range δ = +45 to + 10 ppm consistent with alcohols, aliphatic species and chlorinated aliphatic chains, some of these resonances overlap with the remaining CEES.

NMR analysis of the solid products formed indicate only the presence of BCEE even though the reactions contained only small amounts of liquid and significant gel/solid material. For reaction 044H and 044J the only significant carbon species belong to BCCE. So either this is a polymerization with THF to make longer ether species, or the "gel" like properties of the precipitate are not related to a reaction of the BCEE. If it was polymerizing (significantly) the ratio of the ether resonance (a) to increase with respect to the Cl carbon environment (b) giving an endgroup analysis. The ratio is approximately 1:1 arguing against extensive polymerization.

The solution ^{1}H NMR spectrum in Figure 3 shows the beginning reaction where HD was treated with a small amount of $LiAlH_4$. The spectrum shows many peaks in addition to the original mustard peaks, indicating that a chemical reaction is taking place in addition to the gelling process. The $LiAlH_4$ was obtained from a solid pellet, and a small chunk (5 mg) was placed directly on the surface of the neat mustard (400 µL), without use of solvents. Over several hours a physical change was observed, and the mixture appeared to thicken and gel.

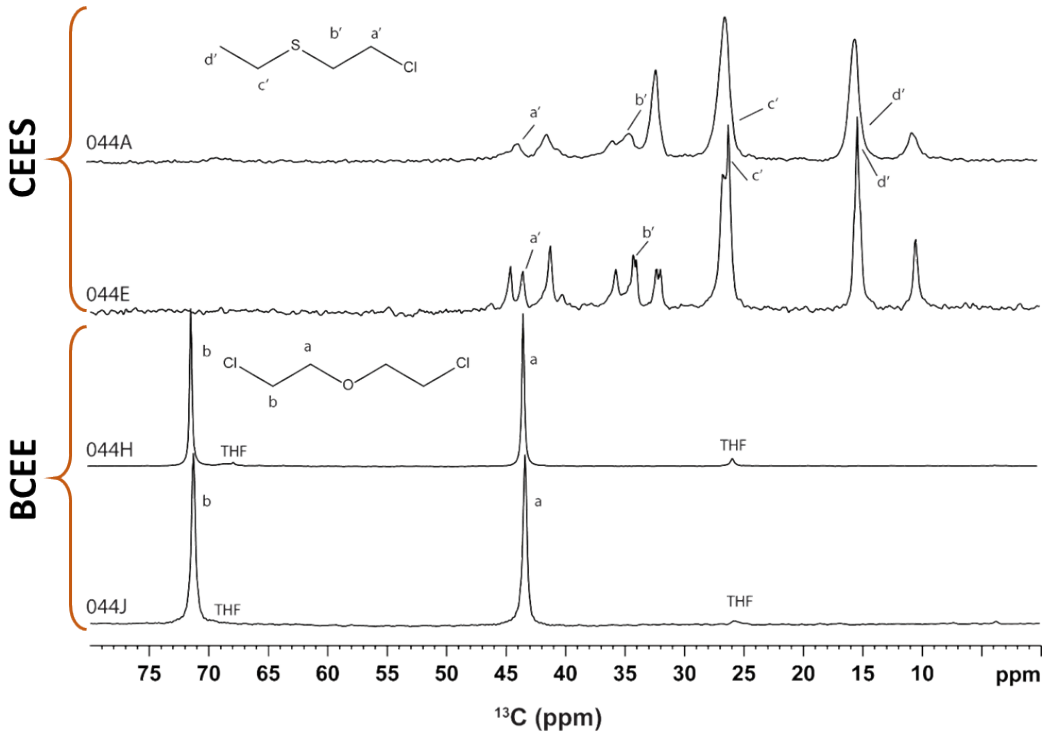

Figure 2. Solid state ^{13}C MAS NMR analysis of solid reaction product.

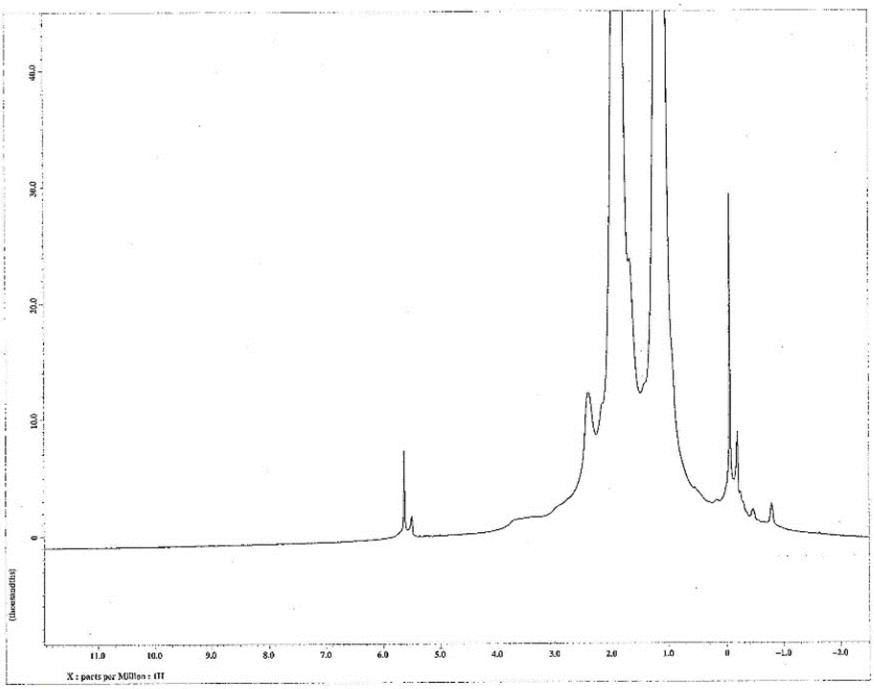

Figure 3. Solution ^{1}H NMR spectrum at the beginning of a reaction of HD and $LiAlH_4$ pellet.

Subtask 1.3: Synthesize Alkylaluminium Chlorides from HD

Since HD chemistry is significantly different from G agents, some other reaction schemes were explored.[2] A series of reactions based on Friedel-Crafts reactions were done using the conditions that are listed in Table 2. The goal was to find a catalytic approach that would consume the HD with a minimal amount of metal and reagents. Mg or Mg/Al alloy were added as solid metal turnings or powder with various catalysts or cosolvents. I_2 was added to all the reaction mixtures to corrode the metal oxide surface to expose the HD to non-oxidized metal.

Table 2. Reaction information for magnesium reactions analyzed via ^{13}C MAS NMR.

Sample ID	Agent	Metal	Corroder	Catalyst
81A	373 µL HD	14.93 mg MgAl	19.12mg I_2	37 µL THF/$CuCl_2$
81B	393 µL HD	15.57 mg	19.64mg I_2	39.4 µL THF/$CuCl_2$
83A	386 µL HD	16.29 mg	19.28 mg I_2	39 µL THF
83B	200 µL HD	16.07 mg MgAl	21.93 mg I_2	40 µL THF
85A	400 µL HD	15.64 mg MgAl	22.29 mg I_2	40 µL d-DMSO

There were signs of reaction for some of the compositions. Figure 4 shows the NMR tube with sample nb097p85A. A solid mass is formed in the reaction, although there is still liquid HD on top of the solid, and the analysis of the liquid shows that it is still HD without reaction products. Inverting the tube multiple times was not sufficient to mix the solid and liquid components.

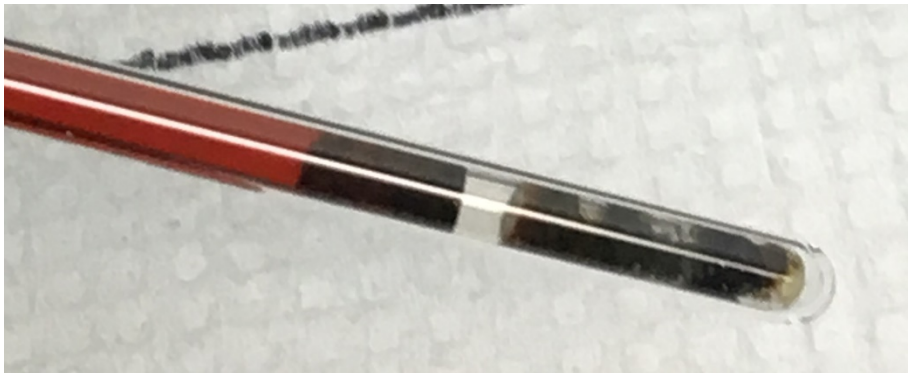

Figure 4. Reaction mixture in NMR tube of HD + MgAl metal + I2 + DMSO, sample nb097p85A.

Two reaction runs with chloroethyl ethyl sulfide (CEES) were done for comparison to preliminary simulant results at Sandia National Labs (Sandia). Solid residue was also observed, but no reaction products were detected corresponding to the CEES. Prior experiments at Sandia using the simulant chloroethyl phenyl sulfide (CEPS) revealed full reduction of CEPS to ethylthio-benzene.

There was no evidence of HD reaction products in solution or mixed with the residual HD. Some samples formed a thick plug of porous solid material that increased the viscosity. It was possible that HD was reacting with the metal to form a solid that we could not analyze. We have not found a way to demonstrate that a reaction occurred.

These reactions required more reagents, particularly I_2, which is dense, heavy, and potentially toxic. This reagent was needed to form the active Mg or Al reagent for the Friedel Crafts reaction, and to transform the metal reagent into a reactive species. Additional solvents and $CuCl_2$ catalyst (saturated solution of solid $CuCl_2$ in THF solvent) were also added to some of the mixtures.

Since a considerable amount of residual HD was observed, it would be necessary to do a toxicity study of the reaction mixtures to determine whether the toxicity has been reduced by the reaction. Due to the expense of this testing, it would be preferable to optimize the reaction so that toxicity studies of only a few of the reaction mixtures are necessary.

For these samples, the resonances from the unreacted HD were observed at δ = + 43 and +34 ppm, while the THF resonances were observed at δ = +25 and +67 ppm. In 85A, the DMSO-d6 (deuterated) gives a minor multiplet resonance at 39.5 ppm. The relative concentration of these HD carbon species remains essentially unchanged during the reaction, as shown in Figure 5. This suggests that the reaction chemistry does not degrade the HD into new speciation.

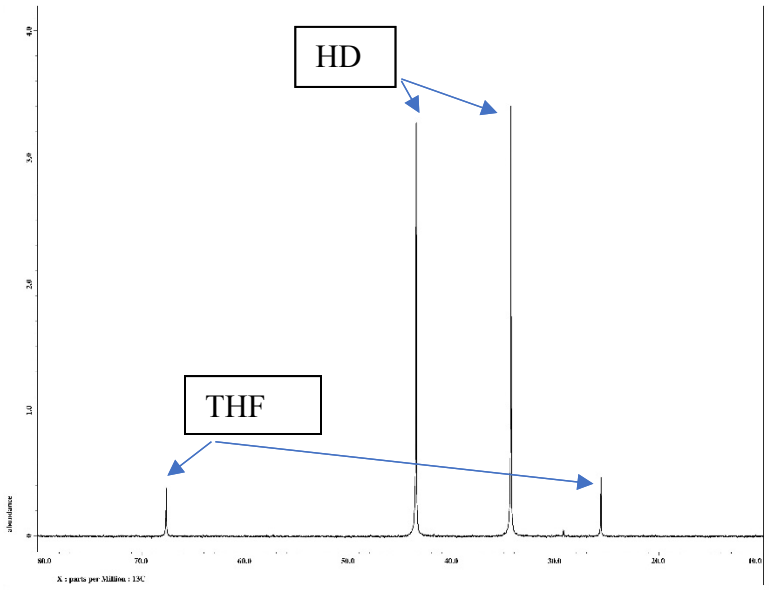

Figure 5. ^{13}C MAS NMR spectra showing no reaction products with HD.

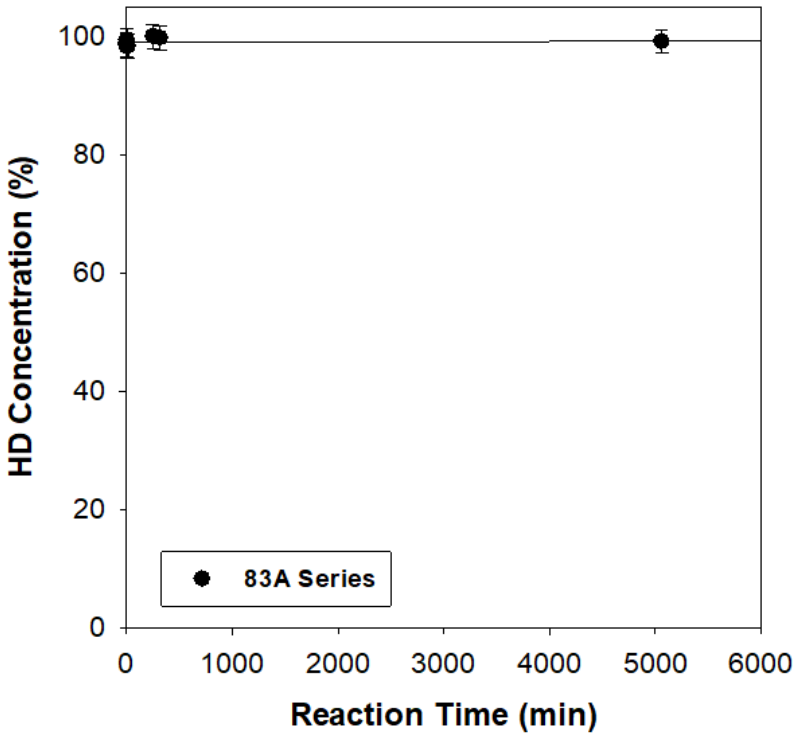

Figure 6. Magnesium chemistry with HD as monitored by solution ^{13}C NMR spectroscopy.

Task 2: Elimination of GB Using $LiAlH_4$

Subtask 2.1: Optimize DFP Reactions Using LiAlH4

Combining reactive mole equivalents of DFP and $LiAlH_4$ powder resulted in an extremely violent initial reaction. The reaction remained a cloudy, liquid solution for the first 10 minutes and did not change in appearance or liquidity over the next several days. Figure 7 shows the solid state ^{31}P MASNMR analysis of the solid product from the reaction. There are no solid environments observed in the solid precipitate products, suggesting that this gel is still very liquid-like (lower viscosity) such that there is significant mobility. In addition, no significant concentration of polyorganophosphates was observed between δ = -20 to -60 ppm that would reflect polymerization. The unreacted DFP remaining in the precipitate corresponds to ≈ 60% of the total P concentration.

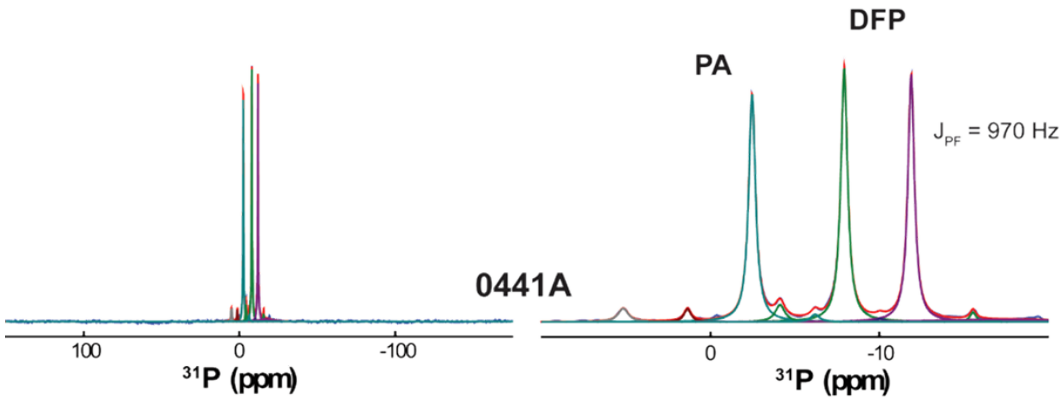

Figure 7. Solid state ^{31}P MAS NMR of DFP precipitates when DFP and $LiAlH_4$ are combined.

Even though enough $LiAlH_4$ was used to react all of the DFP, there appeared to be significant amounts of unreacted DFP based on the amount of liquid still in the reaction vial. There are two possible explanations for the significant amount of DFP still remaining in the reaction. First, $LiAlH_4$ is extremely reactive towards organophosphates and it is possible that as the reaction products are formed $LiAlH_4$ reacts with the reaction products in addition to DFP. It can be observed in Figure 7 that there are several small peaks that visible indicating other reaction products. Secondly, $LiAlH_4$ is reactive towards moisture and may lose some amount of reactivity since reactions are performed in open atmosphere.

It may be possible to mitigate both possible causes discussed above by encapsulating the $LiAlH_4$. This could be done by mixing paraffin wax or long chain alkanes with the $LiAlH_4$ at high concentrations. It has been reported that 27% by weight concentrations of $LiAlH_4$ in paraffin wax can be done to encapsulate $LiAlH_4$ powder.[3] It was demonstrated in the report that the $LiAlH_4$ is safely protected in the wax from environmental exposure. It is expected to be possible to create higher amounts of $LiAlH_4$ in paraffin wax because the application intended here (agent destruction) is different. Tablets of $LiAlH_4$ powder mixed in paraffin wax is hypothesized to control the rate of reaction by slow dissolution of the wax into the neat simulant/agent solution releasing $LiAlH_4$ that should promote self-mixing from formation of micro bubbles. It is

expected that the slow release of the $LiAlH_4$ will yield higher destruction rates. Scaling up reactions beyond a few milliliters of simulant/agent and using $LiAlH_4$ will require research into the encapsulation and safe delivery of $LiAlH_4$.

Due to the high reactivity of $LiAlH_4$, it may be possible to synthesize an $LiAlH_4$ analogue ($LiBH_4$) *in situ* in the neat simulant/agent. Lithium borohydride is a strong reducing agent like lithium aluminum hydride and can be synthesized as follows: [4]

$$NaBH_4 + LiCl \Rightarrow LiBH_4 + NaCl$$

This reaction was attempted directly in DFP and resulted in significant amounts of micro bubbling. A fine white precipitate formed and settled out of solution. This was most likely the formation of sodium chloride (NaCl). Solid state ^{31}P MAS NMR analysis of the gelled reaction product revealed multiple overlapping resonances corresponding to both solid and liquid like species, including phosphoric acid (PA), see Figure 8. There are 5 distinct solid environments (labeled 1-5 in expansion) that give rise to a set of SSB manifolds with the chemical shift δ between -1 and – 9 ppm, and anisotropy Δδ ranging from -85 to -145 ppm. These different environments are related, but have different P coordination environments. There is also the unreacted DFP that shows up as a doublet at δ = -10 ppm (overlapped with the previous discussed resonances) and corresponds to 40% of the total P concentration. There is also a liquid-like (no ssb) resonance at δ = +5.5 ppm (6%).

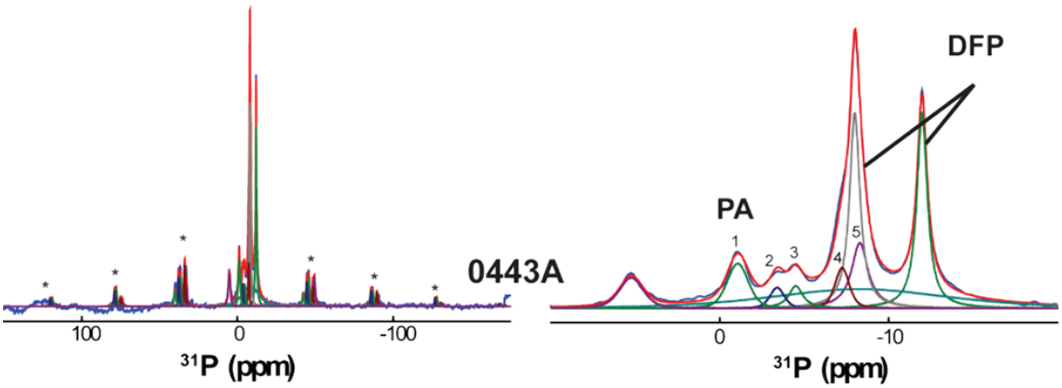

Figure 8. Solid state ^{31}P MASNMR of DFP precipitates when DFP, $NaBH_4$, and LiCl are combined.

The proof-of-concept reaction was demonstrated to be successful in gelling and destroying neat DFP. Although $LiBH_4$ is a less powerful reducing agent compared to $LiAlH_4$, the handling of $NaBH_4$ and LiCl is much easier and safer. Although $LiBH_4$ is moisture sensitive and requires special handling, it is not necessary because the $LiBH_4$ is synthesized in situ in the agent. Reactions to synthesize $LiAlH_4$ are not as easy which is the reason $LiBH_4$ was chosen for this proof-of-concept reaction. Research would need to be performed to evaluate quantities of material and reaction rates on DFP and agents.

Subtask 2.2: Validate GB Destruction Using $LiAlH_4$

Combining 0.445 mL GB and 0.0328 g $LiAlH_4$ (sample 69B) results in significant amounts of bubbling, formation of precipitates, and smoking. After a few minutes, the NMR tube was tested for pressure buildup and none was observed. Gelling was not observed, although the solution may have become more viscous.

The ^{31}P NMR analyses revealed the formation of two reaction products from the reaction of $LiAlH_4$ and GB: methyl phosphine and isopropyl methylphosphonic acid, see Figure 9. The presence of the fully reduced methyl phosphine at a chemical shift of -163 ppm [5-6] indicates the strength of the reducing potential of the $LiAlH_4$. The isopropyl methylphosphonic acid is the primary hydrolysis product of GB, and may indicate a reaction with lithium hydroxide or aluminum hydroxide that is formed when $LiAlH_4$ comes in contact with residual water.

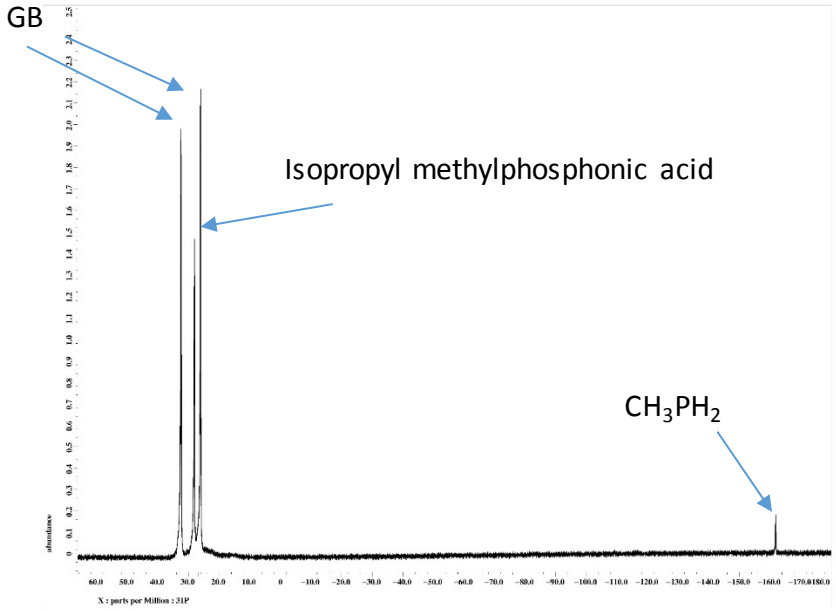

Figure 9. Breakdown products of GB + $LiAlH_4$ using ^{31}P NMR.

Solution ^{31}P NMR analysis, Figure 10, revealed 27% destruction of the GB by the time (20 minutes) the first NMR spectra was collected. There was no additional change in the amount of GB consumed over five days. The observation of no pressure building shortly after the reaction started and the lack of change of the reaction over five days suggests the reaction is a quick-and-done type reaction.

Observation of the methyl phosphine product that the GB was fully reduced, losing all its P-O bonds and reduced from P(V) to P(III). No compounds with intermediate amounts of reduction were identified. CH_3PH_2 is very volatile and rapidly evaporates from the sample. The volatility of the compound makes quantitative methods difficult for determining the amount of the compound that is formed, but the amount of residual GB can be measured. The compound auto-ignites when exposed to oxygen in the air to form methylphosphonic acid (*hypothesized based on*

phosphine plus oxygen reaction) as evident by the observed flame above a container. The flame we observed was small but the compound is classified as pyrophoric, so there is an explosion hazard if it accumulates in a low oxygen enclosed container.[7] After reaction, there was a gray-white solid residue from the $LiAlH_4$. This solid residue was not collected and analyzed but it is likely a combination of Li and Al oxides and fluorides, and residual GB.

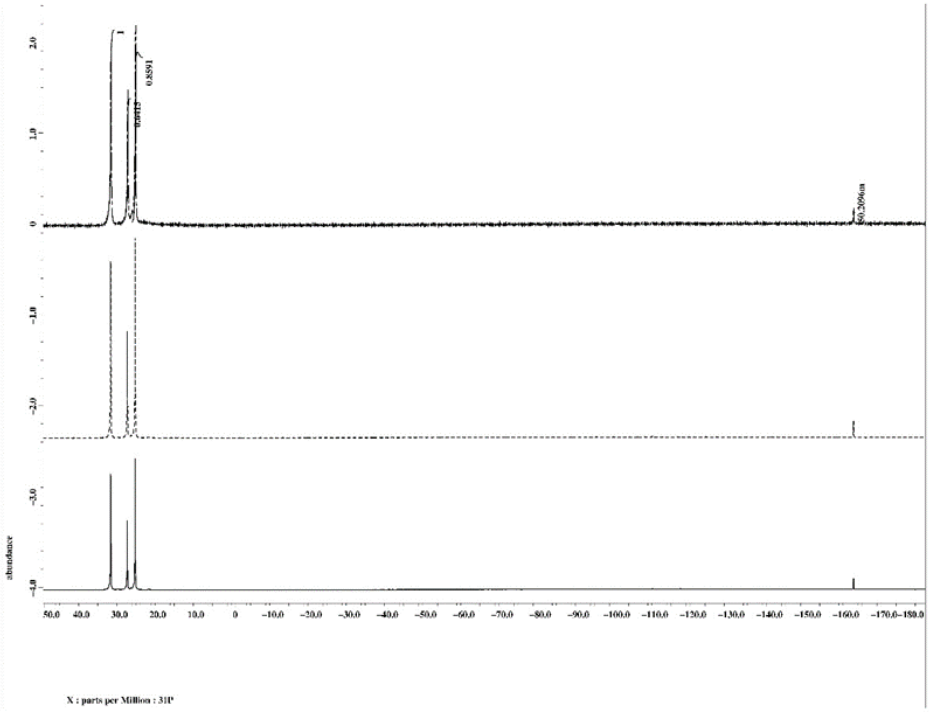

Figure 10. Reaction of GB and $LiAlH_4$. Reaction of GB and $LiAlH_4$ by solution ^{31}P NMR. There is little reaction after the first burst of bubbling. Bottom panel: first spectrum 15 min after mixing; Middle panel: 4 hr after mixing; Top panel: 6 days after mixing, showing peak integrals.

Since GB is fully reduced to CH_3PH_2, a GB molecule consumes 3 of the 4 hydrogens on each $LiAlH_4$ molecule according to the reaction stoichiometry, rather than reacting in a 1:4 molar ratio that might be anticipated if a less reduced intermediate product was formed. To fully reduce GB to CH_3PH_2 requires a theoretically calculated 24% by volume amount of $LiAlH_4$. Based on the observation of methylphosphine formation, $LiAlH_4$ could slowly be introduced over time such that minimal volume displacement occurs. As methylphosphine leaves the solution, more $LiAlH_4$ can be added to eventually reach 24% by volume $LiAlH_4$.

If the reagent begins as a chunk of material, in the NMR tube reactions, some chunks remain that appear to be unreacted. This may be due to insufficient agitation in the tube or some passivation of the surface of the reagent.

Task 3: Elimination of GB Using Li_3N

Subtask 3.1: Optimize DFP Reactions Using Li_3N

Reactions on the destruction of DFP using Li_3N and water were investigated and optimized for the quantity of Li_3N and water to add to the reactions. The effect of ratio of DFP:Li_3N:H_2O was investigated to understand what drives the reaction.

Based on the proof-of-concept reaction using Li_3N performed on GB at CBC in 2015, DFP appears to be significantly more difficult to neutralize than GB using the $Li_3N + H_2O$ reaction chemistry. More $Li_3N + H_2O$ is required (compared to GB reaction) to achieve similar neutralization amounts of DFP in 24 hours.

DFP + H_2O (no Li_3N) as a control reaction revealed minimal amounts of DFP neutralization after several days. This result confirms Li_3N as a key reactive ingredient for neutralization. When the reactions are performed, water is added after DFP and Li_3N are combined. The combination of DFP and Li_3N does not appear to react as there is no change in color of the Li_3N or appearance of micro-bubbling. It is only when water is introduced into the reaction that micro-bubbling immediately appears and the Li_3N slowly begins to change color to a whitish/grey color.

Neutralization kinetics for DFP are not entirely conclusive because reactions were performed directly in small diameter (5 mm) Teflon NMR inserts. Mixing in NMR inserts via the micro-bubbling is not as effective as in a vial. Figure 11 provides kinetic information on DFP reactions.

Figure 12 shows the solid state ^{31}P MAS NMR spectra of the solid precipitation product formed from the reaction of DFP with Li_3N and water. The precipitate reveals 2 P-containing species are formed. There is unreacted DFP showing up as a doublet with a P-F J coupling of 970 Hz at $\delta \approx -10$ ppm. There is a second species observed at $\delta = -1.18$ ppm. This environment corresponds to a solid, non-mobile, species as a series of ssb that are observed. The chemical shift anisotropy $\Delta\delta \approx -78$ ppm, with a CSA asymmetry parameter of $\eta \approx 0.6$. This is labeled as PA or crystalline phosphoric acid because of the chemical shift, but the non-zero asymmetry parameter suggests a non-symmetric P environment, where H_3PO_4 is predicted to have $\eta = 0$. This assignment is probably incorrect, but this is clearly a solid P environment. In addition, this solid P species gives rise to a very sharp set of resonances in the spinning side band (ssb) manifold, revealing that it is not a highly-disordered species. The unreacted DFP corresponds to ≈ 11% of the total P concentration in this sample. No polyphosphate species are observed ($\delta = -20$ to -100 ppm).

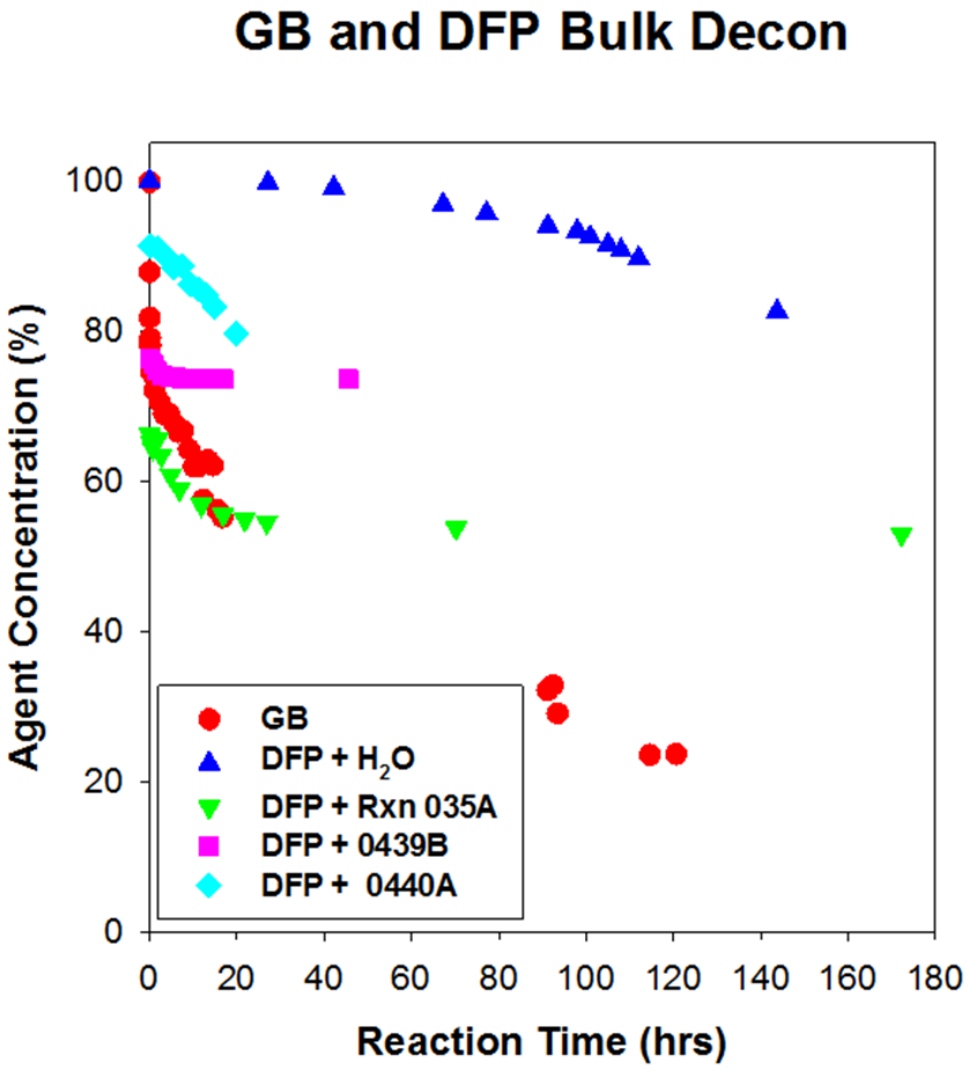

Figure 11. Comparison of DFP and GB reactions as monitored by solution ^{31}P NMR.

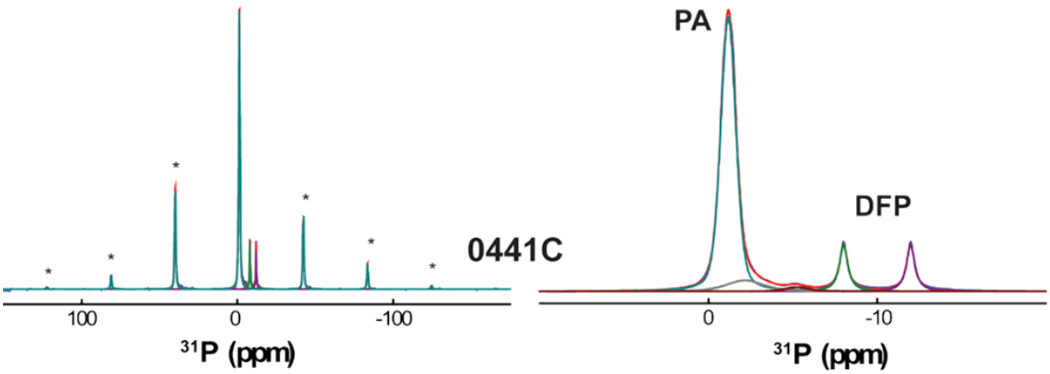

Figure 12. Solid state ^{31}P MAS NMR analysis of solid product from reaction of DFP with Li_3N and water.

Subtask 3.2: Validate GB Destruction Using Li_3N

GB was 50% neutralized in 10 minutes and 90% in one day using 21% additives (Li_3N + H_2O) to the reaction, Figure 13. The specific quantities for the reaction (85B) are outlined in Table 3. Approximately 99% of the GB was destroyed in two days. Complete gelling of the solution occurred in six hours and is a contributing factor to the decrease in reaction kinetics with time. The reaction had very little unreacted Li_3N at the bottom of the NMR rotor. This is because there were approximately 3 moles of H_2O to 1 one mole of Li_3N. Slight excess amount of water (more than 3:1 H_2O:Li_3N) would have likely resulted in complete reaction of the Li_3N. One molecule of Li_3N can react with 3 water molecules because each Li_3N molecule has three reactive lithium atoms.

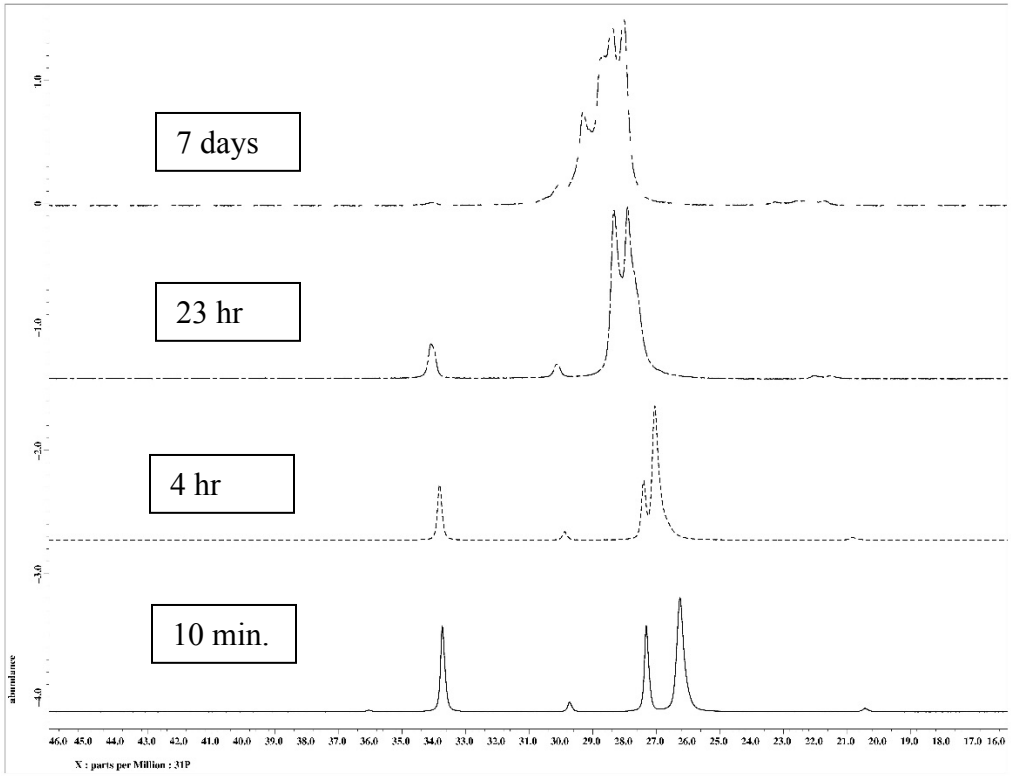

Figure 13. Solution ^{31}P NMR spectra of reaction run 85B, GB + Li_3N + H_2O. The solution gelled in about 4 hr. The top panel shows a broad, low resolution peak for isopropyl methylphosphonic acid due to the high viscosity of the sample.

Table 3. List of GB + Li_3N + H_2O reactions

RXN ID	GB (mL)	Li_3N (g)	H_2O (µL)	H_2O:Li_3N (mol ratio)
69C	0.400	0.0422	16	0.73
85B	0.382	0.0340	54	3.0
87B	0.245	0.0163	12.6	1.5

If the mole ratio of Li_3N to H_2O is significantly reduced (Reaction 69C), then only ≈23% of GB is destroyed in six days. For this reaction, complete gelling was not observed, although the sample was partially gelled. Those quantities are about 0.733 mole of H_2O to 1 mole of Li_3N. Reaction 87B (Figure 14) had approximately 1.5 mole of H_2O to 1 mole of Li_3N and exhibited ≈15% destruction in 10 minutes and ≈60% over six days. This reaction was also only partially gelled. These reactions emphasis the importance of the mole ratio of H_2O:Li_3N in the reaction and that there needs to be three times as many moles of water in the reaction than Li_3N.

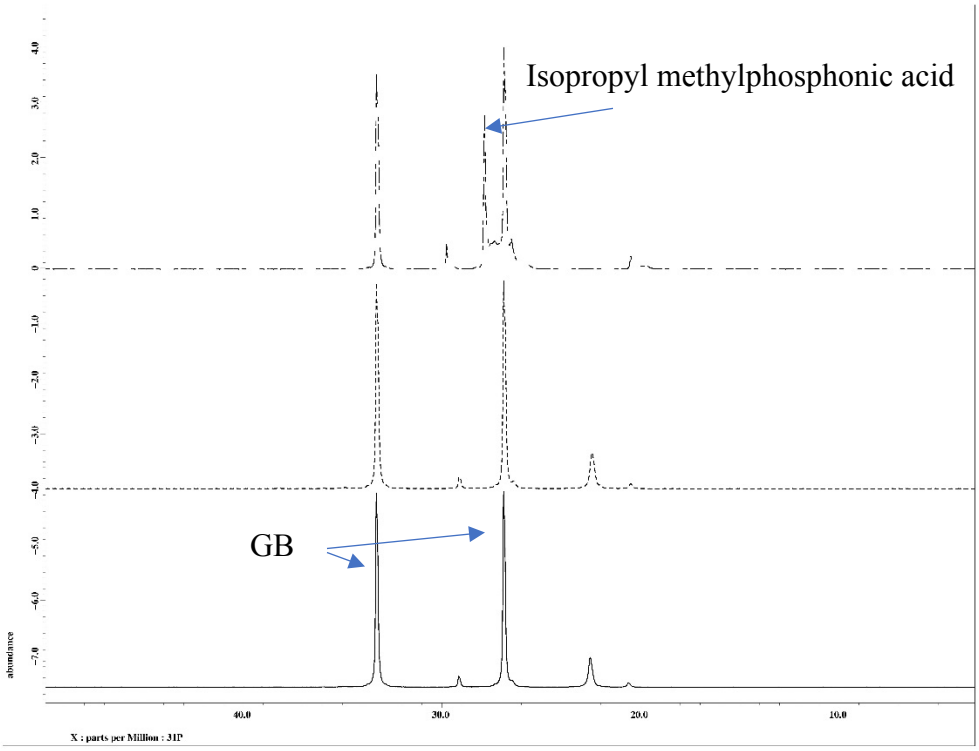

Figure 14. Solution ^{31}P NMR spectrum of GB and Li_3N (run 87B). Bottom panel: Spectrum from 4 min. after mixing; Middle panel: spectrum after 18 hr reaction time; Top panel: spectrum after 13 days of reaction time.

Reactions (e.g., 69C and 87B) with small mole ratio quantities of water appear to have a substantial amount of unreacted Li_3N in the bottom of the NMR tube, see Figure 15. Figure 15 also indicates the partially gelled part of the solution. Since there is poor mixing in NMR tubes, it is hard to say for certain that more water was the main reason for significantly enhanced reaction kinetics but most likely the contributing factor as explained above. It is known Li_3N and H_2O react to form LiOH and NH_3: [8]

$$Li_3N + 3H_2O \Rightarrow 3LiOH + NH_3$$

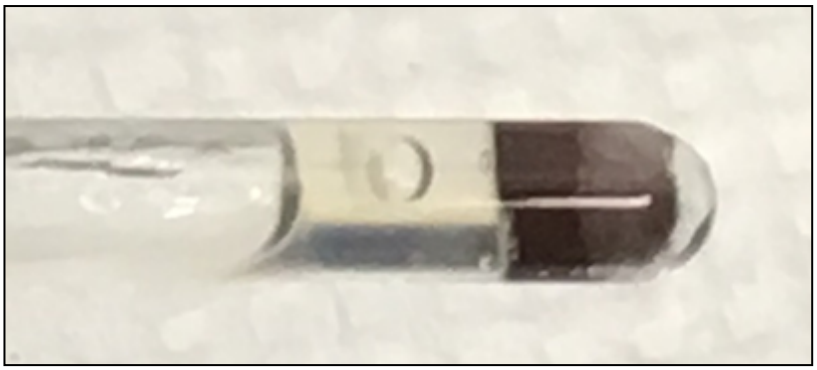

Figure 15. Photo of the NMR tube containing the reaction of GB + Li_3N + H_2O (69C), showing the brown residue of unreacted Li_3N at the right, and the gelled translucent liquid to the left of it. Some of the fluid has drained away.

Lithium hydroxide is a strong base and is hypothesized to be the key chemical reacting with the GB. It was observed that the 69C reaction did not exhibit much micro-bubbling compared to the 85B reaction. The bubbling is most likely NH_3 being released which helps to mix the solution as the bubbles rise to the surface. It is also important to note that the reactions get very hot during the early stages of reaction. The proposed reaction mechanism of GB + Li_3N + H_2O is shown in Figure 16.

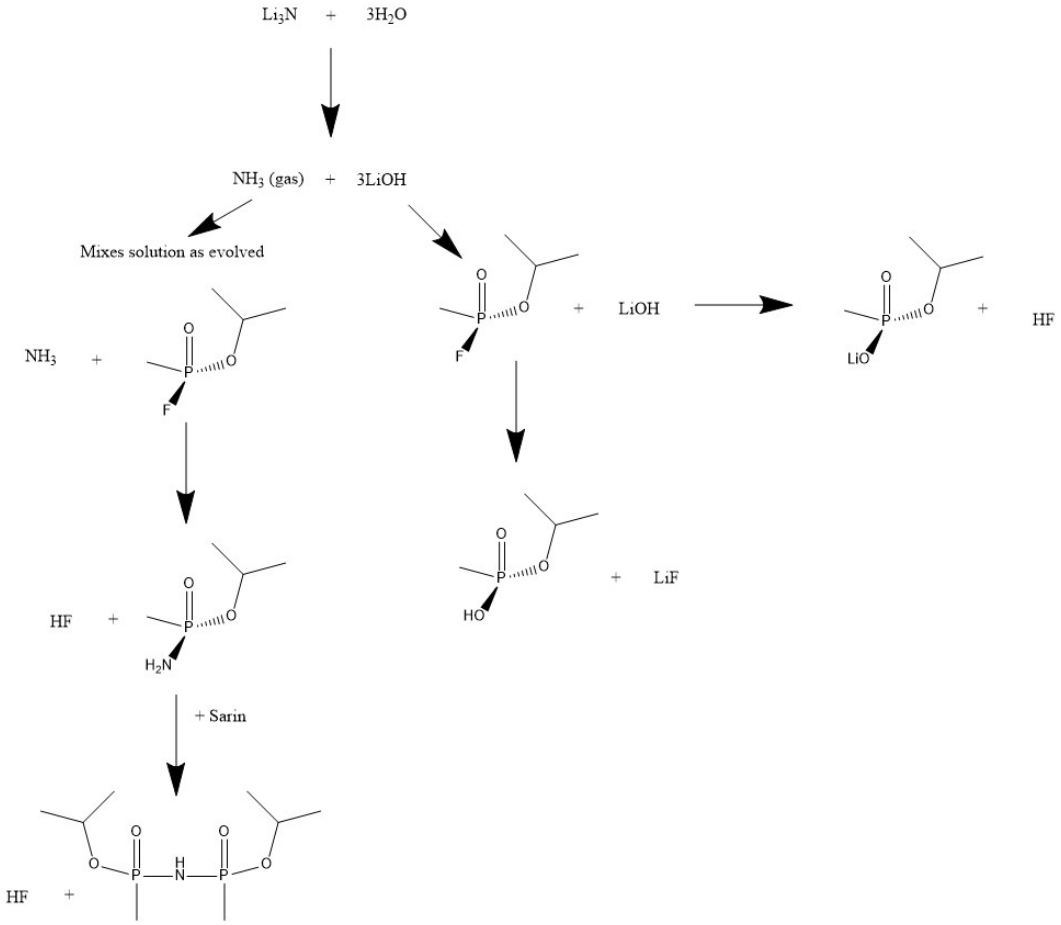

Figure 16. Proposed reaction mechanism of GB + Li_3N + H_2O.

A few additional reactions were performed to determine if Li_3N + H_2O is a requirement, or if lithium hydroxide or ammonium hydroxide could be used. It was observed that reacting Li_3N and H_2O *in situ* with the neat agent is critical for the performance in destruction of the agent. See Table 4 for a list of reactions performed and the observed destruction.

Table 4. Reagent ratio for Li_3N reactions with GB.

Sample Ref. No.	Li_3N:GB (w/w)	Li_3N:H_2O (w/w)	Product consistency	GB remaining
P69C	0.083	2.64	Partly viscous plug	64% GB
P85B	0.083	0.64	Viscous, does not flow	1% GB
P87A	0.021	0.66	Partly solidified	63% GB
P87B	0.061	1.29	Not solidified	50% GB
P121D	0.065[a)]	0.22[b)]	Viscous liquid	5% GB

a) Added as LiOH and NH_4OH (aq.); corresponds to a ratio of about 0.188 LiOH:GB.

b) Including water consumed from making LiOH and NH_4OH from Li_3N. Not including that water, corresponds to about 0.89 Li_3N:H_2O.

The solid Li_3N is in the form of a red/purple powder. Li_3N was added before the agent, and the container was inverted several times to mix the powder with the agent. Several reaction runs were done with a range of amounts of water to determine the effect of the water and the amount that is optimal. It was found that little or no reaction occurred without water, indicating that the Li^+ does not extract fluorine or fluoride from the GB molecule. As a result of this observation and literature,[9] we conclude that the reaction of $Li_3N + H_2O$ forms lithium hydroxide and ammonia, which react by hydrolysis with the agent. The major product that was observed was GB acid (isopropyl methylphosphonic acid), as expected for hydrolysis reactions. It is possible that the GB reacts with some water first, and then the product HF reacts with the Li_3N. We were not able to detect LiF in the NMR. It appeared that there was minimal bubbling of the mixture (ammonia gas).

The sample with the least residual GB was P85B, and this sample had the most Li_3N and the most water. The sample became viscous. The reaction mixtures sat for 2 weeks at room temperature to determine the final amount of GB remaining. It was observed there was a slow reaction continuing for the second week. The continual decreasing rate of reaction over time is due to (1) consumption of the alkali reagent and (2) increase in viscosity of the solution.

To test the hypothesis that the Li_3N reaction was hydrolysis, separate reaction runs were performed using LiOH solution, NH_4OH (30% aqueous) solution, and a mixture of LiOH and NH_4OH (30% aqueous) solution. Reactions are listed in Table 5. LiOH was added as a solid and did not show any effect, probably due to low solubility in GB. NH_4OH solution and the mixture of LiOH and NH_4OH both reacted with GB. There was a noticeable increase in viscosity, but the mixture still flowed because there was more water present for these samples compared to the Li_3N samples. There appeared to be more products formed in the NMR spectrum, but we were not able to assign the identity of the products. Additionally, even though the LiOH and NH_4OH solution reactions yielded high GB destruction, the amount of volume was significantly higher than $Li_3N + H_2O$ reactions.

Table 5. LiOH and NH_4OH reactions against GB.

RXN ID	GB (mL)	Reactant 1	Reactant 2	Comments
121C	0.400	n/a	0.120 mL 30% ammonium hydroxide solution	Minimal destruction in 24 h
121B	0.400	41 mg $LiOH•H_2O$	n/a	Minimal destruction in 24 h
121D	0.150	14.7 mg $LiOH•H_2O$	0.045 mL 30% ammonium hydroxide solution	75% destruction in 24 h

A reaction was performed using a mixture of $LiAlH_4$ and Li_3N, see Figure 17. No water was used, since water would react with the $LiAlH_4$. Quantitation of a sample of the final solid material after a week of reaction time indicated that there was 25% of the original GB remaining.

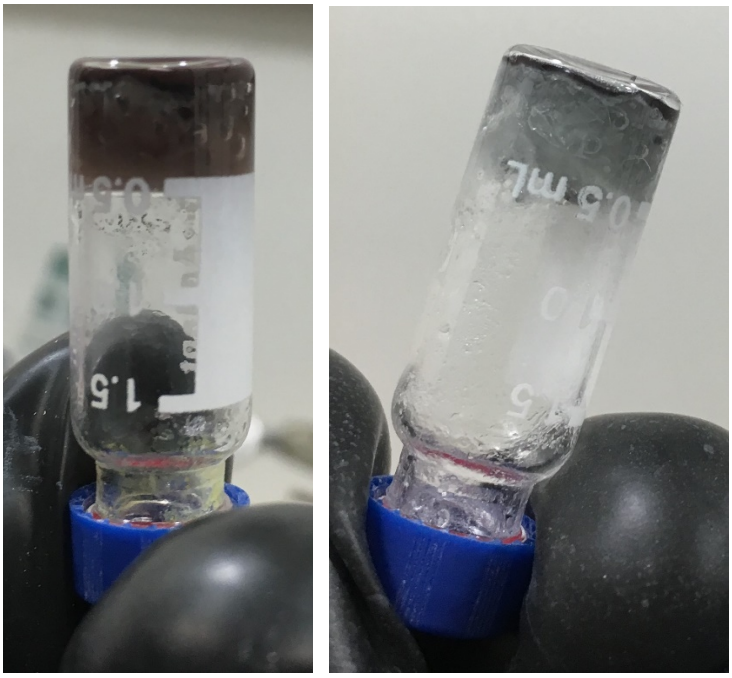

Figure 17. Reaction mixture of GB + $LiAlH_4$ + Li_3N, sample nb0018P27B. Left photo: One-week reaction time. Right photo: Two-week reaction time. Both samples have 25% residual GB.

Task 4: Elimination of VX

Subtask 4.1: Validate VX Destruction Using $LiAlH_4$

A reaction of 19.8 mg of $LiAlH_4$ as a solid pellet was reacted with 0.55 mL of VX. The VX sample bubbled when $LiAlH_4$ was added. It was not clear if all the pellet reacted, since pieces of it seemed to remain. The liquid became more viscous, but did not totally gel. The solution ^{31}P NMR spectrum showed only VX, which was likely to be a smaller amount of liquid VX. Molecules that cannot freely tumble in solution cannot be observed in a typical liquids NMR experiment. Figure 18 shows the same reaction performed in a vial showing partial solidification.

Reaction of 500 µl 2.0M $LiAlH_4$ in THF with 10 µL of VX (107B) and reaction of 400 µl 2.0M $LiAlH_4$ in THF with 60 µl of VX (107D) were done in THF solution. In both cases, the VX reacted to completion to form methyl phosphine. The spectrum from the first reaction mixture is shown in Figure 19. Because it was in solution, no gelling or solidification was observed. It is worth noting that methyl phosphine is a volatile product and causes a pressure buildup. It is toxic, but less toxic than VX or GB.

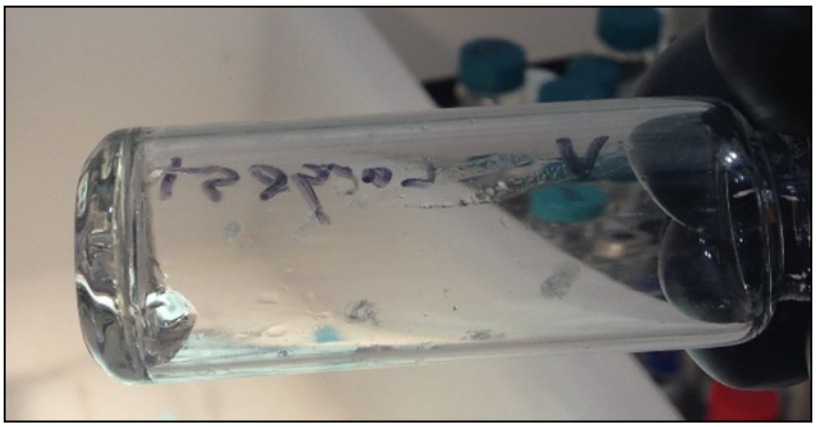

Figure 18. Picture of VX and $LiAlH_4$.

When small amounts of $LiAlH_4$ are added, a significant amount of VX remains, see Figure 19 and Figure 21. Adding an excess of $LiAlH_4$ will drive the reaction to completion, where the only phosphorus-containing product seen is the full-reduced methyl phosphine as illustrated in Figure 20. The methyl phosphine peak disappears over time as it is a volatile chemical species.

Figure 23 is the proposed reaction pathway for the reaction of VX with $LiAlH_4$. The formation of methyl phosphine is confirmed, but the identification of the other reaction products is unknown. Suggested reaction products are shown in Figure 23.

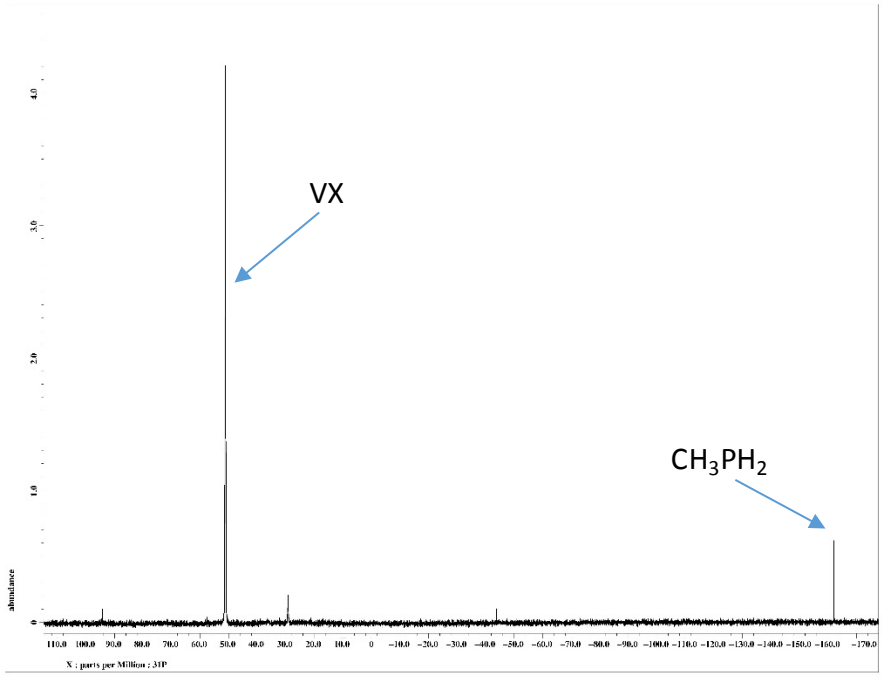

Figure 19. ^{31}P NMR spectrum of mixture with excess VX reacted with LiAlH4

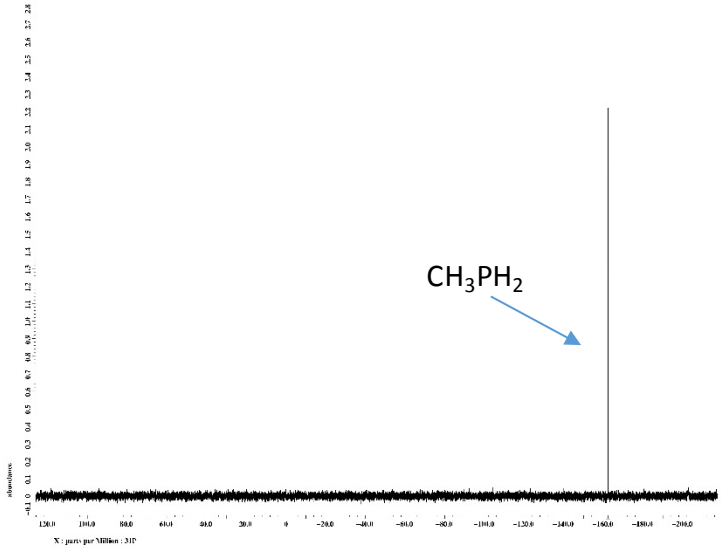

Figure 20. Solution ^{31}P NMR spectrum of a reaction mixture with excess $LiAlH_4$ reacted with VX, showing all the VX has been consumed.

A sample with only 0.01 mL of VX was run, and another with 0.06 mL of VX, and both of these samples went to completion to only CH_3PH_2 remaining in the NMR spectrum. It is possible that H_2S was formed as a volatile product, but this compound was not detected.

Another reaction was done to attempt to measure the weight loss of the sample due to loss of volatile compounds. No weight loss was measured, possibly because the sample absorbed water from the atmosphere to replace the volatile products, Figure 22. As a result, we have not yet developed a quantitative method for measuring the quantity of VX that is converted to volatile compounds. However, a considerable amount of VX remains in the reaction samples that used 10% w/w reagent to VX.

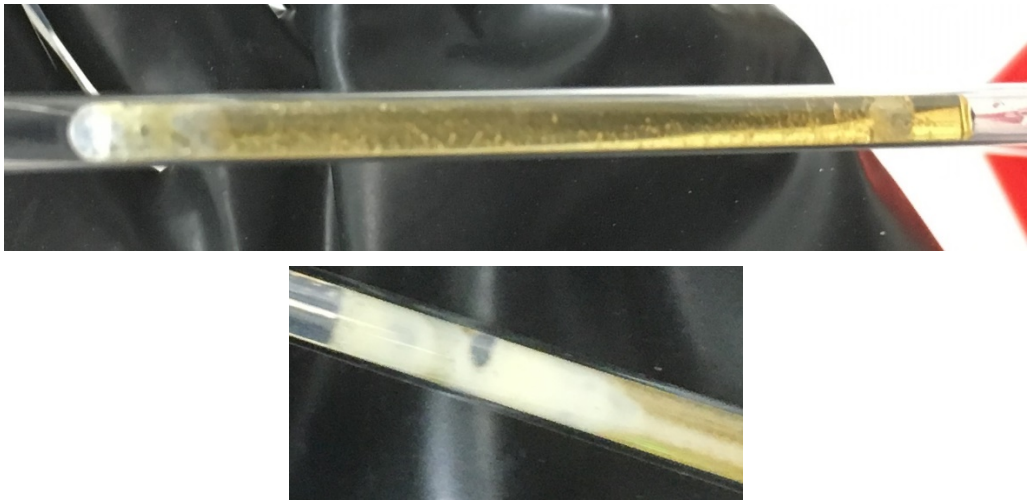

Figure 21. Reaction mixture in NMR tube of VX + $LiAlH_4$, sample nb097P103A. Top photo: solid powder reagent at the bottom of the NMR insert. Bottom photo: foaming liquid after agitation to mix the solid.

Figure 22. Reaction mixture in vial of VX + $LiAlH_4$, sample nb097P135A. After sitting for a week uncapped, the reagent absorbed enough water from the atmosphere to expand from about 0.15 mL to about 1 mL in volume, absorbing the VX.

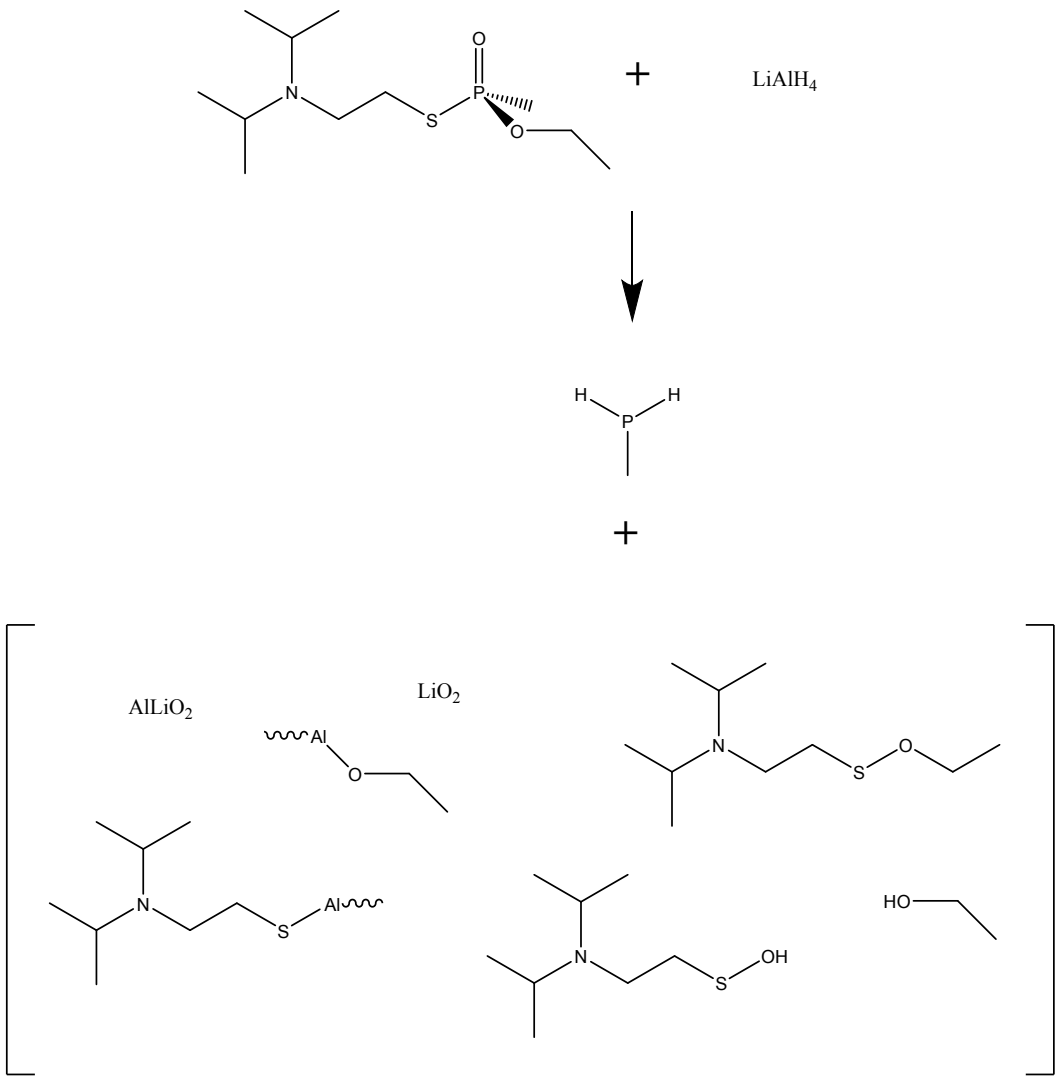

Figure 23. Proposed reaction pathway for $LiAlH_4$ + VX. Products in brackets are hypothetical.

Subtask 4.2: Validate VX Destruction Using Li_3N

Reaction of 19.8 mg Li_3N and 30 µL H_2O were done with 452 µL VX. The NMR solution gelled. The reaction mechanism is related to the reaction of GB. The spectrum using solution ^{31}P NMR is shown in Figure 24, showing some reaction products. The peaks are broadened because of the gelling of the liquid.

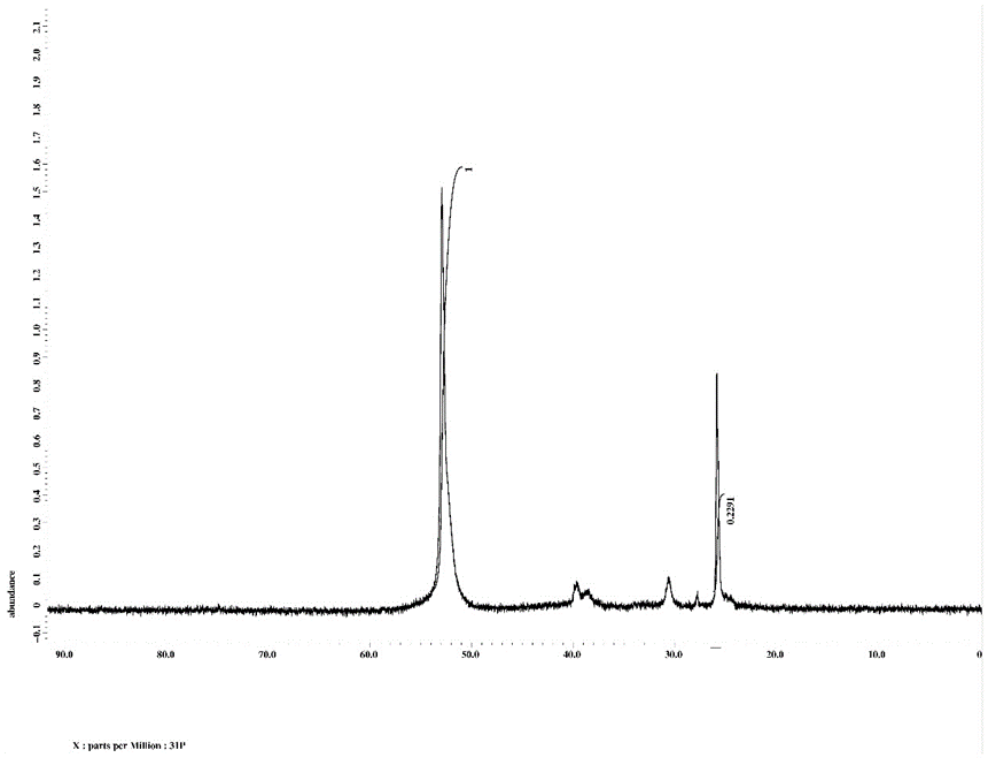

Figure 24. Solution ^{31}P NMR spectrum of VX reacted with Li_3N.

When combining 10% w/w Li_3N + H_2O to VX at total volume of 0.5 mL, only 45% destruction was observed after 4 days of reaction time. Figure 25 shows the inverted NMR tube revealing unreacted Li_3N (brown solid) at the top and a highly viscous VX mixture. With sufficient mixing in a larger container, it is anticipated that the 10% w/w quantity would achieve greater than 45% destruction.

Figure 25. Reaction mixture of VX + Li_3N + H_2O, sample nb097P103B.

Task 5: Large Scale Live Agent Testing

Subtask 5.1: Validate GB at Large Volumes

Reactions with $LiAlH_4$

A reaction with a 5 mL quantity of GB was vigorous enough to react most of the 0.5 g pellet of $LiAlH_4$, although there was still unreacted reagent that was visible in the reaction vial. During reaction, if the cap was removed from the vial, periodic flames and flares of the flammable gas (methyl phosphine) were observed. The reaction mixture formed a viscous brown paste with the GB, shown in Figure 26. The amount of GB remaining was 26% after two days, and 23 wt% after a week. Increasing the amount of $LiAlH_4$ is expected to decrease the amount of GB after similar amounts of time.

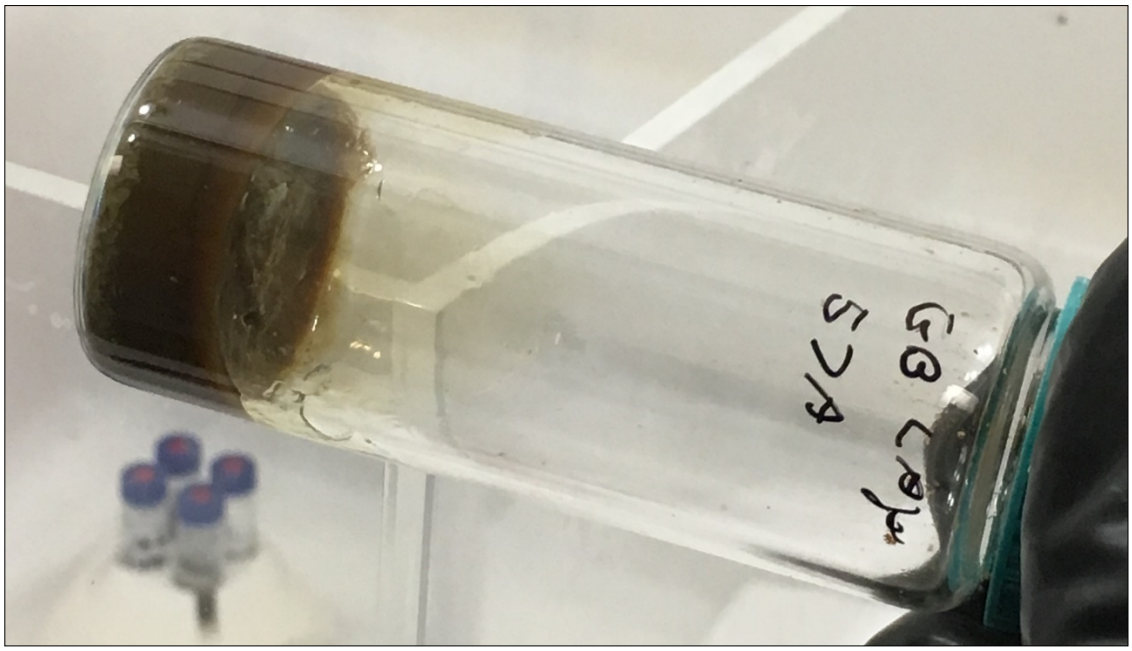

Figure 26. Reaction Mixture of GB + $LiAlH_4$, sample nb0018P57A, after 2 days of reaction. The amount of GB remaining was 26%, measured relative to an internal standard added by weight to a subsample of the mixture prior to analysis.

Because of the generation of flammable gas from $LiAlH_4$, milder reducing agents were tested. Reactions were done using $LiBH_4$ (sample NB0018P103C) and $NaBH_4$ (sample NB0018P103D) reacted at 10% ratio with 1 mL of GB. Some fizzing was observed, but there were no flames above the vials. For both, a wet slurry was formed that was not completely solid. After 8 days of reaction, the amount of residual GB was 7% for both $LiBH_4$ and $NaBH_4$ reactions.

Reactions with $Li_3N + H_2O$

GB was reacted with $Li_3N + H_2O$ at 5 and 10 mL volumes. For a 10 mL volume of GB (sample nb0018P89A), and a ratio of 9.1 wt.% Li_3N and 4% H_2O, the mixture forms a solid brown mass in about 4 hr. The residual amount of GB is 16% in 4 hr., and 9% after 5 days. The mixture is shown in Figure 27 after 4 hr. When water was added to the mixture of GB + Li_3N, there was bubbling and the temperature went up to 65°C. The heat was due to reaction of water with Li_3N.

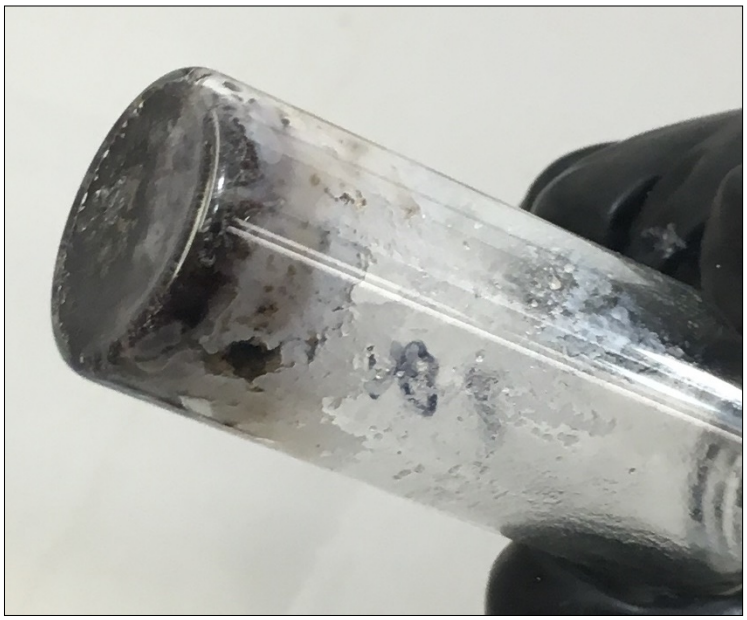

Figure 27. Reaction mixture of GB + Li_3N + H_2O, using 10 mL GB, 9% Li_3N and 4% H_2O, after 4 hr reaction time.

This reaction appears to be effective in forming a solid product. The reaction has visible excess unreacted Li_3N, although we cannot determine how much. Further studies were done to minimize the solid reagent. Optimization on small scale (1 mL) reactions indicates that the minimum amount of Li_3N reagent that can be used to decontaminate the GB is 5% Li_3N with 10% (excess) H_2O. However, repeated runs have shown variation in the amount of solidification using this amount of reagent. For two replicates with almost identical amounts of reaction, one completely solidified and the other only partially solidified, Figure 28. A similar problem has been observed for GD reactions.

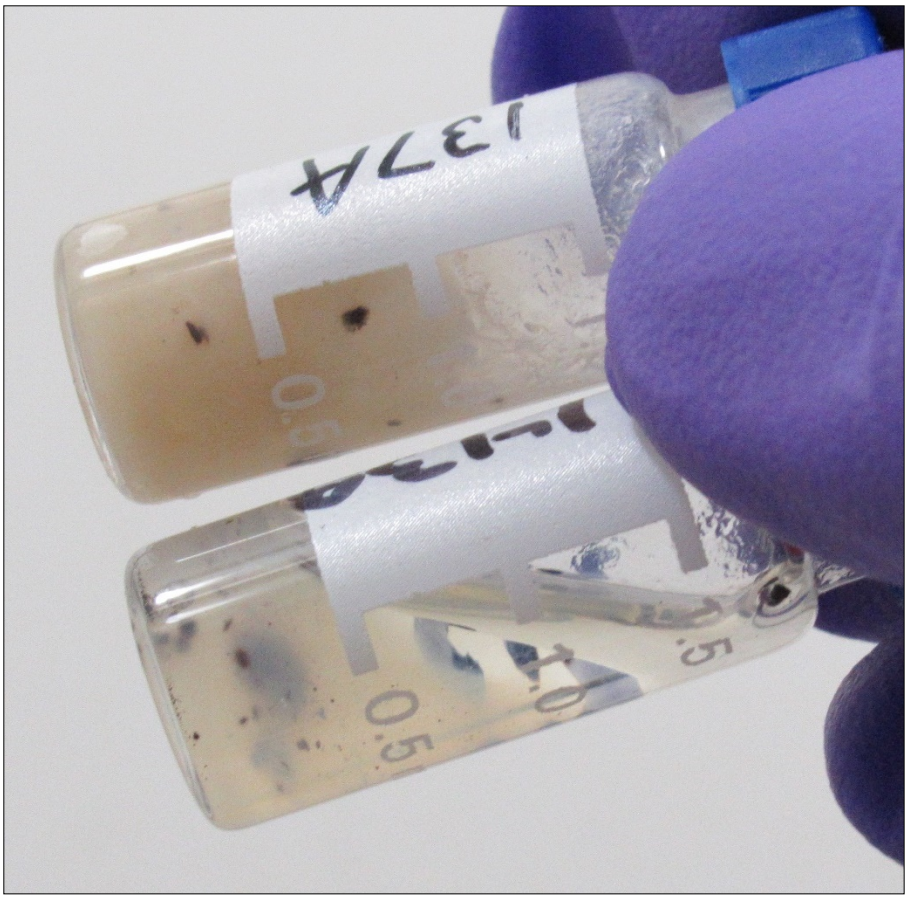

Figure 28. Reaction vials of GB + 5% Li3N + 10% H2O (samples 137A and 143A) showing one vial contents have solidified, and the other has not.

As a result, before a 100-mL reaction was done, we refined the reagent composition to have more assurance that the product proceeded as expected. We added the Li_3N reagent as a pellet rather than a powder so that the handling was simpler. This effort included testing different pellet formulations to determine whether the pellet broke up during the reaction so it was entirely consumed. This effort is described in Task 6.

A reaction run was begun with 100 mL of GB and the same ratio of Li_3N and water (10 mL water and 5 g Li_3N pellets). In this case, the water was added first before the Li_3N to avoid local exothermic reactions of the water coming into contact with Li_3N before it was mixed in the GB. This change in procedure was also due to the DF reaction study, for which water reacted energetically with DF without Li_3N being present.

For the GB reaction, a vigorous reaction was not observed, either with water or Li_3N. The temperature rise of the reaction mixture was not higher than 35°C. GB was reacted to less than 2% of the starting material in 6 days (Figure 29 left). The formation of partly solid product was observed, but it proceeded much slower than the reaction. The reaction product was not completely solid even after a month. It is possible that the delay is due to the length of time that it takes for the pellets to react.

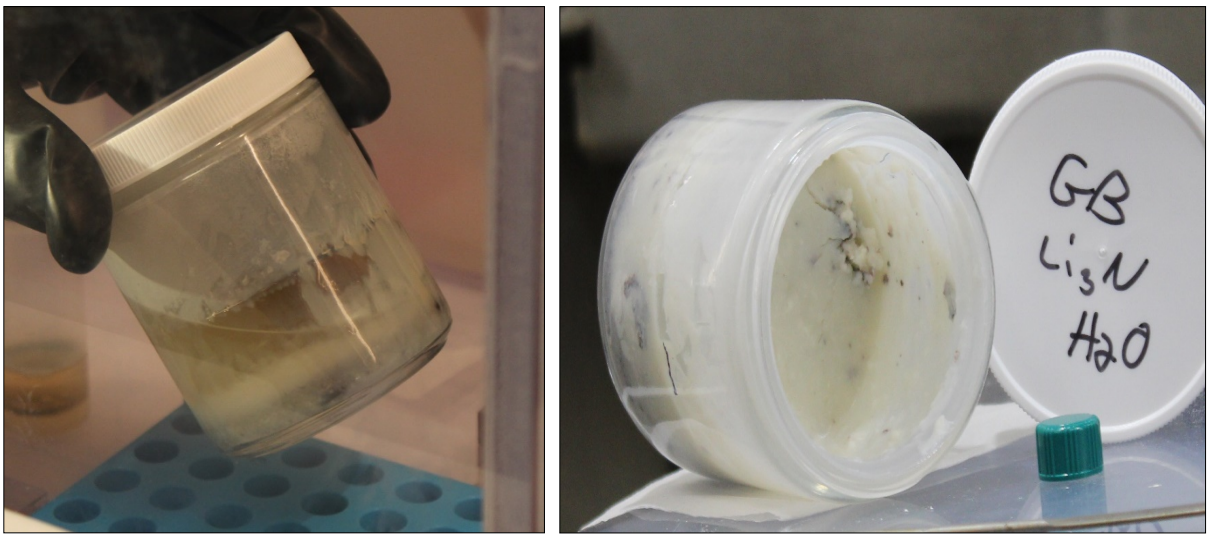

Figure 29. Left: Reaction Mixture of 100 mL GB with Li_3N + H_2O, after 6 days. The amount of residual GB is 2%. Right: Solid product after addition of another 1 mL of water and 0.5 g Li_3N.

Video and still photos were taken to document the reaction. Studies to analyze the chemical composition of the reaction product were done when the reaction went to completion. In order for full solidification to be observed, shown in Figure 29 right, it was necessary to add another 1 mL of water and 0.5 g Li_3N with stirring of the product mixture.

Because of the surprising lack of complete solidification of the products for the GB reaction with the original amount of reagents, additional studies were done using dimethyl methylphosphonate (DMMP) as a simulant for GB. DMMP is easily obtained commercially, and it is much less toxic, so it is easier to perform multiple tests compared to GB. DMMP is much less reactive to hydrolysis, so initial small-scale studies were done to show that solidified products were formed with this simulant. Measurements of the products showed that DMMP hydrolyzes to a small extent (25-50%) but most of the ^{31}P-containing extractable product remains DMMP, a liquid. This result indicates that it is not necessary to use a CA to form the solid, and the acid product GB acid (or a salt of it) is not a necessary component of the solid. It now appears likely that the solid is mostly LiOH and possibly an ammonium salt that has expanded in volume to absorb or incapsulate the liquid.

Several different reaction conditions were studied with DMMP to study the solidification process: 1) The method that has been used previously was to add Li_3N powder or pellets to CA first, followed by slow addition of water using a pipet or syringe. 2) Add Li_3N first, followed by fast addition of water by quickly adding in the measured amount without mixing, which could form a local high concentration of water at the surface. 3) Add water first, mix so the liquid is homogeneous, followed by addition of Li_3N powder. (This method seemed preferable for reaction of DF as the CA.)

Method 2 was the best method for causing rapid and complete solidification, but the water was added rapidly enough that it caused boiling at a temperature of 90-100 C. Stages in the reaction are shown in Figure 30 and Figure 31.

Figure 30: Photos from sample P55B. Left: Add Li3N to 100 mL of DMMP; Middle: Add 10 mL water with a pipet; Right: mixture is boiling after 20 min. of reaction time.

Figure 31. Final product for sample P55B. This order of addition caused rapid reaction, and the sample completely solidified in a few minutes.

From a test on a 10 mL volume of DMMP, method 3 was slow, so it was unexpected that method 3 was very fast and vigorous using a test volume of 100 mL. Also unexpectedly, the solid did not completely and rapidly solidify. The fast reaction may have been due to clumps of powder adding to the liquid quickly. A video of the reaction was taken. As a result, it was concluded that this kind of addition order was very unpredictable and it could produce excessive heat but also incomplete solidification. This method had been eliminated for the present.

Method 1 or adding Li_3N as tablets: The methods produce slower reactions, but often the reaction was incomplete since the tablets either do not break up or else the tablets or powder settle to bottom and do not react effectively with the added water. It appears that a layer of hydroxide product can cover the unreacted Li_3N to prevent the solidification reaction, even if there is enough hydroxide to decontaminate a CA like GB. This can lead to incomplete solidification.

Adding water rapidly to CA after Li_3N was suspended in it can lead to very fast reaction and vigorous boiling. Determining the optimal addition rate for larger volumes of CA may require a metering pump to control the engineering problem of addition of solid to water in a controlled, nonhazardous way. This problem was not anticipated or considered before. Mixing by diffusion of large volumes of reagents is much slower than small volumes.

Another alternative that was considered was to use capsules to contain the Li_3N powder. Two types of empty capsules were purchased. Vegetarian capsules (made of cellulose) dissolved in 5 mL DMMP/water and had a reaction to solidify the product, shown in Figure 32 left. A capsule made of gelatin did not dissolve under the same conditions and no reaction was observed, shown in Figure 32 center.

Caustic solution (10% NaOH) can be used instead of water to form a solidification reaction, shown in Figure 32 right, which may slow down the reaction of water with Li_3N and help to decontaminate the CA, although reaction kinetics was not measured.

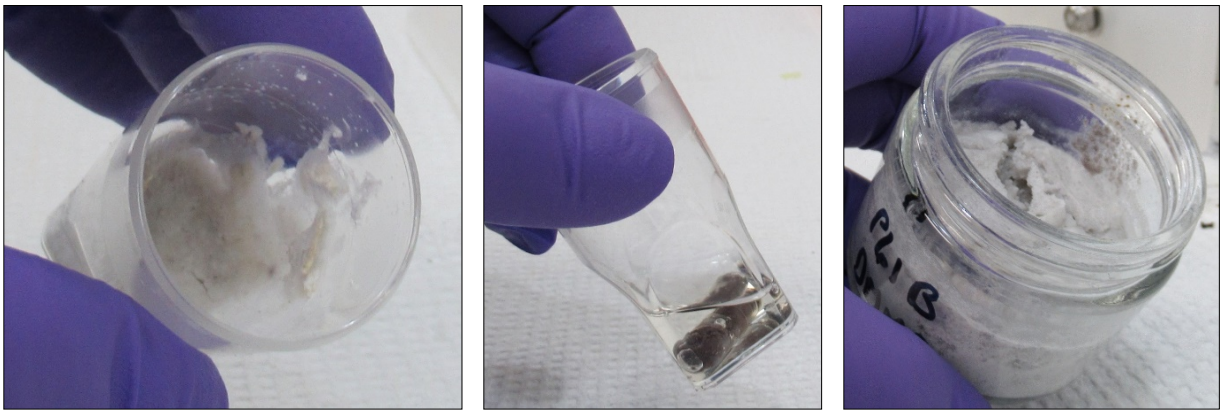

Figure 32. Reaction samples of DMMP with $Li_3N + H_2O$ with different conditions. Left: Vegetarian capsules (made of cellulose) dissolved in DMMP/water and had reaction to solidify the product. Center: Gelatin capsule did not dissolve under the same conditions and no reaction was observed. Right: Caustic solution (10% NaOH) can be used instead of water.

Additional experiments, including a reaction using 1 L of CA, were performed. Water was added to the DMMP and mixed via swirling the reaction chamber. Tablets were then added to the chamber. Addition of water to DMMP before addition of Li_3N can lead to vigorous reaction and sparking, if the water is not well mixed. Videos of the experimental trial was recorded. Figure 33 shows the reaction vessel for the 1 L DMMP reaction.

Figure 33. Reaction vessel for 1 L reaction of DMMP. After addition of the reagents, the temperature and pressure in the sealed steel container increased, shown by the pressure gauge on the right. The pressure eventually rose higher than 13.6 atm (200 psi), and the temperature of the outside was 171°C.

This trial is essential to demonstrate reaction conditions that are safe for a GB reaction. There should be conditions that can lead to a "middle ground" reaction, which does not generate excess heat and pressure but which completely consumes the Li_3N and forms a solid product.

Another series of experiments was a study of the effect of density of the aqueous solution. Since the densities of CA liquids varies from near the density of water to higher than water, the water

can remain on top of the CA in a layer. By adding salt to the water, the aqueous reagent becomes dense enough to sink. Since the Li_3N pellets also tend to sink, it was proposed that the reaction could be controlled by adjusting the density of the water phase with saturated NaCl. Alternately, by adding KOH to the water, it would become denser and possibly less reactive with Li_3N. Several reactions were done to test these ideas with CA and simulants at CBC and Sandia. The advantages of these modifications are not simple for the purpose of controlling the reactivity. The issue of bringing powder or pellets of solid into contact with liquid water reagent was discussed in a technical report. The extra requirement of adding salt to the water reagent adds an extra burden on field operations. The goal of the project was to keep the method preparations and required reagents to the minimum amount. However, it is clear that keeping the most simple and flexible approach leads to a wide variation in the rate and extent of reactions. If there is a constraint on the amount of time that is needed for reaction to take place, then further studies on the requirements for the reagents and preparations steps will be needed.

We solicited feedback from potential users of this technology at the CBOA 21 User Feedback for Technology Concepts, held on 25-26 May 2021 at the Joint Expeditionary Base Little Creek-Fort Story (JEBLCFS), VA. The feedback gave us a better idea of the range of conditions that the users might be comfortable with, depending on the applications that are required. The technology was given the acronym QILIN, "Qualitative Inactivation using Lithium Nitride," for CBOA 21. (A qilin is a mythical Chinese animal.) In general, comments from interested potential users indicated that the users would prefer a method that required little training and minimal logistical burden on warfighters. They expressed an interest in this approach for handling found CA materials, since the alternatives that are currently available include doing nothing, transporting the materiel, or blowing up the materiel, particularly munitions, with explosives.

A 1 L reaction of GB will be done at the Chemical Transfer Facility (CTF), since their facility is approved for handling liter quantities of CA. Funding for this operation was transferred to CTF before the end of the project. The study was delayed due to COVID restrictions and due to further laboratory studies to make sure that the reaction can be done safely on this scale. A stepwise procedure was developed for the operators. The Standard Operating Procedure was under review from safety officials. The results will be included in a future technical report from CCDC-CBC.

Subtask 5.2: Validate VX at Large Volumes

Reactions with $Li_3N + H_2O$

VX was reacted with $Li_3N + H_2O$ at 10 mL volume. For a 10 mL volume of VX (sample nb0018P85B), and a ratio of 9 wt.% Li_3N and 3.5% H_2O, there was no visible sign of reaction. The mixture forms a solid brown mass but with liquid and VX remaining. The residual VX in the liquid layer was 47% after 8 days. Then an additional 0.5 mL (5%) of water was added. After 5 h, no liquid was observed to remain in the vial. After another day of reaction, the amount of residual VX was measured at 27 wt% in the upper grayish layer. After 5 days of reaction after the second addition, the residual VX was 14%. Photos of the reaction mixture are shown in Figure 34.

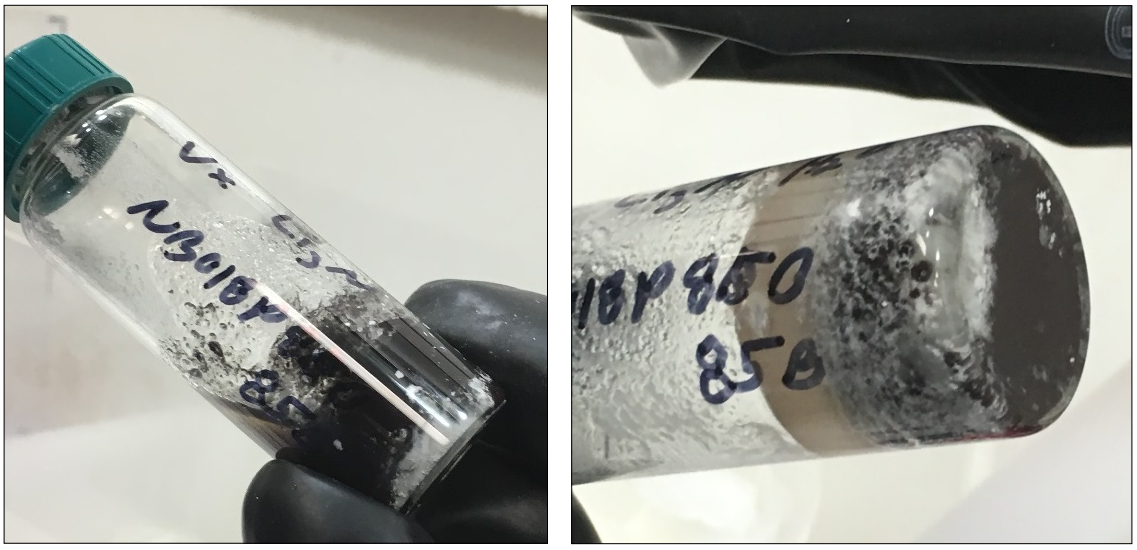

Figure 34. Reaction mixture of 10 mL VX + $Li_3N + H_2O$, using 10 mL VX, 9% Li_3N. Left: 3.5% H_2O after 5 days reaction time; Right: additional 5% H2O after additional 5 hr and manual stirring.

The reaction of VX with $Li_3N + H_2O$ was also done at 100 mL scale, using 102.5 ml VX, 8.06 g of Li_3N pellets received from Sandia on 2/25/19, and 10 mL of water. A series of photos was taken for time-lapse video, as well as regular speed video. The images were assembled by Sandia into a video of the reaction as it progressed. The photo of the reaction mixture after 12 days is shown. The mixture has completely turned to solid material, Figure 35.

Figure 35. Solid reaction product formed from reaction of 100 mL VX with Li_3N + H_2O.

The solid material was studied to determine the composition. Current understanding is that solidification occurs by formation of an ionic solid of the reaction products, rather than by formation of a molecular polymer. The working hypothesis is that the solid is an ionic solid formed from the VX acid product with the amines from the VX thiol or VX disulfide reaction product along with amines formed from reaction of the Li_3N solid. The proposed reaction scheme is shown in Figure 36.

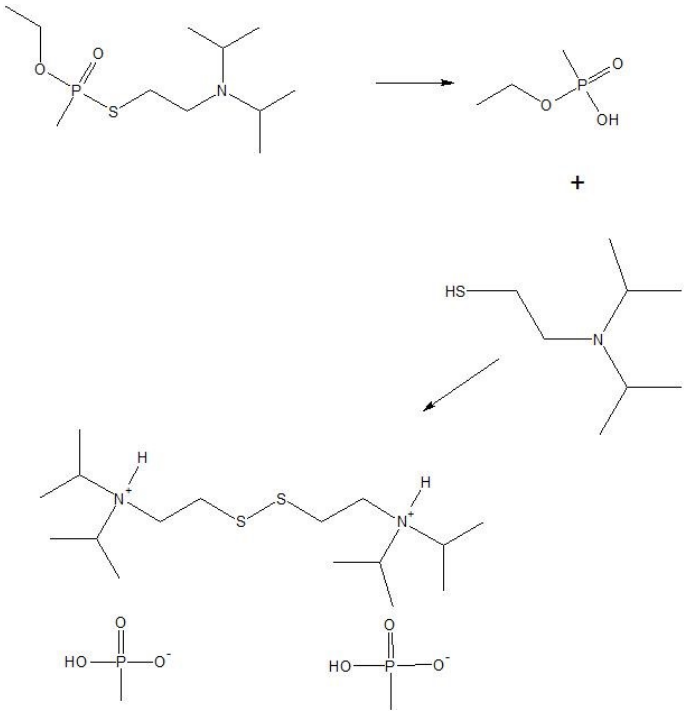

Figure 36. Reaction scheme showing formation of solid ionic products from VX.

The solid completely dissolved in dilute HCl but not in neutral water or chloroform. The solid was then re-precipitated by adding NaOH solution to the solution in HCl. The solid was rinsed and redissolved in dilute HCl. Liquid-phase NMR measurements of both of the HCl solutions indicated that the ^{13}C peaks (Figure 37) that are observed are the same and are consistent with VX acid and VX disulfide.

As a result of these measurements, we conclude that the weight of evidence is that the solid is an ionic precipitate of the reaction products, rather than any type of polymerization or permanent insoluble material. However, these products cannot be reformed into VX, so it is reasonable the material has been significantly detoxified. Approximately 6-7% of the solid is in the form of EA-2192 even after sitting for several months. EA-2192 is a toxic decontamination product of VX that is nonvolatile but is water soluble and toxic through ingestion or injection. Theoretically, the EA-2192 could be separated from the other solid material and purified, although we do not have a separation method that could accomplish that task.

This reaction indicates that the best general kind of approach for the project is to find a reagent that forms an insoluble product in solution with the CW agent. A small amount of reagent is added to the CW agent, and the product that is formed crystallizes out of solution. This reduces back reaction, and it allows the CW agent to continue reacting to completion. The worst kind of reaction, for this project, would be one in which the product tends to encapsulate the agent and stop the reaction from proceeding, either by separating the reagents or by increasing the viscosity. VX may be a particularly favorable kind of agent, because it has a molecule with both acid and amine groups.

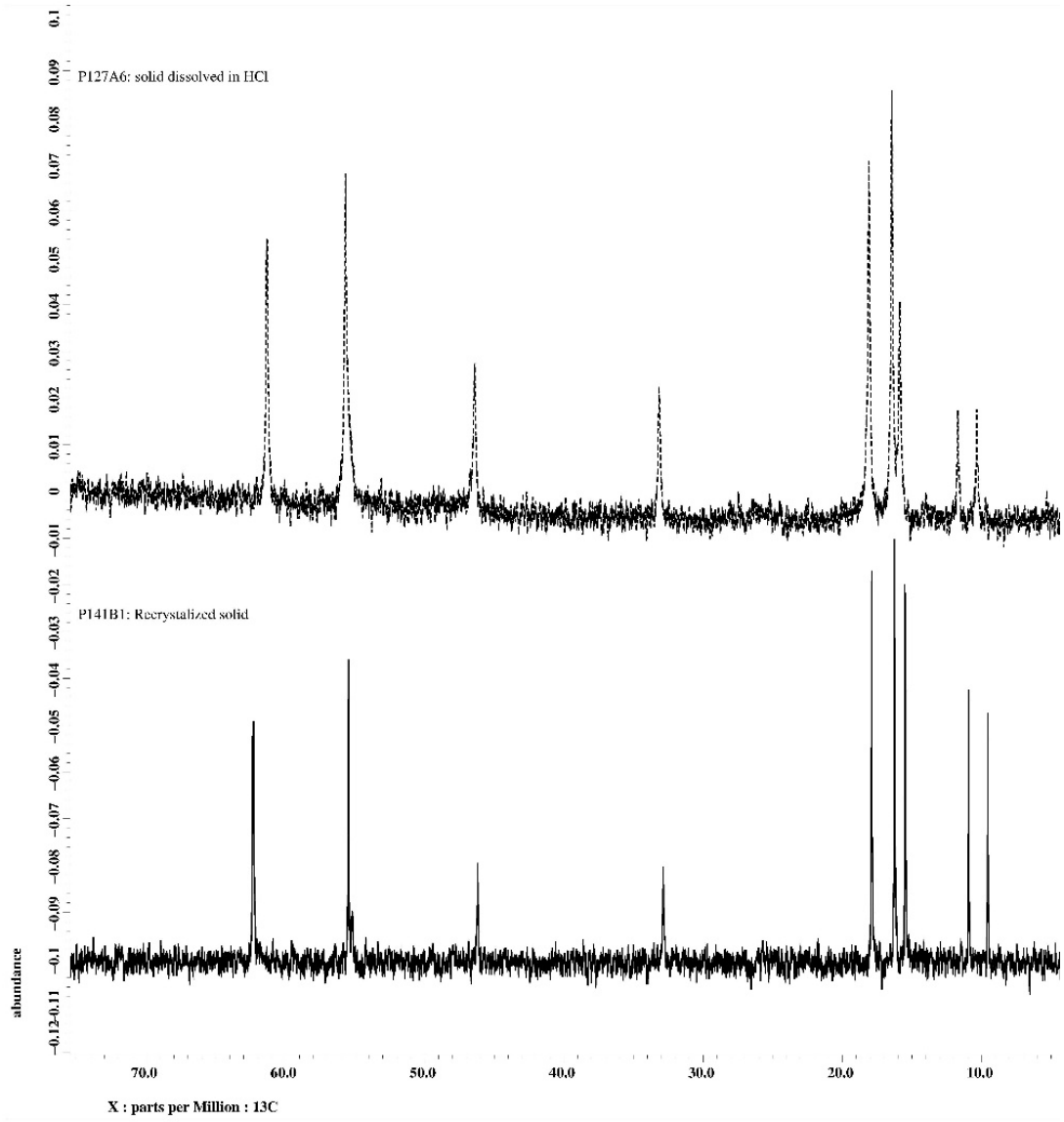

Figure 37. C-13 NMR spectra of VX solid product, dissolved in dilute HCl solution. Top: first solution; Bottom: after recrystallization and rinsing.

Results of work to characterize the solid material were written in a separate report that included NMR (^{13}C and ^{31}P spectra), Liquid Chromatography/Mass Spectrometry, and Raman spectra. The report is D.J. McGarvey, W. R. Creasy, and M. K. Kinnan, *Characterization of Solid Reaction Products from the Reaction of VX with Li_3N+H_2O for the Tactical Disablement Project*, CCDC CBC Technical Report No. CCDC CBC-TR-1635, Aberdeen Proving Ground Edgewood Area, Feb. 2020.

Subtask 5.3: Validate HD at Large Volumes

Based on the limited success with the sesquahalide chemistry discussed previously, HD was reacted against $LiAlH_4$ and $Li_3N + H_2O$. A number of other reagents were also tested.

Reactions with $LiAlH_4$

When a $LiAlH_4$ pellet was added to HD, a small amount of micro bubbling was initially observed. There was no heat or evidence of a strong reaction. When the reaction mixture was sampled, no reaction products were observed. Quantitation of the HD relative to an internal standard showed that 85-90% of the HD that was added was still present even after 49 days of reaction (sample nb0018p65B, Figure 38). We conclude that the HD was not reduced or reacted by the reagent. However, when the vial sat with the cap off, the $LiAlH_4$ likely reacted with water from the atmosphere and expanded to absorb the HD in a gray or white paste (Samples nb097p143B, nb0018p65A, nb0018p65B). The chunks of $LiAlH_4$ were gone. The brownish color of the original HD faded, indicating that the compound that caused the color was reduced. As a result, the agent was converted into a viscous solid in these conditions, but the toxicity was probably not decreased since there was no apparent reaction with the HD.

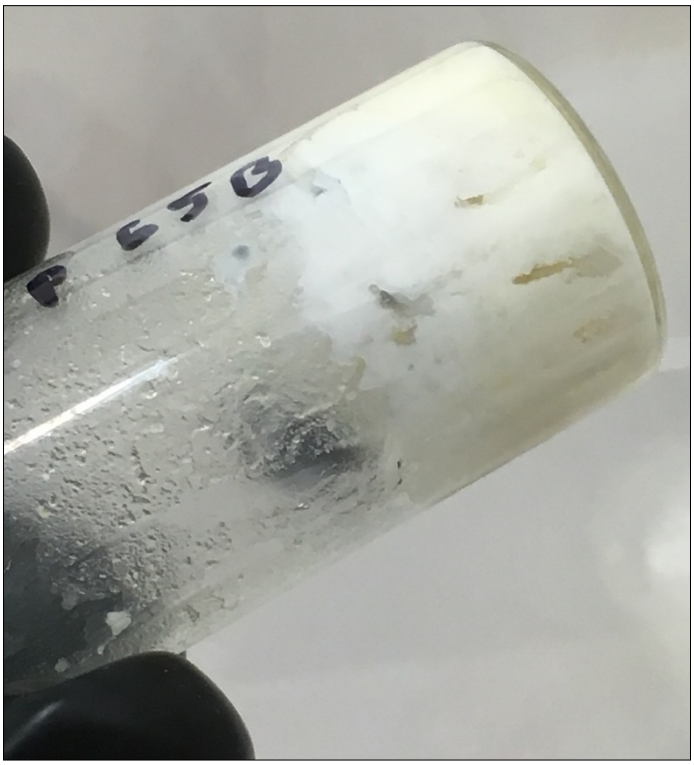

Figure 38. Reaction mixture of HD + $LiAlH_4$, sample nb0018P65B, using 5 mL HD and 0.9 g $LiAlH_4$ (14.5 wt%). After standing for a week uncapped, the reagent expanded to absorb the HD to form a paste.

An HD reaction was done with $LiAlH_4$ that was purchased as a solution in tetrahydrofuran (THF) solution at a 2.0 M concentration (Sample nb097p143A). This solution was miscible with HD, so no solids separated. There was no evidence of reaction, except that the color of the HD faded, shown in Figure 39, and no reaction products were observed in the NMR spectrum.

Figure 39. Reaction mixture of HD + $LiAlH_4$ in THF solution (right, sample nb097P143A), compared to the original HD (left), showing that the reagent removed the color.

Reactions with $Li_3N + H_2O$

When HD was added to Li_3N solid with no water, no reaction was observed. When water was added, there was heat and pressure due to reaction of the water with Li_3N. When the reaction was sampled for quantitation, there was still 80 wt% of the original HD left and no reaction products were observed.

However, for one of the reaction runs (nb097p89B), the reaction mixture reacted rapidly and formed a charred black solid mass with 36% w/w reagent, shown in Figure 40. No reaction products were extracted from the residue and no HD was extracted either. It is possible that the $Li_3N + H_2O$ reaction was hot enough in this case to cause reaction or evaporation of the HD. When repeating the reaction at lower quantities (22% w/w) of reagent, the reaction did not proceed as previously observed (Figure 41). We have not been able to identify the conditions and reproduce this kind of reaction. Since the water did not dissolve in the HD, it may have reacted more vigorously with the reagent powder as they both floated to the top of the HD. It is also possible that the H_2O was added faster to this sample. It is not clear what caused the reaction with the HD to form charred residue, and it does not seem that it can be done reproducibly.

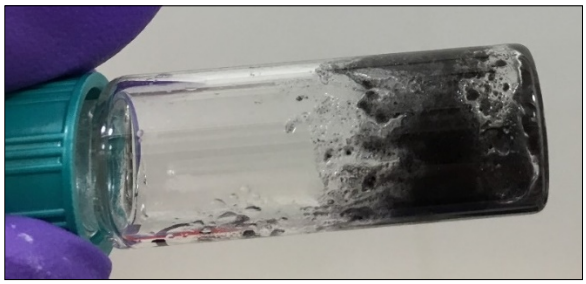

Figure 40. Reaction mixture of HD plus $Li_3N + H_2O$ (36% w/w), sample nb097P89B.

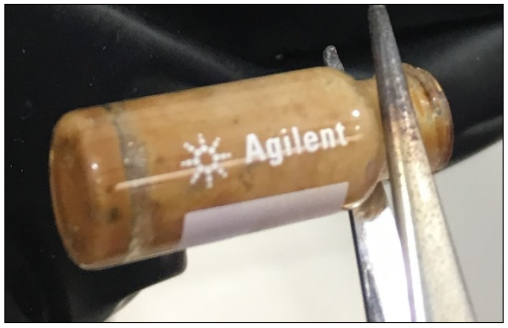

Figure 41. Reaction mixture of HD with $Li_3N + H_2O$ (22% w/w), sample nb097P143D.

Studies were done using 10% of H_2O as a reagent and 20-30% propylene carbonate as a cosolvent. The reaction mixture formed some solid, and the liquid appeared to be a single layer. However, a considerable amount of HD was unreacted, so the reaction did not go to completion.

Experiments were done using Li_3N pellet with an aqueous solution of Fe(II) acetate as a catalyst. Another experiment was done using Li_3N pellet with triethanolamine as a multifunctional alcohol. (See simulant study in Subtask 6.3.2.2.).

Other Reactions

Although both $LiAlH_4$ and $Li_3N + H_2O$ met the limited goal of forming a solid reaction product, neither of them were effective at reacting with the HD to decrease the toxicity. As a result, we did a survey of other possible reagents at a number of ratios. See Table 6.

Table 6. Reagents surveys to look for reactivity with HD.

Primary Reagent	Wt. Ratio to HD	Secondary Reagent	Vol. Ratio to HD	Sample No.	Residual HD percent, days of reaction
Mg-Al Turning/Powder	4%	THF or THF/$CuCl_2$	8%	NB0018P19C, NB0018P19D	No major reaction prod. after 14 d
HTH solution[a)]	8%			NB0018P75A	90% after 26 d
STB[b)]	8%			NB0018P75C	93% after 28 d

STB[b)]	8%	THF cosolvent	20%	NB0018P75D	81% after 28 d
$Fe_2(CO)_9$[c)]	10%			NB0018p99A	No reaction prod.
Fe(II) acetate[c)]	10%			NB0018P99C	No reaction prod.
Fe(II) sulfate[c)]	11%			NB0018P99D	No reaction prod.
$NaMoO_4$[d)]	12%			NB0018P99B	No reaction prod.
$NaOCH_3$[e),f)]	35%			NB0018P99E,	30% after 9 d
$NaOCH_3$[e)]	24%	MeOH	10%	NB0018P101B	55% after 6 d
$NaOCH_3$[e)]	55%	MeOH	15%	NB0018P101C	12% after 6 d
Li metal[e)]	7.6%			NB0018P101A	90% after 30 d
Na metal[e)]	7.9%			NB0018P107A	92% after 17 d
Na metal[e)]	7.9%	Heat to 160C		NB0018P107A	71%
$LiBH_4$[e)]	8.3%			NB0018P101D	100% after 2 d
HTH solid	20%	Propylene carbonate	20%	NB0018P123C	48% after 2 months
$NaOCH_3$[e)]	30%	Propylene carbonate	20%	NB0018P123B	30% after 2 months
Li metal in ethylene diamine	10%			NB0018P139B	90% after 1 month

a) HTH is $Ca(OCl)_2$ in water

b) STB is supertropical bleach, $Ca(OCl)_2$ and NaOH in water

c) Fe(II) compounds were added to attempt to form HD Heel, a solid found in many stored ton containers of HD

d) Possible oxidizer

e) Possible reducing agent

f) Reagent was added incrementally over several days to a total of 35%.

Almost all of these reagents were surprisingly unreactive. That includes HTH (high test hypochlorite, or $Ca(OCl)_2$ in water), STB (supertropical bleach, or $Ca(OCl)_2$ and NaOH in water), and Na metal. (Reaction of HD with Na metal was rapid only when it was heated to 160 °C, above the melting point of the metal.)

The most promising reagent was $NaOCH_3$, which showed reaction and formation of a solid residue. A photo of the reaction mass is shown. However, the reaction requires a larger amount of reagent than the target amount, 68% by weight. For 24 wt%, the amount of residual HD decreased to 55% after 6 days. For 55 wt%, the residual HD decreased to 12% after 6 days, (Figure 42).

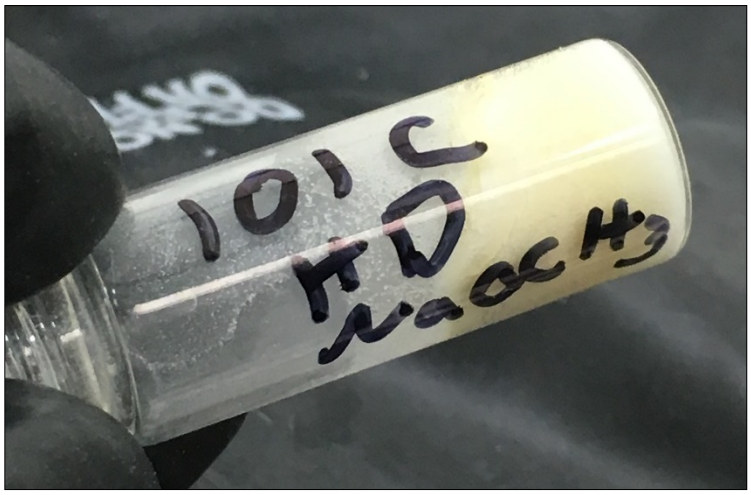

Figure 42. Reaction mixture of HD with $NaOCH_3$, 55 wt% ratio. The photo was taken after 2 days of reaction time, and there was still 88% residual HD. After 6 days of reaction time, the residual HD was 12%.

We hypothesize that the reactions do not occur for most of these reagents because of unfavorable solvent affects in the presence of pure HD. The reactions are expected to proceed by formation of a three-member sulfonium ion intermediate, and this ionic intermediate is not stabilized in the nonpolar HD.

Since the reactions had limited success, HD reactions were studied with a polar solvent added. The presence of a polar solvent may stabilize the sulfonium ion intermediate, which could speed up the reaction. Reactions were done using the solvent propylene carbonate. Reagents were $Li_3N + H_2O$, $NaOCH_3$, HTH ($CaOCl_2$), or $NaMoO_4$. Results are included in Table 6. The cosolvent improved the reactions to a small extent, but not enough to meet the project goals.

Another small-scale reaction study of HD was done with the reagent tetrakis(dimethylamido) titanium (IV), $[(CH_3)_2N]_4Ti$. Transition metals like Ti are heavier than the previous reagents that we have studied, but Ti has the advantage of being tetravalent and it is well known to form a variety of solid materials.

Using a mixture with 20% by volume (15% by weight to HD) of the Ti compound with HD and no water, a solid formed after two weeks and continued to become harder in 5 weeks (Figure 43). The reagent reacts vigorously with water, so water was not added. Most of the HD was still present, and there were no indications of reaction products, using a quantitative ^{13}C NMR analysis.

Even though this reagent did not destroy HD, it may be worth pursuing this reagent or other similar reagents to look for one that reacts with HD. Similar tetravalent compounds can be purchased with hafnium and zirconium, as well as titanium compounds such as $Ti(OCH_3)_4$.

Figure 43. Reaction of HD with [(CH3)2N]4Ti, sample NB0049P17A after two weeks of reaction time.

Subtask 5.4: Validate GD at Large Volumes

Reactions with $LiAlH_4$

The GD sample bubbled when $LiAlH_4$ was added. After two weeks of reaction, there was still 93% of the GD remaining relative to the acid product. A small peak of the volatile CH_3PH_2 was observed and disappeared over time from the NMR spectra due to evaporation from the reaction mixture. Chunks of the reagent remained unreacted, shown in Figure 44. The sample did not become noticeably viscous.

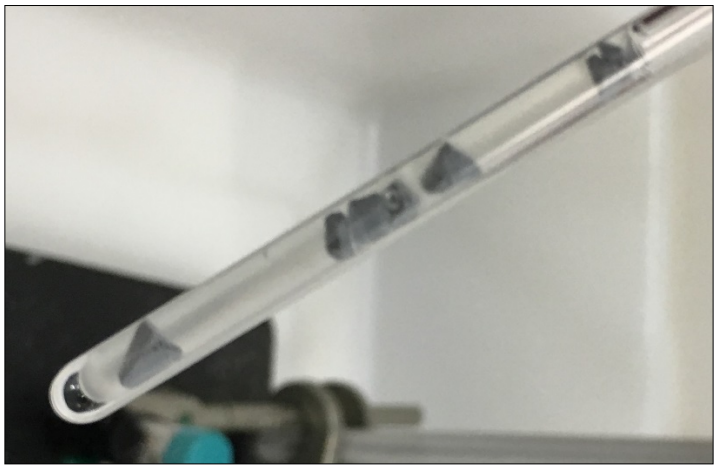

Figure 44. Reaction mixture of GD + $LiAlH_4$ in an NMR tube, sample nb097P141A. The chunks are unreacted LiAlH4 after 4 days.

Reactions with $Li_3N + H_2O$

Two similar samples were run with GD. After a week of reaction time, the residual amount of GD fell to 0.2% and 4% after 8 days of reaction, and the sample became cloudy and more viscous.

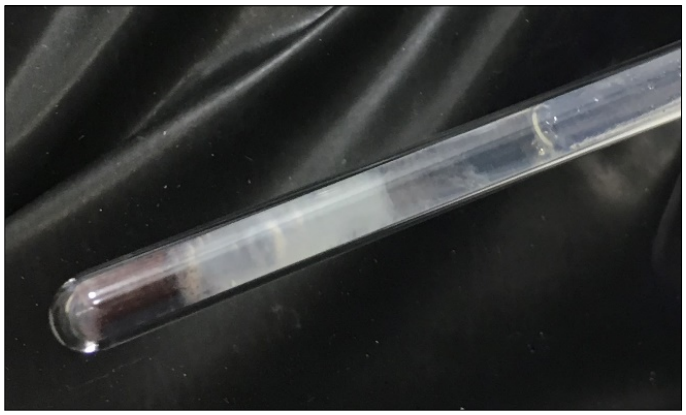

Figure 45. Reaction mixture of GD + $Li_3N + H_2O$ in an NMR tube, sample nb097P149A. Brown solid is unreacted Li3N. Cloudy region is gelled, viscous material.

A reaction with 10 mL of GD was done to validate the result on a larger volume. A similar result was observed using 9 wt% Li_3N and 4 wt% H_2O. The reaction mixture is shown in Figure 46. The sample was solidified after 3 hr, and the amount of residual GD was not detectable after 1 day of reaction (<1%).

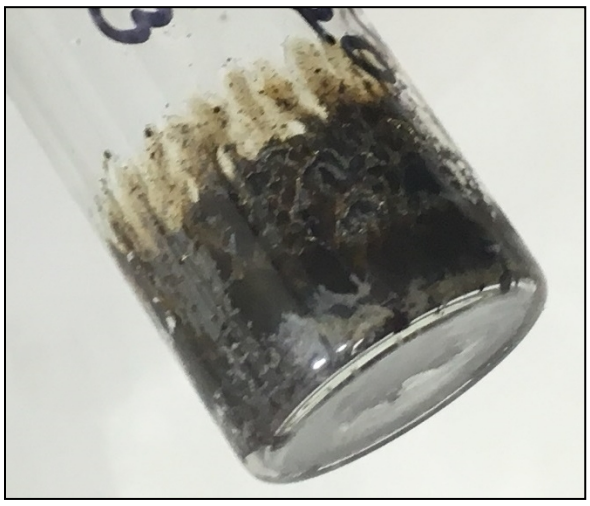

Figure 46. Reaction mixture of 10 mL GD + $Li_3N + H_2O$, using 10 mL GD, 9% Li_3N and 4% H_2O after 1 day of reaction time (sample NB0018P89B). The residual GD was below detection limits (<1%).

Reactions with GD are generally similar to GB. A 100 mL scale GD reaction was performed. For the reaction, 100 mL of GD was transferred to a glass jar, and 10 mL of water was added and mixed. Li_3N was added last in the form of 5 g of pellets made using Sandia's pellet press. This addition order and physical form of the Li_3N were done to keep the reaction rate slow to minimize hazards from rapid heat release and boiling. For this reaction, the rate was moderate and no boiling was observed, although there was some fog or smoke formation. A video was recorded.

The reaction proceeded without closing the jar. Within two weeks, the residual GD was reduced to 2% as determined by quantitative ^{31}P NMR, indicating that the decontamination was effective. Some tablets of Li_3N persisted in the decontamination product, and they did not seem to completely react. The product was approximately 50% solidified. Additional aliquots of 3 mL of water were added for three successive weeks, for a total of 9 mL of water in addition to the first 10 mL addition. The additional water made little difference in the composition of the product, which remained at about 50% solid. Figure 47 shows the end reaction.

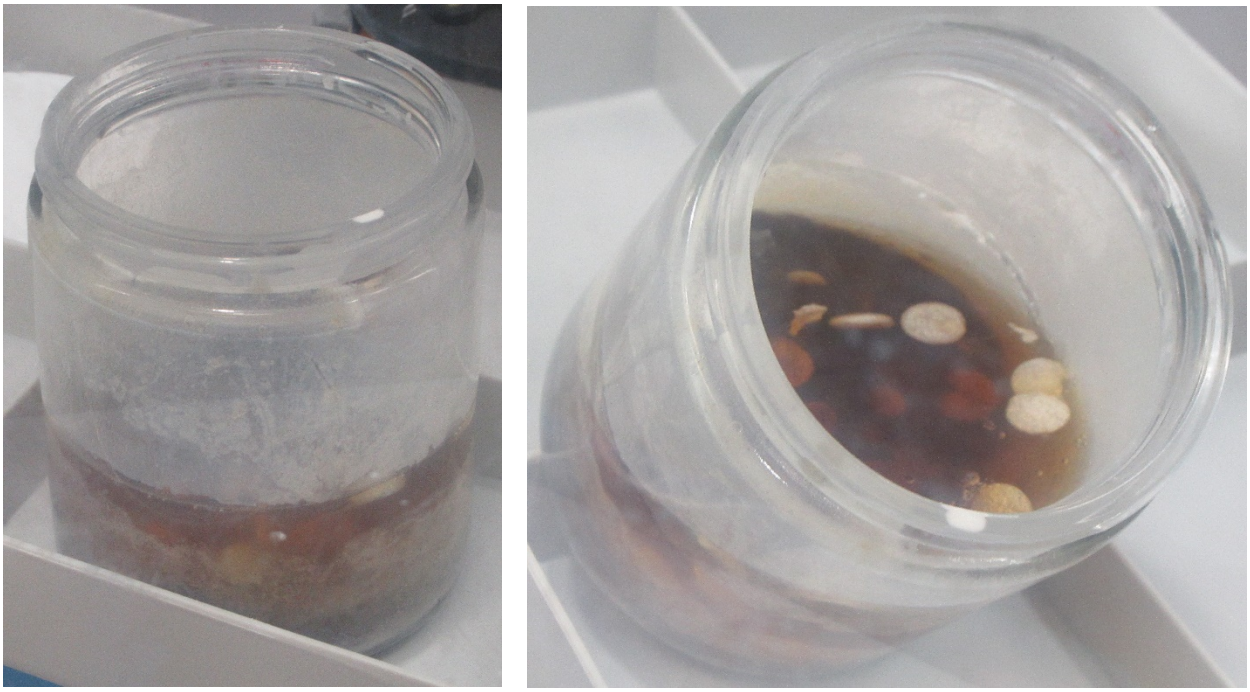

Figure 47. Reaction product of 100 mL GD + 5 g Li_3N + 10 mL water, with extra 9 mL of water added periodically, after 1 month total reaction time. Remaining, partially reacted Li_3N pellets are visible in the right photo.

It is not clear why the GD product failed to solidify, as the previous reactions of GB, DMMP, and VX did solidify. A more careful consideration of the amount of water that is needed for stoichiometric reaction was done. The ratio of 5 g Li_3N to 10 g water was developed on an empirical basis to obtain decontamination in smaller scale reaction studies and in an attempt to meet at target of 10% reagent to agent ratio and to use the same amount of reagent for all agents. The detailed calculation using this ratio is shown in Table 7.

The amount of water that is needed to neutralize the GD to GD acid (0.56 moles) is about the same as the amount needed to react with Li_3N (0.57 moles) to form $3LiOH + NH_3$. In ideal reaction conditions, the same water could serve both purposes, forming a Li salt of GD acid. (The product from reaction with ammonia has not been identified.) In this case, the volume ratio of additives to agent is 13.85%.

Under the worst case conditions, the reactions could compete so that water is needed for both neutralization of the CA and reaction with Li_3N. If enough water is added to complete both reactions, the volume ratio of additives to agent is 24.3%. For the reaction study, the initial amount of 10 mL water was added, but an additional 3 mL amount of water was added each week for three weeks to see if additional solidification was generated. Little change was observed with addition of more water. It is possible that addition of more water as a solvent will dissolve some of the solid, so more of the product remains liquid. As a result, there appears to be a trade-off between rate and amount of reaction and the amount of solidification.

In the actual reaction condition, it appears that the GD reacts preferentially with water to form GD acid, leaving some of the Li_3N unreacted after the GD has reacted to completion. It is possible that the only way for all Li_3N to react is by using a fine powder instead of pellets. The powder reaction presents additional hazards such as rapid heat generation and boiling, which was observed for the QL and DMMP reaction studies. For comparison, the reaction of 100 mL DMMP formed a white solid that appeared to have nearly complete reaction of Li_3N. This may be a consequence of the lower reactivity of DMMP with water, so the DMMP is less effective at competing for water compared to the CA.

It is not clear why the product GD acid is not forming a mostly solid product. Complete solidification has been observed, shown in Figure 46, for reaction with Li_3N powder that reacts faster. It is possible that the GD acid is less polar than GB acid, and the lower polarity decreases the solubility of the LiOH enough at the lower reaction temperature to decrease the formation of the salt product. It is possible that with longer reaction time or with heating, additional ionic product will form and precipitate, forming the solid.

Table 7. Calculated stoichiometry of the reaction of GD with Li_3N + water

CA	GD
Mass (g)	102.20
Vol (mL)	100.00
MW (g/mol)	182.17
Den (g/mL)	1.022
Decon Sites	1
Reagent	Li_3N
Mass (g)	5.00
Vol (mL)	3.85
MW (g/mol)	34.83
Den (g/mL)	1.3
Active Sites	3
Reagent	water
Mass (g)	10.0000
Vol (mL)	10.0000
MW (g/mol)	18.01528
Den (g/mL)	1
Active Sites	1
Moles CA	0.56
Moles H_2O for CA	0.56
Moles Li_3N	0.14
Moles H_2O for Li_3N	0.57
Total moles H_2O	1.14
Wt or vol. H_2O (g or mL)	20.45
% Vol Additives (for 0.56 moles water)	13.85
% Vol Additives (for 1.14 moles water)	24.30

Subtask 5.5: Validate Precursors at Large Volumes

Subtask 5.5.1: QL Studies

QL is chemically similar to VX, but it is in a more reduced state, since the phosphorus atom is in the P(III) oxidation state rather than the P(V) oxidation state. This chemical difference affects the best strategy to use for destroying the compound or making it unsuitable for use as a binary munition.

Reactions with $LiAlH_4$

Two runs were done with QL + $LiAlH_4$. One had 10% reagent, and the other had 5%. Slow reaction was observed when the reagent was first added. After 24 hours, there was clear pressure buildup in the vial and the mixture was becoming viscous. After a week of reaction time for the 10% vial (nb0018p49A), there was a steady flame over the vial when it was opened in air due to combustion of CH_3PH_2 with air. As the pressure released, there was foaming out of the top of the vial and formation of a dome from the dried foam. There was a solid gray residue from the $LiAlH_4$ that was too solid to pipet or pour, Figure 48.

For the sample with 5% $LiAlH_4$ (nb0018p49B), after a week of reaction time there was a gray slurry that could be stirred and appeared wet. There was not an open flame over the vial, but there was some foaming.

Treatment of QL with a reducing agent has advantages and disadvantages. Since it is already reduced compared to VX, it is easier to reduce further with less consumption of the $LiAlH_4$. There is probably more of the reduced product CH_3PH_2 compared to VX. (We were not able to accurately quantify the amount of the volatile product.) Even though this product presents a fire hazard, the methyl phosphine leaves the reaction mixture. An undesirable property of QL is that in normal contact with air or water it can oxidize to a number of P(V) compounds. This will increase the amount of $LiAlH_4$ required to convert to methyl phosphine.

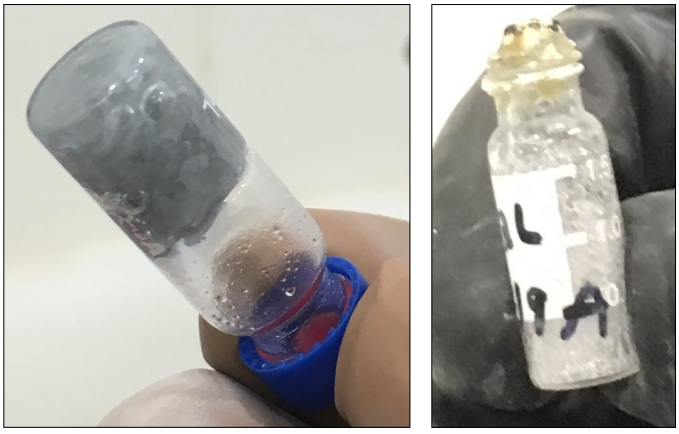

Figure 48. Reaction mixture of QL + $LiAlH_4$, sample nb0018P49A. Left photo: After one week of reaction time, with the vial tightly capped. Right photo: After 8 days reaction time, and after opening the vial so the CH_3PH_2 escaped and flared.

Reactions with $Li_3N + H_2O$

Two samples were done for QL + Li_3N. The first sample was without added water, and there was no sign of reaction. The second sample had $Li_3N + H_2O$. The mixture had bubbling and smoking after the H_2O was added. A white precipitate was formed but there was still runny liquid. QL was present in the liquid as observed by NMR, but an internal standard was not added so a percentage of QL remaining was not determined.

A study with 10 mL of QL was done for confirmation using 10 wt% Li_3N (sample NB0018P91B). Water was added incrementally. After 10 wt% of water was added, there was still 37% QL remaining. After 15 wt% water was added, the QL was undetectable. Further study is needed, but it is possible that the added Li_3N competes with QL for reaction with water, so using less Li_3N or even no Li_3N may reduce the amount of water that is needed for reaction with the QL. But the Li_3N is caustic, so it may also be needed to promote the reaction.

A reaction of 100 mL QL with 10 mL of water and 5 g Li_3N was performed. The reaction mass solidified after 2-4 weeks. Photos and videos were sent to Sandia and a video was produced. Product analysis is more complex than that of VX and it was difficult to determine a product quantitative composition. Photos of the reaction product are shown in Figure 49. The product analysis is discussed in a technical report.

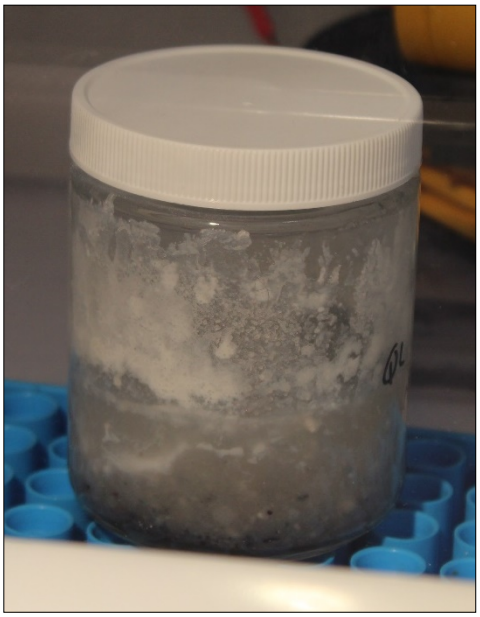

Figure 49. 100 mL reaction of QL with 10 mL water and 5 g Li_3N.

Reaction with H_2O

A previous study[10] showed that QL reacts with water, and this reaction can be used in decontamination. The prior study was done with a ratio of 1:5 QL:water.

A reaction study was done with 10% water in QL. The QL is not completely miscible with water, but it reacts at the interface. In 24 hours, most of the QL reacted with only 12%

remaining. When an additional 10% water was added, the amount of QL was reduced to undetectable levels (<0.05%) in 30 min. A complex mixture of products was observed that were not assigned, but they were not P(III) compounds according to the ^{31}P NMR chemical shifts, so they would not be suitable for CW use.

A report on the reaction runs of QL has been released. Further effort to characterize the products in the reaction mixture were done, since many of the P(V) product compounds were not identified. Sections were added to the report from reaction studies and product characterization that was done in 2006 as part of the Binary Destruction Facility project. These results were previously unpublished but include information about analytical chemistry methods to analyze residual QL and reaction product analysis of other reaction mixtures.

Subtask 5.5.2: DF Studies

DF is a precursor to G agents. Several of the test reactions were done with 5 mL quantities in Teflon® vials rather than in NMR tubes. DF can generate hydrogen fluoride that reacts with glass, so a study of reactivity requires an inert container like Teflon. DF is an important compound and was part of the chemical weapons inventory that was destroyed from Syria, 97% was DF. A technical report was published with a complete discussion of the study of DF.

Reactions with $LiAlH_4$

When DF was added to $LiAlH_4$ (sample nb0018P55A, nb0018P61C), no reaction was observed. The reaction was attempted several times to confirm it. Reactions with both a solid pellet and powder were done.

The only time a reaction was observed was when NaOH solution in water was added followed by a $LiAlH_4$ tablet. This type of reaction was not done for any of the other agents, and it is not a practical approach. It was done to accelerate the reaction. Addition of the NaOH solution caused a flash of flame from the container when it reacted with the $LiAlH_4$. This reaction was probably due to reaction of the $LiAlH_4$ with water, shown in Figure 50, and might not have involved the DF. After one day, there was still 24% DF remaining in the liquid.

Figure 50. Reaction mixture from DF + $LiAlH_4$ + NaOH(aq), sample nb0018P59A. This experiment was to accelerate the reaction of DF with $LiAlH_4$. The flame lasted about 5 sec. before dying out. Photo is a still taken from a video.

Reactions with $Li_3N + H_2O$

DF reacted with $Li_3N + H_2O$. It did not react with Li_3N by itself, and only reacted after water was added. In the case of sample nb0018P59B, water was added rapidly and the reaction was violent, causing splattering of the liquid outside the container (but it was inside a secondary container of acrylic plastic), shown in Figure 51. The reaction may have been a combination of reaction of water with the Li_3N and with DF. Other reactions were not as violent, possibly due to different mixing or to the Li_3N being on the bottom of the container, so the water did not contact it as fast. Using pellets of Li_3N instead of powder controlled the rate of reaction. Water can also be introduced in a slow manner to prevent splattering.

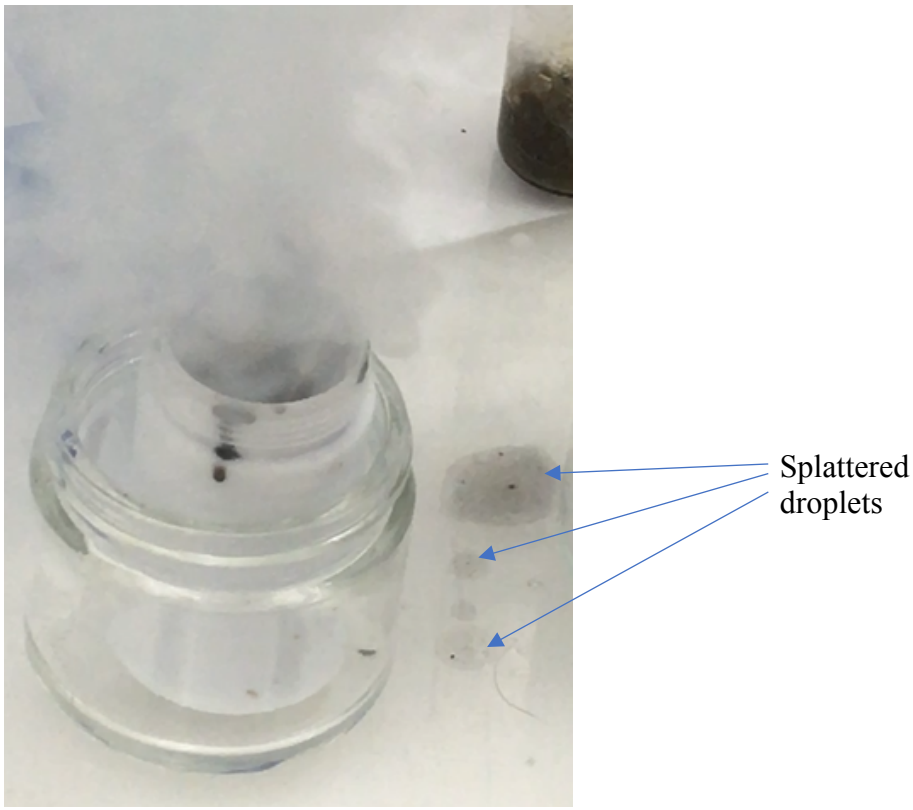

Figure 51. Reaction Mixture from DF + Li_3N + H_2O, sample nb0018P59B. As the water was added, the mixture reacted violently, smoked, and splattered out of the container. Photo is a still taken from a video.

A reaction with 10 mL of DF was done using 6.7 wt% Li_3N and incrementally increasing the amount of water to prevent violent reaction. After addition of 0.3 mL, bubbling, heating, and evaporation of the DF was observed. After 1.0 mL of water was added (7.3 wt%), there was 16% residual DF in the sample. As with QL, further study is needed to optimize the ratio of DF to water. It is possible that the added Li_3N competes with DF for reaction with water, so using less Li_3N or even no Li_3N may reduce the amount of water that is needed for reaction. But the Li_3N is caustic, so it may also be needed to promote the reaction.

Because of the vigorous reaction, an alternative procedure was studied to mitigate possible hazards of the reaction. It appeared that reaction with water alone was enough to degrade the DF (see next section). For a 9-mL reaction, an amount of 1.8 mL of water was placed in a small vial, and the vial was stood in liquid DF that was placed in a larger reaction jar. The large jar was capped with a lid to contain the vapor from the DF reaction. After capping, the small vial was tipped over to let the water mix with the DF. The temperature of the liquid rose to 55-60 C (measured on the outside of the jar with an infrared thermometer). After 5 min., the jar was opened and two tablets (0.53 g) of Li_3N was added. No further vigorous reaction was observed. DF was not detected in 24 h, and the material solidified after a week (Figure 52).

Figure 52. Reaction product of 9 mL DF with H2O+Li3N, after 7 days, sample NB0049P19A.

Using a similar procedure, a 100 mL reaction volume of DF was done. An amount of 100 mL of DF was measured by volume. Then 20 mL of water was placed in a 25 mL vial and the vial sat in the DF liquid. The outer reaction jar was capped. The inner vial was tipped over so the reaction proceeded. A temperature of 50-60°C was obtained on the outer surface of the jar. After 3 minutes, the cap was removed and 5.0 g of Li_3N pellets was added. The reaction produced vigorous boiling and fog formed in the containment enclosure. Boiling continued for about 15 minutes before slowing down. The temperature measured on the outside of the jar was 100°C. After 40 minutes, the temperature dropped to 56°C.

It appears that for the larger volume of DF, it takes longer than 3 minutes for the DF + H_2O reaction to conclude, so it is necessary to allow more time before adding the Li_3N in order to prevent boiling. Since both DF and water have similar boiling points, it is not clear whether one or both were boiling.

Videos and still photos were taken of the reaction.

After 2 months of reaction time, the product was completely solidified, as shown in the right panel of Figure 53. The pH of the solid product was determined by dissolving some solid in water and testing with a pH test strip. The pH was found to be 0-1 units, indicating that even the solid material was very acidic. The low pH implies that the MF primary product should rapidly react to the secondary product, methyl phosphonic acid (MPA). It indicates that the amount of Li_3N was not sufficient to keep the reaction basic.

Figure 53. Reaction of 100 mL DF with water and Li_3N. Left:, after 10 days of reaction time (Sample nb0049P21A), right: after 2 months. The reaction product is initially a mixed liquid (brownish color) and solid (light brown). DF is not detectable by NMR after <1 day. The lid of the jar could not be removed, so a hole was cut in the lid to sample the product. After 2 months, the product is completely solidified.

Reaction with H_2O

Reaction with water alone has been used previously to decontaminate DF.[10] An excess of water was used in the previous study, 1:5 DF:H_2O vol./vol. A 1:1 molar ratio of DF:H_2O would remove one F from the DF molecule to leave monofluoromethylphosphonic acid (MF), giving a. weight ratio of 20% H_2O to DF. The volume ratio is slightly smaller, 18% H_2O to DF, due to the higher density of DF. The second F from DF also can be replaced by water to form methylphosphonic acid as the final product, but the second reaction is slower.

Sample nb0018P53A was done with only water added. Water was added in 40 µL increments to a volume of 0.4 mL DF. After 0.4 mL (10% by volume relative to DF) was added, 28% of the reaction mixture was product and 72% was DF. After 80 µL of water was added, 56% of the liquid was product and 44% was DF. After 120 µL (30% relative to DF), 11% of the DF remained, using NMR detection. More water than the 1:1 molar ratio is needed because some of the DF is reacting to form methylphosphonic acid, consuming two H_2O molecules.

DF can be decontaminated by H_2O alone, without Li_3N. Although the reaction may be nominally faster in basic conditions, the reaction of DF with water is fast regardless.

Reaction with Glass

One trial reaction was done with DF and Li_3N without water (sample nb0018P47A)in a small glass vial. No reaction was visible, but it was observed that in 24 hours, the reaction mixture

was solidified. However, no reaction was observed with DF and Li_3N (without water) in Teflon containers. It is possible that the reaction was between DF and the glass vial. Due to the active fluorine in DF and the potential for forming HF, it is not surprising that glass can be attacked.

Another reaction was performed using 5 mL DF and Li_3N + water in a larger glass vial, using 0.25 g Li_3N and 0.25 g H_2O (5% relative to DF). The reaction mixture did not solidify, and 50% of the DF remained in the vial. The amount of water would not be expected to consume all of the DF, but reaction with the glass also was not effective. It is possible that the larger vial did not have enough surface area relative to the volume of DF to be as reactive.

A reaction between 5.0 mL DF and 0.56 g silica gel (about 10 wt.%) was done. The DF was completely consumed in less than 5 days.

A report on the reaction runs of DF has been published. Further effort to characterize the products in the reaction mixture was done. Sections were added to the report from reaction studies and product characterization that was done in 2006 as part of the Binary Destruction Facility project. These results were previously unpublished but include information about analytical chemistry methods to analyze residual DF agent, and reaction product analysis of other reaction mixtures. There is also information in the previous studies on the reaction rate of MF, the primary reaction product, under some different conditions.

Task 6: Reactive Material Formulation and Packaging

Subtask 6.1: Semi-quantify solubility of coating materials in simulant and live agent solutions.

Simple solubility tests were conducted with diphenyl chlorophosphate (DPCP) and candidate binder materials such as camphene, low melting point (53-58 °C) and high melting point (≥65 °C) paraffin. Camphene was found to be readily soluble in DPCP, while each paraffin was incompletely soluble. Samples swelled, but did not homogenize into solution, see Figure 54.

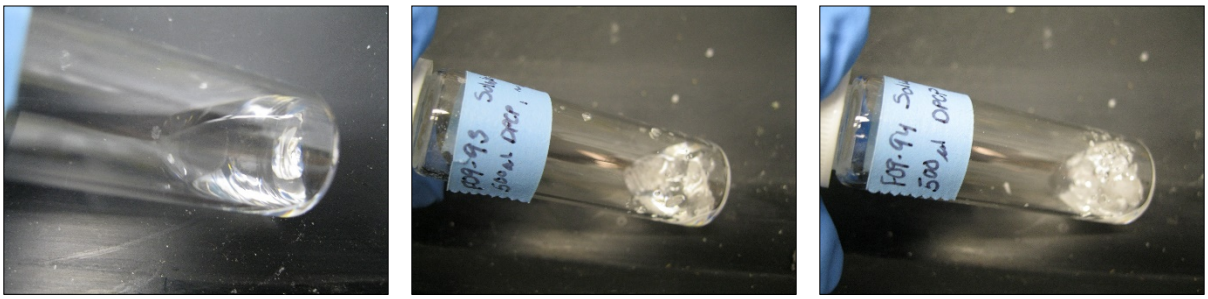

Figure 54 Images of camphene (left), low MP paraffin (center) and high MP paraffin (right) in DPCP. Camphene is fully soluble, the paraffins swell, but do not dissolve.

Exploratory efforts were undertaken to establish a range of solubility and packing density for powders and coating materials. Low and high melting point paraffins were used as coating materials, and blended with a dye for visual tests, or sand for structural tests. Fluorescein dye was used to provide a visual indicator of diffusion into neat simulant (DPCP). Samples were prepared by melting an excess of paraffin and mixing it with fluorescein dye in a conical centrifuge tube. The dye settled to the tip of the tube, which could be trimmed from the cooled, solidified mass. An aliquot was removed from the tip of the wax piece and immersed in DPCP. The dye began leeching into the simulant almost instantly, eventually resulting in a homogenous fluorescent solution (see Figure 55).

Figure 55. Images of wax-encapsulated fluorescein dye (left) in DPCP (center) under UV irradiation (right).

The bulk pellet did not dissolve, which may indicate a greater dye solubility than the paraffin. The rate of diffusion was slowed by dip-coating the pellet in an outer shell of paraffin. Similar results were achieved using both low and high melting point paraffins.

Subtask 6.2: Environmentally Stabilized $LiAlH_4$ Tablets with Protective Coating (UFR1)

Subtask 6.2.1: Coat COTS $LiAlH_4$ Tablets with Protective Material

Commercially available $LiAlH_4$ tablets (Sigma Aldrich, 95% Reagent Grade) tablets were coated with molten (low MP) paraffin to form a core-shell structure (Table 8). Several different approaches were attempted. First, a tablet was suspended on a plastic mesh over a collection tray, and molten wax was poured over the tablet (Figure 56). Multiple coatings were applied, then the tablet was flipped to coat the obverse side. The second method used forceps to hold the pellet and dunk it directly into the molten wax. The wax coated the pellet and forcep tips, so when the tool was removed, the coating was pulled away. Multiple coatings were needed to repair the tool damage. Finally, pellets were added to molten wax, and the wax was decanted away to avoid tool damage. Some bubble formation was noted in the final coat, but the decanting method was the most effective technique. All approaches resulted in a substantial mass of wax added to the pellet, up to 47% of the combined mass.

Sample	Tablet (g)	Tablet + wax (g)	Wax Content (%)
A	0.524	0.989	47.0
B	0.477	0.667	28.5
C	0.499	0.591	15.6
D	0.490	0.581	15.7

Table 8. Wax coated commercially available $LiAlH_4$ tablets.

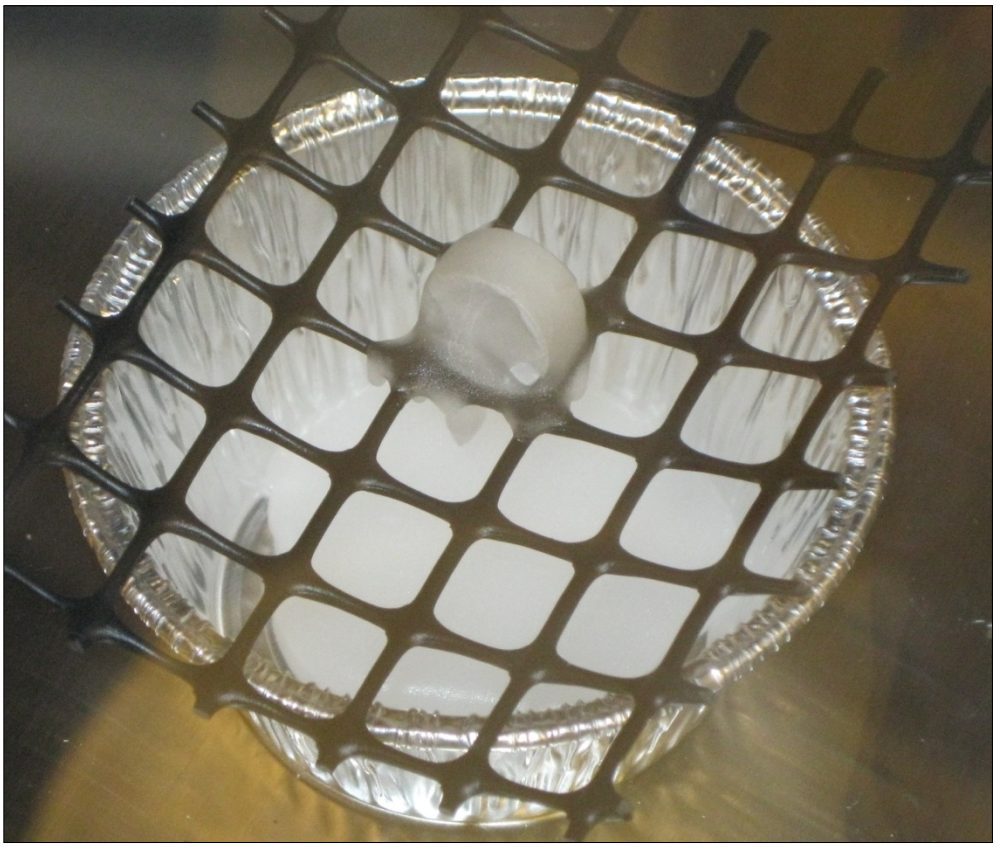

Figure 56: Pellet A on mesh support with first wax layer.

Subtask 6.2.2: Test effectiveness at Sandia

Pellets A-D were contacted with 150 mL DI H_2O and immediately began to react. It is likely that the wax coating was incomplete, allowing water to penetrate immediately upon contact. Residual wax remained after the reaction was complete, indicating substantial inhomogeneity in the coating, Figure 57. Since the coating contributed a substantial mass, yet provided incomplete coverage, this method was deemed unsuccessful and abandoned.

Figure 57. Post-reaction residue from pellet D, with some unreacted pellet remaining.

Subtask 6.2.3: Test effectiveness at CBC

Based on poor performance of these tablets, they were not tested at CBC.

Subtask 6.3: Fabricate Pucks of Protective and Reactive Material (UFR1)

The concentration of solid in the paraffin pellet was evaluated using thermogravimetric analysis. In order to ensure the solid powder was not volatilized during the experiment, test sand was used in place of the fluorescein dye. The stock paraffin was heated in flowing air (100 sccm) to 500°C, and the resulting change in mass was compared to a test dust paraffin pellet subjected to the same conditions (Figure 55). The dust residue after combustion was 34 wt% of the sample, which is well below the desired mass loading of 95-97%. Further efforts to centrifuge the suspension while molten were unsuccessful. Minimal solid compaction was achieved, and the paraffin began to degrade after prolonged exposure to elevated temperatures (Figure 58).

Figure 58. Centrifuged dust-encapsulated pellet after repeat melt/cool cycles. Headspace paraffin had discolored. The color change was pronounced compared to a sample prepared with a single melt process and allowed to settle/cool under ambient conditions.

As an alternative processing method, a known ratio (5 wt% paraffin, balance test dust) was prepared and heated on a hot plate. Once the paraffin was molten, the hot plate was turned off and the sample was stirred to homogenize while allowing to cool. A homogenous, slightly cohesive powder was obtained. In a similar procedure, the same ratio of paraffin to test dust was slurried in iso-octane and allowed to dry. The homogenized powder was packed into a 13 mm Carver die press and compacted under ≈7 metric tons. A robust pellet was produced (Figure 59).

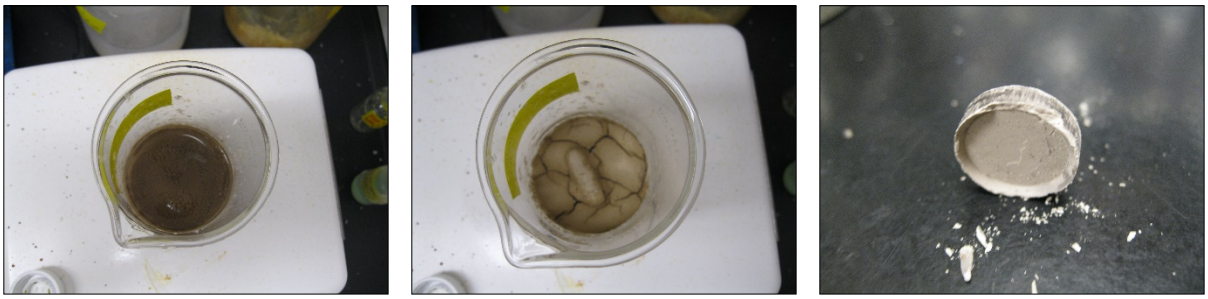

Figure 59. Progression of paraffin/dust/isooctane slurry (left), dried powder (center) and pressed pellet (right).

After initial qualification tests with surrogate powders was complete, the reaction kinetics of DPCP with wax-covered LAH tablets was evaluated. Tablets (approximately 0.5 g from vendor) were dipped into molten low or high MP wax within an argon glovebox. Very slight off gassing was noted when some tablets were added to the molten wax. This behavior was not consistent among all samples, and is most likely due to trapped atmosphere within the tablet, not a reaction with the wax. Two different coating mechanisms were attempted with low MP wax; direct immersion in the melt, and pouring molten wax over the tablet (Subtask 6.2.1: Coat COTS $LiAlH_4$ Tablets with Protective Material). The pour-over method left numerous gaps, requiring several repeat coats to fully enshroud the tablet. As a result, the composite pellet was approximately 47% by mass wax. A simple immersion method was more effective, producing a

coating of 15 wt%. Unfortunately, this method resulted in numerous pin-hole defects. When tablets were immersed in water as a coating stability test, they reacted instantly.

Subtask 6.3.1: Fabricate Pucks containing $LiAlH_4$

Subtask 6.3.1.1: Develop process to fabricate $LiAlH_4$ pucks

Approach 1

Samples were prepared by melting an excess of paraffin and mixing it with powdered sand in a conical centrifuge tube. The sand compacted to the tip of the tube, which could be trimmed from the cooled, solidified mass. The concentration of solid in the paraffin pellet was evaluated using thermogravimetric analysis. The stock paraffin was heated in flowing air (100 sccm) to 500 °C, and the resulting change in mass was compared to a test dust paraffin pellet subjected to the same conditions (Figure 55). The dust residue after combustion was 34 wt% of the sample, which is well below the desired mass loading of 95-97%. Further efforts to centrifuge the suspension while molten were unsuccessful. Minimal solid compaction was achieved, and the paraffin began to degrade after prolonged exposure to elevated temperatures (Figure 58).

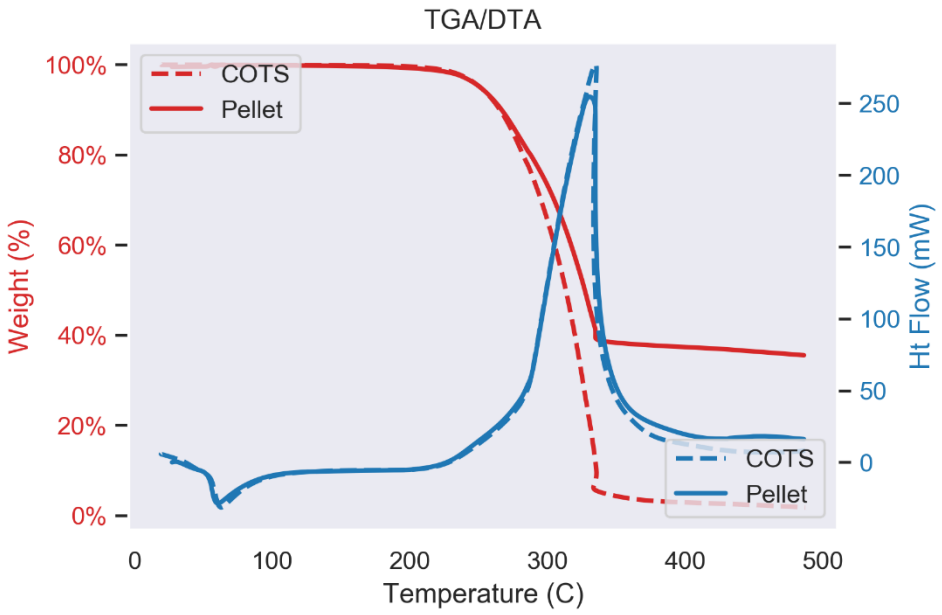

Figure 60. TGA/DTA plot of COTS low melting point paraffin (solid lines) and synthesized dust pellet (dashed lines). The mass difference at 500 °C corresponds to the mass of dust contained in the pellet; 34 wt%.

Subtask 6.3.1.2: Test effectiveness at CBC

When an $LiAlH_4$ pellet (F09-154C) was tested, it was found that the reaction with GB was fairly violent (sample NB0018P105A). The reaction was similar to $LiAlH_4$ powder and commercially

available $LiAlH_4$ tablets (no binder). There was significant amounts of initial bubbling and eventually flame bursts were observed. Based on these observations, 5% w/w binder in the pressed pellets is not enough binder to slow the rate of reaction with neat agent.

Subtask 6.3.2: Fabricate Pucks containing Li_3N

Subtask 6.3.2.1: Develop process to fabricate Li_3N pucks

A series of Li_3N pucks were prepared using 3%, 5% or 10% low melting point paraffin wax as a binder. An aliquot of wax was weighed and melted, and the corresponding amount of Li_3N was added to achieve the desired mass loading. The slurry was stirred and iteratively returned to a hotplate to soften the wax until a visually homogenous mixture was achieved. To prepare a pellet, an aliquot of mixed powder was added to a 13 mm Carver press die and pressed to a pressure of ≈7 metric tons. The starting powder mass and final pellet mass were recorded and tabulated below.

A companion test series without binder was conducted, and found to produce good quality pellets. One pellet was dropped from a height of approximately 30 cm without any apparent damage. Immersion into water resulted in an effervescent reaction, but was considerably milder than a reaction with bulk powder (no flame). The following tables and figure provide details of the tablets that have been fabricated using a press: Table 9, Table 10, Table 11, Table 12, Table 13, and Figure 61.

10% low MP wax in Li_3N			
Sample	**Powder (g)**	**Pellet (g)**	**Δ (%)**
F09-153A	0.2952	0.2882	2%
F09-153B	0.3276	0.3224	2%
F09-153C	0.3724	0.3644	2%
F09-153D	0.3274	0.3250	1%
F09-153E	0.4109	0.4069	1%
F09-153F	0.3520	0.3384	4%
F09-153G	0.4148	0.4083	2%
F09-153H	0.3030	0.2954	3%

Table 9. Li_3N tablets fabricated with 10% w/w low melting point wax.

5% low MP wax in Li_3N			
Sample	**Powder (g)**	**Pellet (g)**	**Δ (%)**
F09-135A	0.3461	0.3406	2%
F09-135B	0.2843	0.2808	1%
F09-135C	0.1993	0.1853	7%
F09-135D	0.3186	0.2296	28% (damaged & re-pressed pellet)
F09-135E	0.3184	0.3137	1%
F09-135F	0.3592	0.3508	2%
F09-135G	0.2808	0.2788	1%
F09-135H	0.1572	0.1524	3%

Table 10. Li_3N tablets fabricated with 5% w/w low melting point wax.

3% low MP wax in Li_3N			
Sample	**Powder (g)**	**Pellet (g)**	**Δ (%)**
F09-138A	---	0.292	---
F09-138B	0.2898	0.2814	3%
F09-138C	0.3581	0.3500	2%
F09-138D	0.4751	0.4654	2%
F09-138E	0.2986	0.2945	1%
F09-138F	0.3523	0.3441	2%
F09-138G	0.3045	0.3008	1%
F09-138H	0.1458	0.1221	16%

Table 11. Li_3N tablets fabricated with 3% w/w low melting point wax.

5% low MP paraffin in LAH			
Sample	**Powder (g)**	**Pellet (g)**	**Δ (%)**
F09-154A	0.3511	0.3407	3%
F09-154B	0.2630	0.2562	3%
F09-154C	0.3035	0.3021	0%
F09-154D	0.3348	0.3323	1%
F09-154E	0.2973	0.2952	1%
F09-154F	0.4899	0.4877	0%
F09-154G	0.3518	0.3483	1%
F09-154H	0.4442	0.4408	1%

Table 12. $LiAlH_4$ tablets fabricated with 5% w/w low melting point wax.

Neat Li_3N			
Sample	**Powder (g)**	**Pellet (g)**	**Δ (%)**
F10-22A	0.3034	0.2949	3%
F10-22B	0.2836	0.2809	1%
F10-22C	0.3271	0.3262	0%
F10-22D	0.3032	0.3017	0%
F10-22E	0.3685	0.3677	0%
F10-22F	0.3174	0.3156	1%
F10-22G	0.3705	0.3578	3%

Table 13. Li_3N tablets fabricated with no wax.

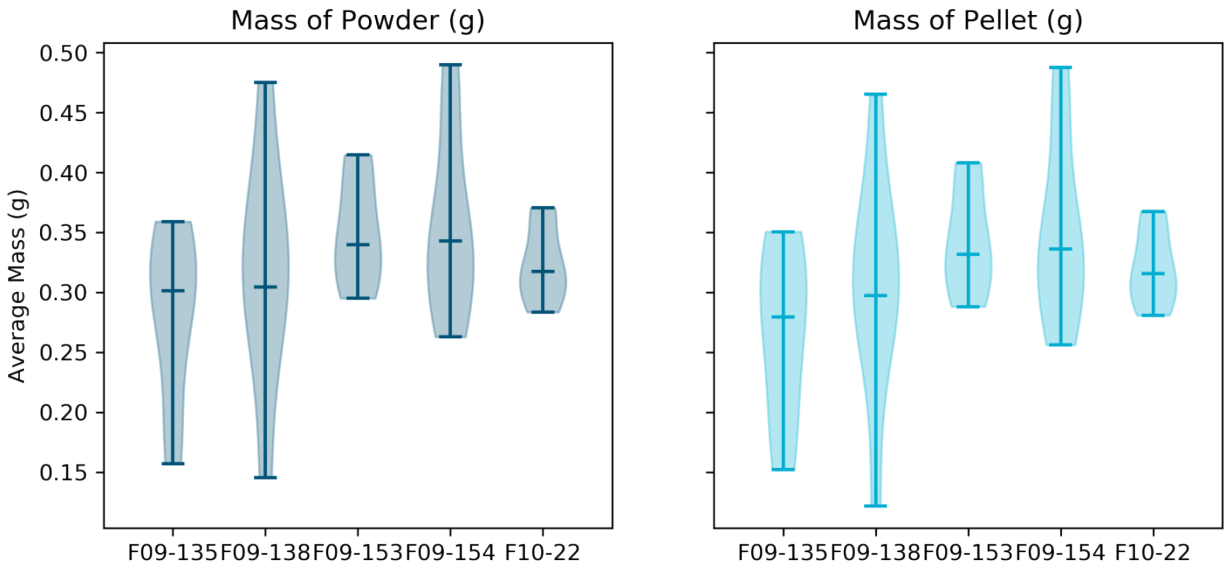

Figure 61. Summary of all Tables and shows starting mass of powder and final mass of pellet.

Additional pellet presses were acquired in order to fabricate pucks with varying diameters. A ¼" diameter die press was used to prepare small, trial scale pellets. These pellets were well-suited for samples of approximately 0.02-0.05 g. A much larger die press (30 mm) was used to prepare a puck for large scale or field tests. Unfortunately, the Li_3N powder was too soft to maintain structural integrity with this size pellet die (Figure 62). Since the applied pressure scales with the diameter of the die, it is very likely that the available press was unable to provide sufficient pressure to compress the powder.

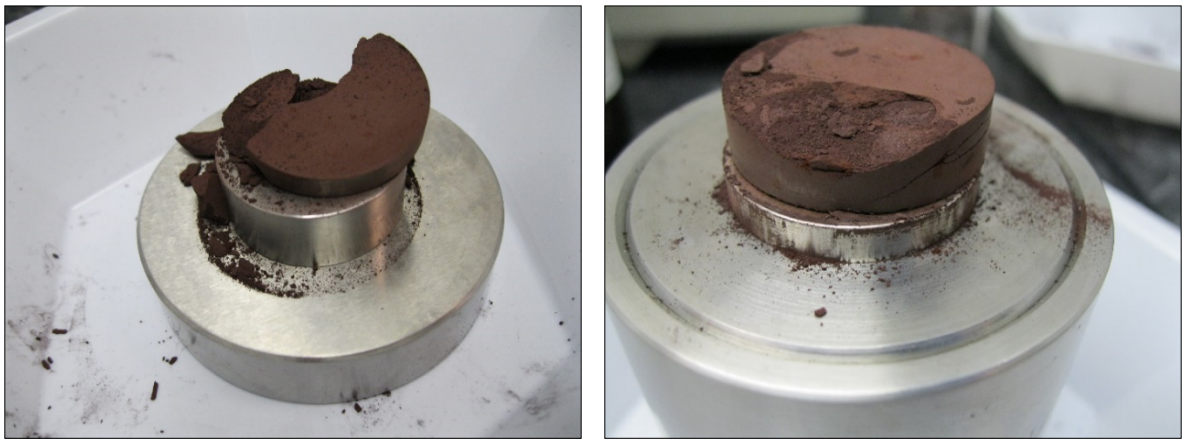

Figure 62. Large Li_3N pellets could not be formed successfully.

Subtask 6.3.2.2: Test effectiveness at Sandia

The reactivity of Li_3N pucks was evaluated with a simple method of monitoring pH and temperature when the puck was added to water. Each puck, approximately 0.3 g, was added to 50

mL of DI H_2O and monitored with an Orion VersaStar temperature corrected pH probe. The probe output (both pH and temperature) was continuously monitored during the reaction, and in one case, for an extended period after reaction. When the pellet was added, an effervescent reaction began almost immediately. The exothermic production of LiOH caused an increase in pH to ≈12.5, and a corresponding temperature increase (Figure 63). The unbuffered solution remained at high pH as the solution cooled in a subsequent extended test (Figure 64).

The efficacy of pressed Li_3N pellets was compared to a similar mass of loose powder in BCEE. A pellet (0.0425 g Li_3N) and 0.0480 g Li_3N powder with 1000 µL BCEE each were mixed with water on a 3 eq basis to Li_3N. After no initial reaction was observed in either vial, successive aliquots of water (100, followed by 1000 µL) were added to achieve a reaction. The powder sample began to effervesce and a distinct phase separation was noted. The pellet sample did not visibly react, but the liquid clouded over time.

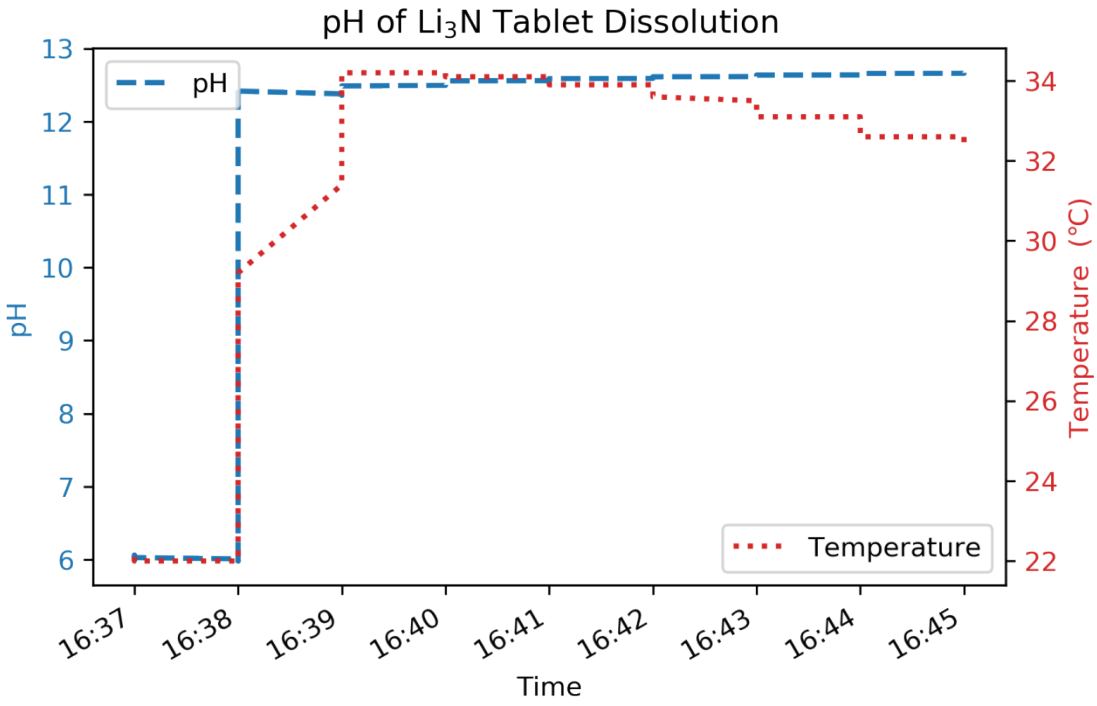

Figure 63: pH (left axis) and temperature (right axis) increase upon addition of Li_3N puck to 50 mL DI H_2O. Time is in hh:mm.

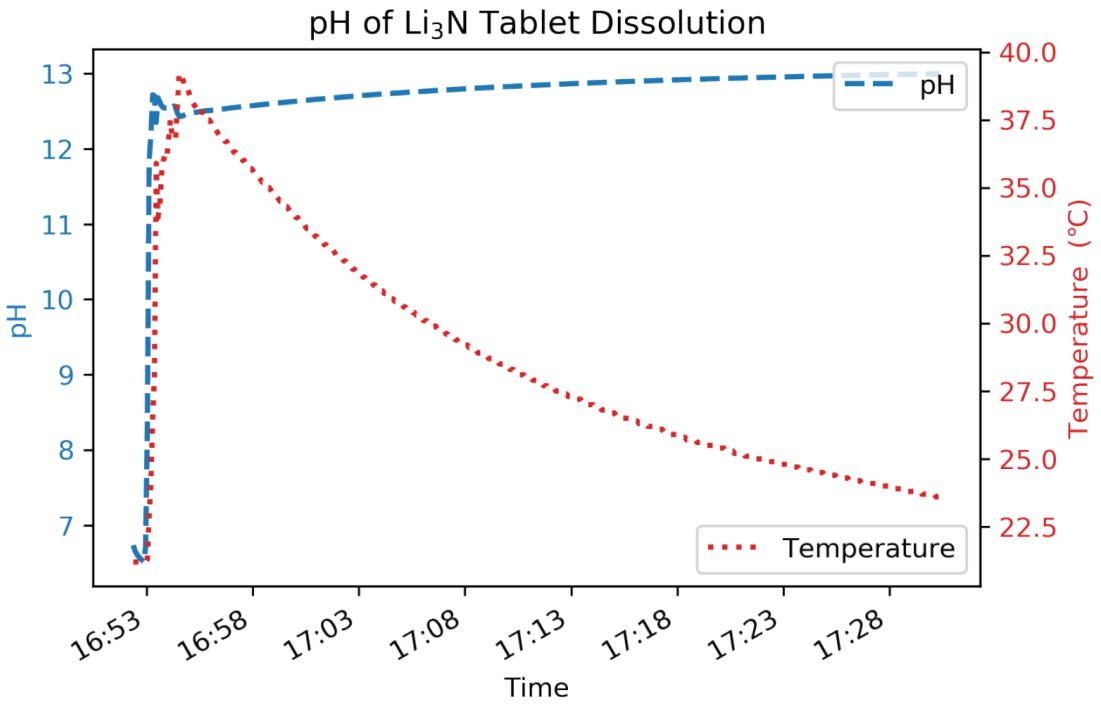

Figure 64: Extended monitoring of Li_3N dissolution after puck was fully consumed. Once the reaction was complete, the solution returned to room temperature while the pH remained constant.

Further reaction optimization was undertaken at Sandia using BCEE as a surrogate. Since the pellet did not remain in good contact with water due to differing density and solubility, an effort to increase the aqueous solution density was made. A saturated solution of potassium carbonate (K_2CO_3, 112 g in 100 g DI H_2O) was used to improve liquid contact with the pellet, as shown in Figure 65.

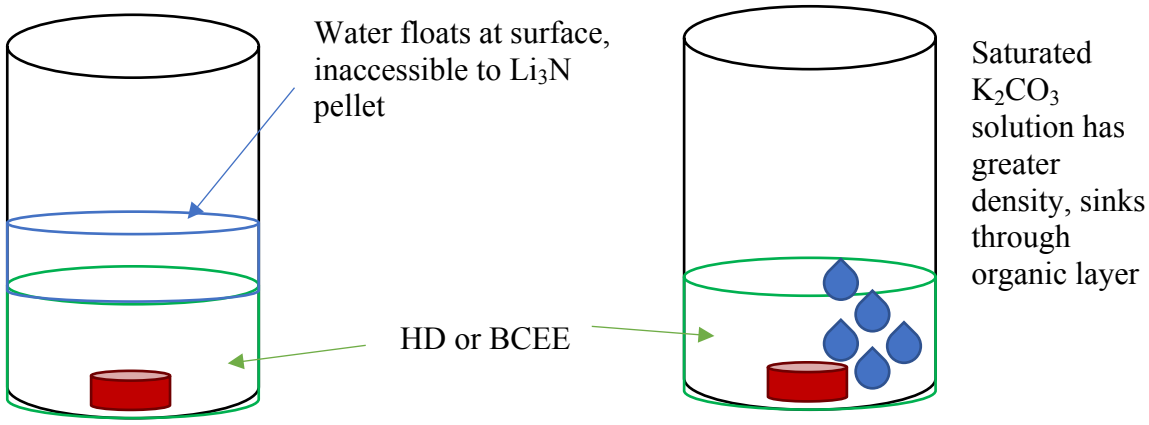

Figure 65. Illustration of using high density salt solutions to overcome mixing limitations of water and HD (BCEE)

Initial efforts with potassium chloride had limited success, as the solution did reach the pellet, but did not substantially react with the Li_3N. A second attempt with saturated K_2CO_3 was more successful, for a variety of reasons. First, K_2CO_3 is highly soluble in water, to a literature value of 112%. Secondly, K_2CO_3 produces a moderately basic solution (pH 10-11), which can enhance the hydrolysis rate.

Non-aqueous solvents were tested for further improvements in density match and miscibility with BCEE. Simple alcohols, ranging from short chain lengths (methanol) to surfactant-like (dodecanol) were used as the solvent and Li_3N reaction activator. Reactivity with the Li_3N powder was inversely proportional to chain length, with menthol producing a violent reaction, and dodecanol producing no immediately perceptible reaction. The reaction with alcohols was expected to produce lithium hydroxide and the corresponding aklylamine, Figure 66. An example reaction is shown in Figure 67 for the reaction of BCEE, propylene glycol, and methanol. Polyols, including propylene glycol and glycerin, were used as reagents to improve miscibility and produce multidentate alkylamines as a product. Viscous mixtures of solvent afford some degree of control and miscibility with Li_3N, as they do not immediately react on contact. Analysis of reaction products via Raman spectroscopy indicates partial consumption of the surrogate.

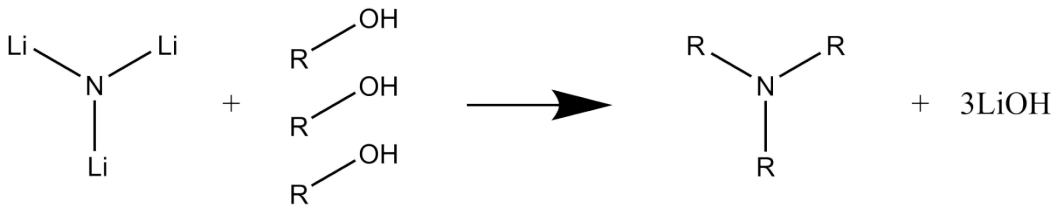

Figure 66. Hypothesized reaction of lithium nitride and methanol.

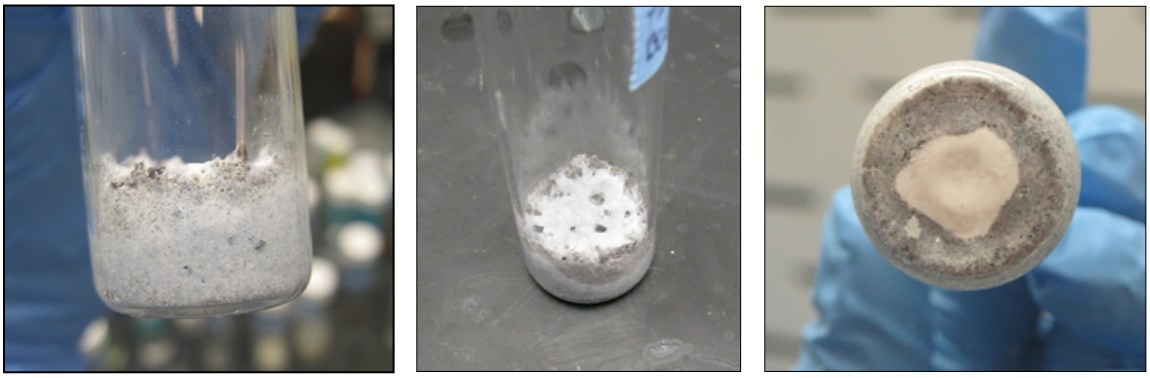

Figure 67. Images of reaction product from Li_3N with propylene glycol and methanol equimolar mixture.

Methanol as an organic solvent in place of water was found to be an effective reagent to activate Li_3N. The solubility of HD (or surrogates) should be slightly higher in methanol and other

alcohols than water. Additionally, the alkyl products produced from hydroxyl cleavage should produce alkylamines as opposed to ammonia. The alkylamines were expected to be more reactive (greater contact time) with the HD/surrogates than gaseous ammonia. Reactions using methanol as the solvent were effective for the decomposition of CEPS, as monitored by the decline of a C-Cl peak via Raman spectroscopy (Figure 68). A greater reaction rate was achieved by adding sodium dodecylsulfate (SDS) as a surfactant to the solution. Methanol, ethanol and an equimolar mixture were used as solvents in comparison to water, all with added SDS to enhance solubility. The ethanol/SDS solution exhibited the greatest decrease in the chlorine peak.

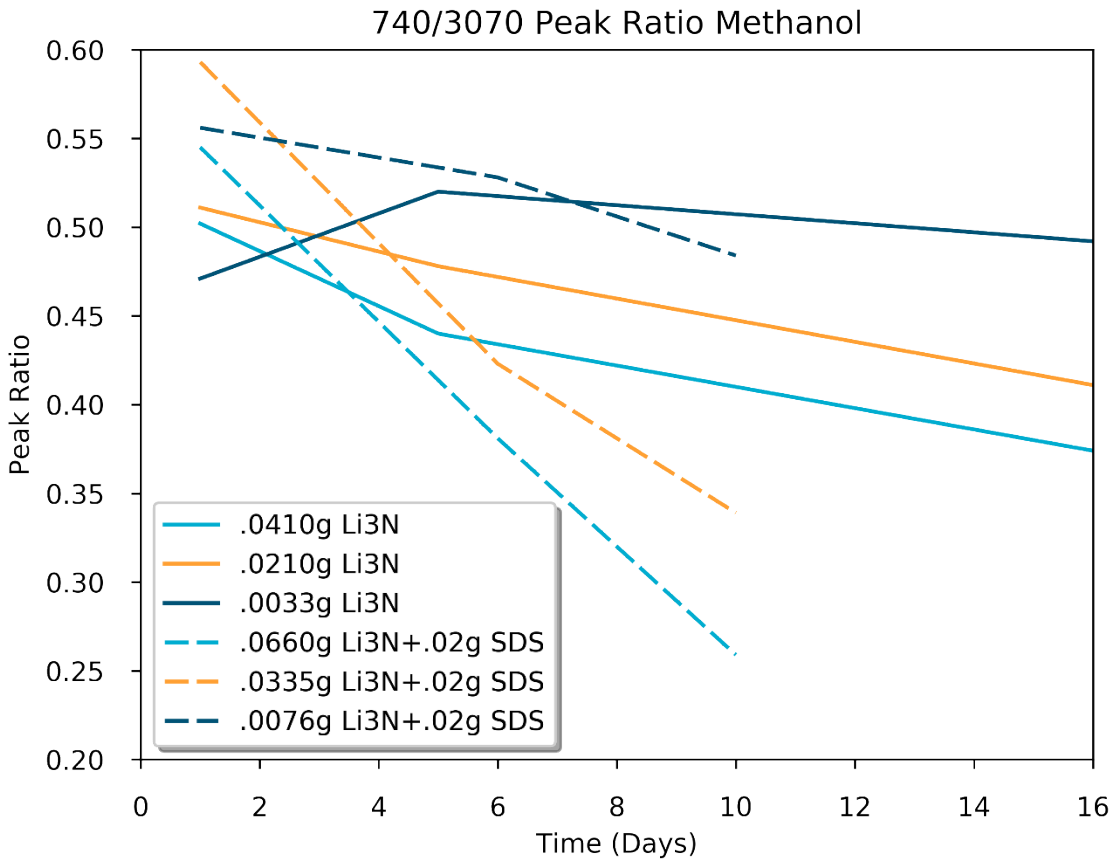

Figure 68. Peak ratio of C-Cl to C-OH peak measured by Raman spectroscopy for methanol at varying ratios of Li_3N. Neat solvent reactions are shown in solid lines, and solvent with surfactant reactions are shown in dashed lines.

Other solvent/reagent mixtures were evaluated to find an effective means to solubilize and react HD/surrogates. Since the biological mechanism of HD is alkylation of DNA, using amine groups as a target was explored. Pyridine was considered an ideal candidate, as it could function both as solvent and reagent via the cyclic amine functional group. In place of water, a solvent mixture of pyridine and methanol was added to Li_3N and BCEE. The alcohol was expected to activate the Li_3N, and the pyridine was expected to serve as a solvent and additional amine source. In contrast to typical reactions between Li_3N and water, this reaction was mild. No noticeable

exothermic behavior occurred. After resting overnight, the entire system formed a translucent gel, as shown in Figure 69. In order to further elucidate reaction behavior, neat pyridine was added to BCEE. A pink solution developed and evolved to dark red after 16 hours, eventually resulting in a dark red precipitate (Figure 71). A subsequent reaction with a small amount (5 vol%) of water reduced the reaction rage; resulting in a pink color only after 5 days. Extraction with water or hexane resulted in the pink solution migrating into the aqueous phase. Investigation of the proposed amination products suggested that this was not a useful mechanism.

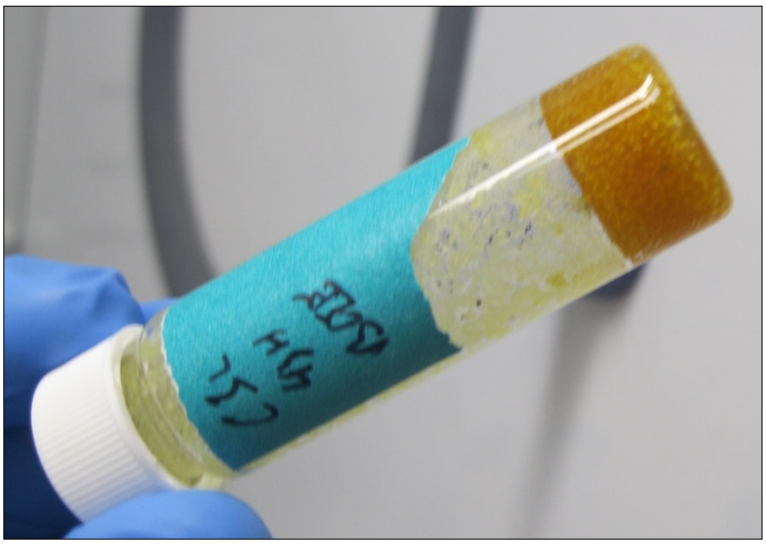

Figure 69: Gelled BCEE/Li_3N/py/MeOH reaction after resting overnight. Typical LiOH reaction products (grey/white powder) did not form.

Other amine-containing reagents were investigated, including urea and thiourea. Thiourea presented a particularly appealing approach, as the reaction product (oxygen urea) could itself further react with HD, as illustrated in the conjectural reaction scheme (Figure 70). Under ideal conditions, this could result in polymerization of the HD. While some color change was observed, no change was detectable by Raman spectroscopy.

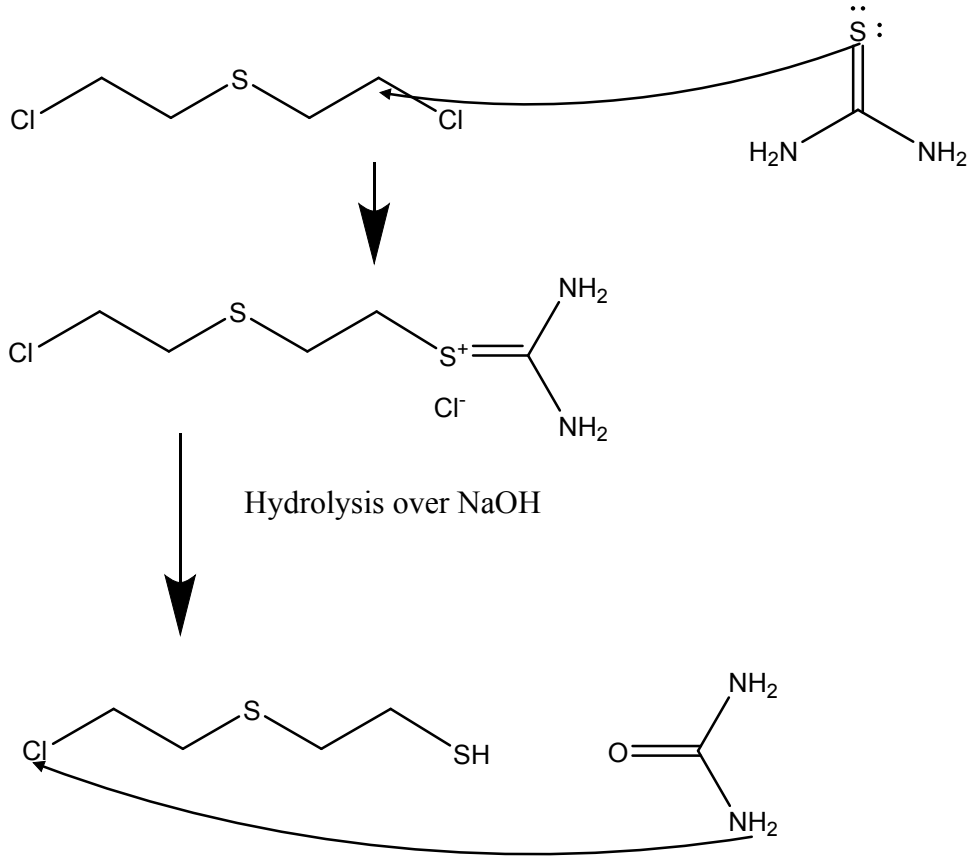

Urea product can undergo subsequent nucleophillic attack with remaining HD.

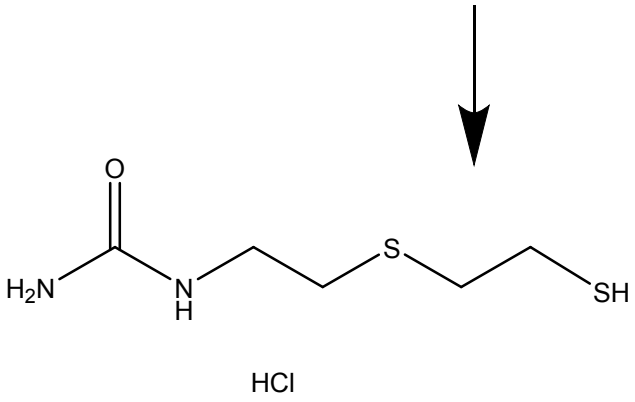

HCl

Figure 70: Conjectural reaction mechanism of HD and thiourea.

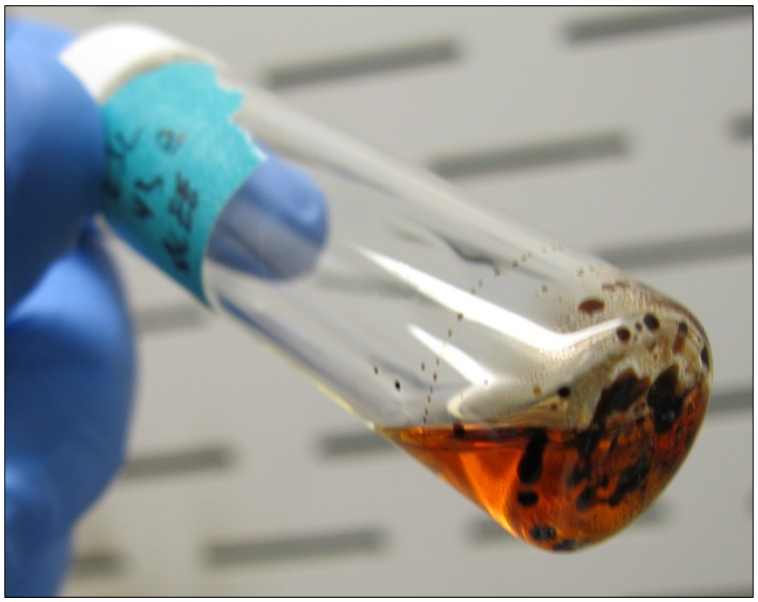

Figure 71: Neat BCEE/py reaction after 5 days showing dark red coloration and solid precipitates.

Figure 72: Reactions of BCEE with Li_3N and thiourea. The solution developed an orange coloration, but did not polymerize or exhibit other signs of surrogate decomposition.

Tablets consisting of 9% w/w/ $LiAlH_4$ dispersed in Li_3N were pressed and sent to CCDC-CBC to determine if the $LiAlH_4$ aids in breakup of the Li_3N powder.

In addition to S_N2 nucleophilic substitution of HD by Li_3N and reaction products, E_2 elimination may also be possible. In this scenario (Figure 73), ammonia or another nucleophile reacts with hydrogen on the alkyl carbon, displacing terminal chlorine and generating a C=C bond. This reaction mechanism is more likely under strongly basic conditions, such as expected when Li_3N reacts in aqueous solution. Notably, this mechanism does not involve a sulfonium ion intermediate, which can lead to problematic oligomerization in aqueous solution. Formation of a vinyl end group could be further utilized to initiate polymerization. Reaction conditions were tested using KOH solution to vary the pH values from 9, 11, and 13. Control solutions were tested in parallel following the same conditions, without Li_3N. The Li_3N and surrogate (BCEE) were mixed before adding alkaline solution dropwise. The reaction rate of the Li_3N was proportional to solution pH. The pH 9 solution produced irregular, step-wise off gas events with the Li_3N; the pH 11 solution produced more steady results, and the pH 13 solution yielded consistent reactions, allowing a steady dropwise addition of the aqueous solution. The product solutions were extracted with hexane and examined using Raman spectroscopy. No substantial consumption of the reactions was observed (Figure 74). The poor reaction performance was attributed to limited solubility of the surrogate in aqueous solution. Despite highly reactive alkaline conditions with elevated temperature (from Li_3N decomposition), the bulk of the surrogate remained inaccessible.

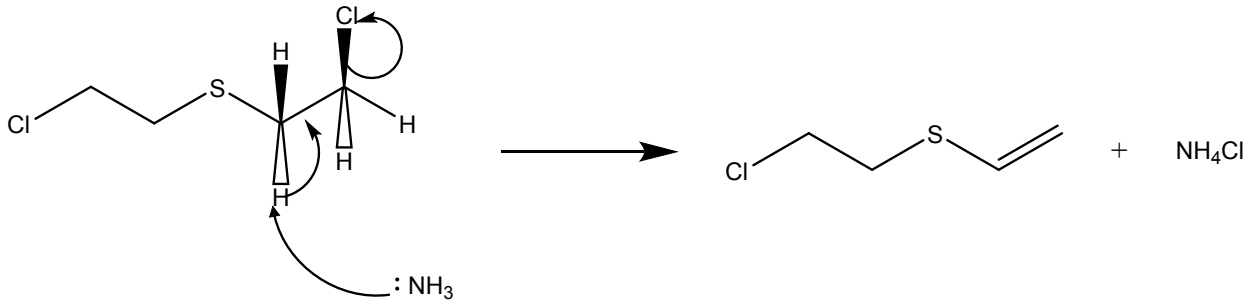

Figure 73: E2 elimination possible mechanism generating a vinyl sulfane.

Upon analysis of these results, aqueous solubility appears to remain a challenge for the E2 (and S_N2) reactions. A non-aqueous basic solvent, such as was attempted with pyridine (see Figure 71) may be more favorable for elimination reactions than substitution reactions. This is a promising avenue for a subsequent study.

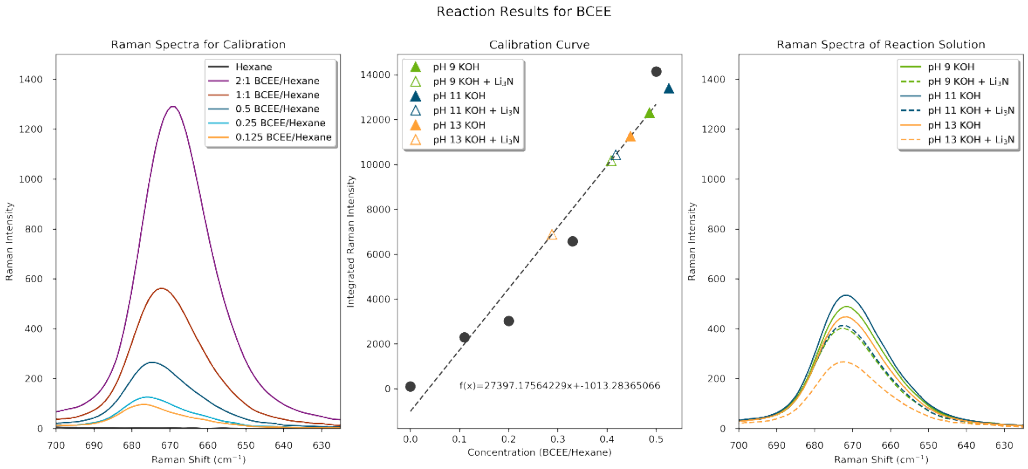

Figure 74: Raman spectra and calibration curve for pH reaction series. Nominal extraction is 0.33 BCEE:hexane.

Solvent compatibility, whether water or low molecular weight alcohols, remained challenging. Structurally, the most compatible alcohol with HD (or oxygen surrogate) is the hydrolysis product thiodiglycol (or diethylene glycol for the surrogate). Since low molecular weight alcohols have been shown to be effective for activating Li_3N, diethylene glycol (DEG) should likewise provide sufficient hydroxyl groups to react with the Li_3N. A trial sample consisting of equal volumes BCEE and DEG was added to Li_3N. The reaction was significantly less vigorous than typical water or alcohol reactions with comparable amounts of Li_3N. A subsequent test was mild enough to allow for pH monitoring via moistened test strip placed at the mouth of the vial. Highly alkaline conditions (dark blue) were noted immediately. An amine-containing volatile gas was evolved without the presence of water. Aqueous hydrolysis in pH 9, 11, and 13 solutions was repeated, with the addition of 30 wt% H_2O_2. Since the surrogate was dissolved in its own hydrolysis product, improved miscibility with the aqueous solution was anticipated. Unfortunately, the continuing production of hydrolysis product/solvent was not sufficient to stabilize the BCEE, and the emulsion broke upon addition of the alkaline oxidizing solution.

Surrogate miscibility with nucleophilic reagents remains challenging. Diethylamine (DEA) has emerged as a leading multifunctional reagent and solvent to address this limitation. In neat form, it is fully miscible with BCEE. As a secondary amine, it is a good nucleophile for abstracting chlorine ions from the surrogate. DEA thus achieves the two necessary conditions to neutralize BCEE, and by analogy, HD. When mixed in a stoichiometric ratio (1 mole BCEE to 2 moles DEA), a crystalline precipitate develops after many hours (Figure 76). Increasing the ratio of DEA corresponds to greater consumption of BCEE (Figure 75), but oddly less formation of the crystalline solid. Triethylamine is similarly miscible with BCEE, but less reactive. Based on these results, it is likely that the DEA forms a quaternary product (2-(2-chloroethoxy)-N,N-diethylethan-1-aminium chloride {BCEE-$HNEt_2$}) when reacted with BCEE (Figure 78). The quaternary product of triethylamine and BCEE (2-(2-chloroethoxy)-N,N,N-triethylethan-1-aminium chloride {BCEE-NET_3}) is carbon saturated and cannot react further. In experiments using triethylamine, no crystalline solids were observed, only a color change (yellow) indicated any reaction progress at all. In contrast, the BCEE-$HNEt_2$ has one remaining reactive proton, and

can further react with BCEE. A charged oligomer may result from successive reaction steps (Figure 78). Formation of a solid crystalline product, and in some cases a yellow color, indicated ongoing reaction progress over several days. In Figure 77, a series of volumetric reactions using (from left to right in each image) 1:1, 1:0.75, 1:0.5, 1:0.25, and 1:0.125 BCEE:DEA progressed from 1 to 7 days. Development of crystalline deposits was more rapid in vials with more DEA. A yellow tint developed first in the vials with the least DEA, but eventually was observed in all vials.

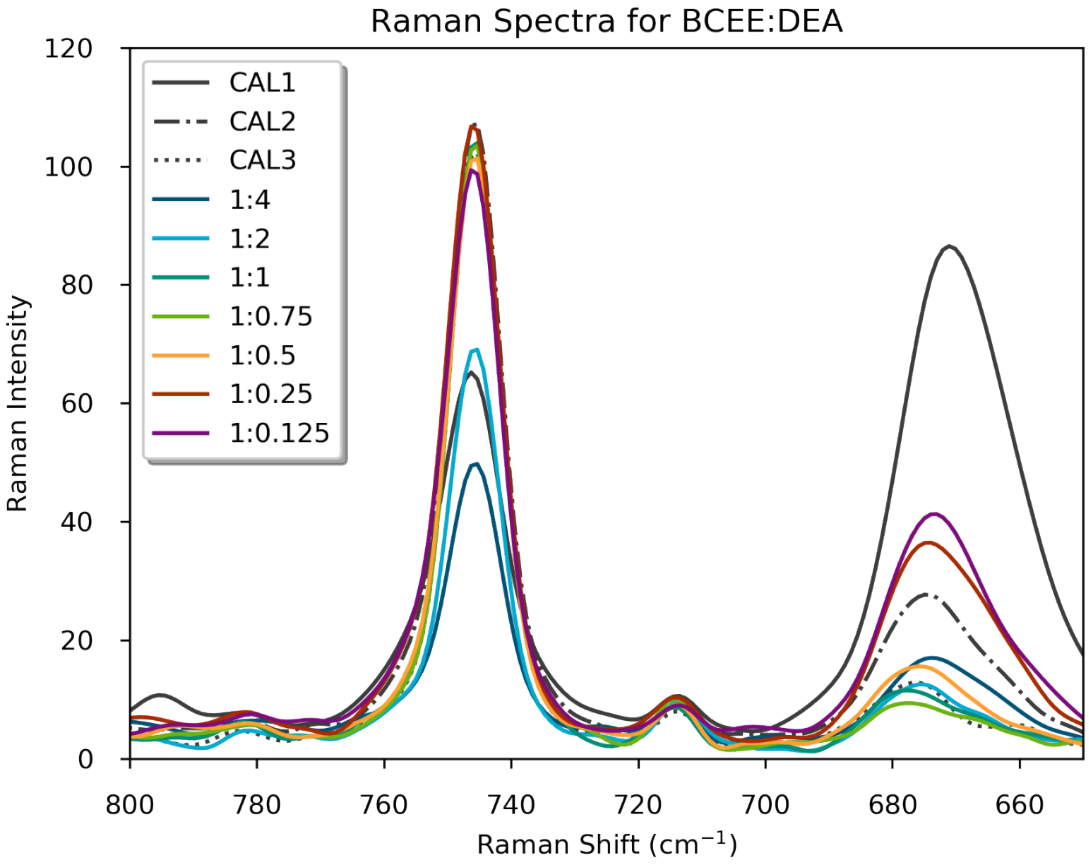

Figure 75: Raman spectra of serial dilutions of BCEE and diethylamine (DEA). Reduction in BCEE correlated to concentration of DEA.

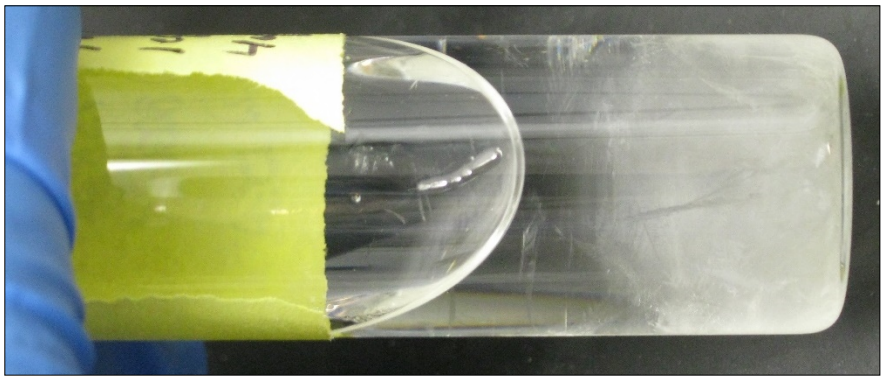

Figure 76: Mixture of BCEE and DEA (1:4 ratio) showing formation of fine needle-shaped precipitates.

Figure 77: Series of BCEE:DEA mixture ratios after several days; (left) 1 day, (right) 7 days.

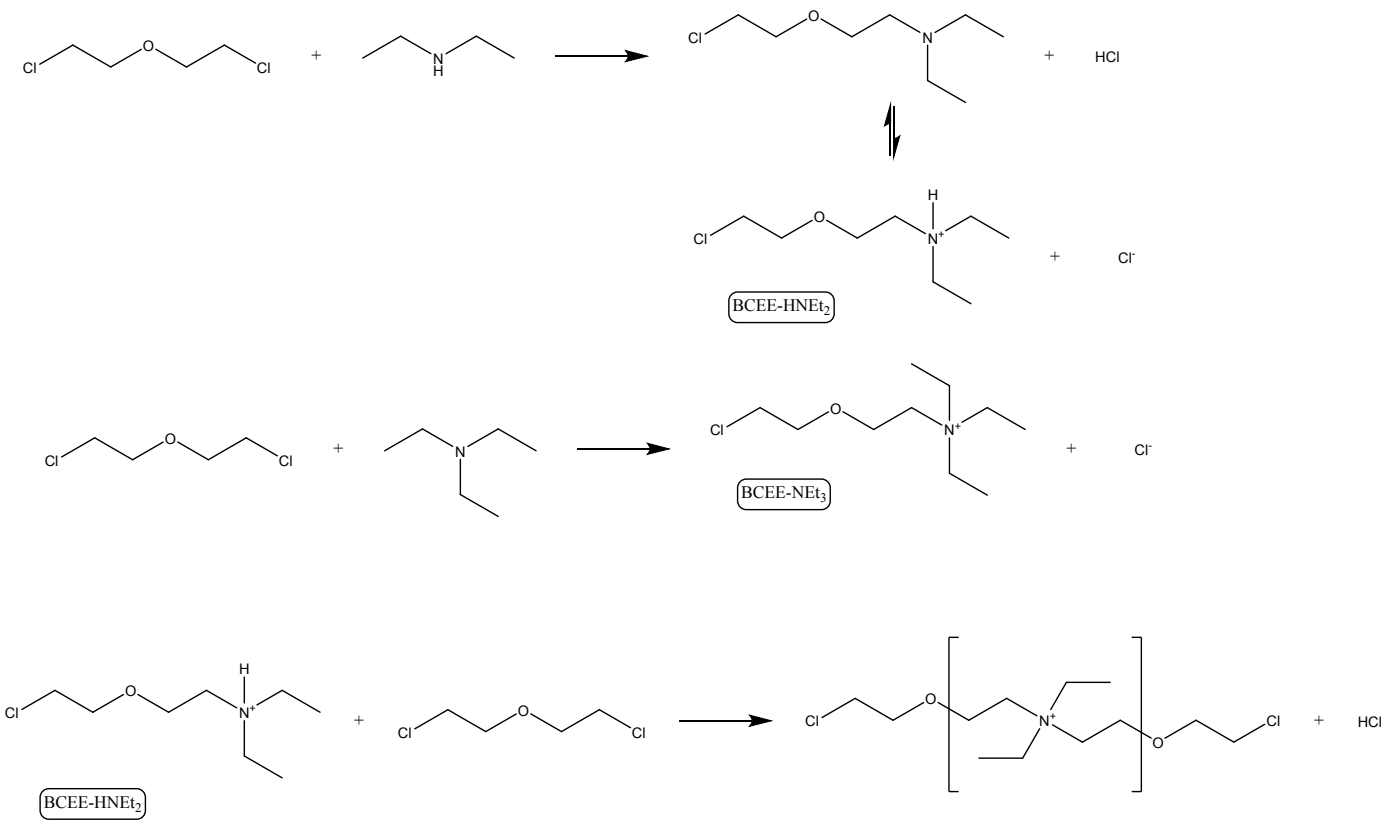

Figure 78: Proposed reaction scheme of BCEE and DEA forming a quaternary amine product.

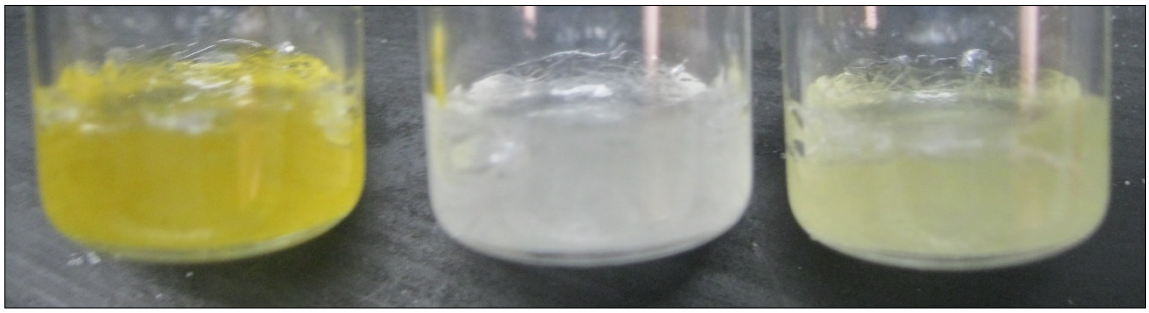

Figure 79: Vials containing 2:1, 1:1 and 1:2 ratios of BCEE:DEA after a reaction time of x days.

Diethylamine also forms crystalline deposits in the presence of AlLi alloy wire.

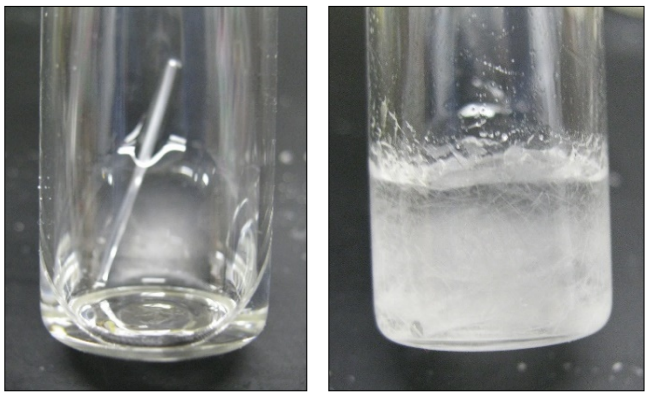

Figure 80: Vials containing DEA, BCEE and AlLi wire (left), or DEA and AlLi wire (right) after x days of reaction time.

Use of dimethylamine as a solvent and reagent has shown some success but is not entirely sufficient to completely consume the surrogate (BCEE), Figure 81. The reaction will progress as indicated by the formation of crystalline deposits and eventual orange color development. However, some amount of starting surrogate was consistently found in the recovered product. Additives, such as isopropanol, have resulted in similar semi-crystalline products. Interestingly, addition of isopropanol resulted in precipitation of large, flat platelets instead of the typical needle-shaped crystals. The isopropanol may form a complex or otherwise determine the structure of the final product.

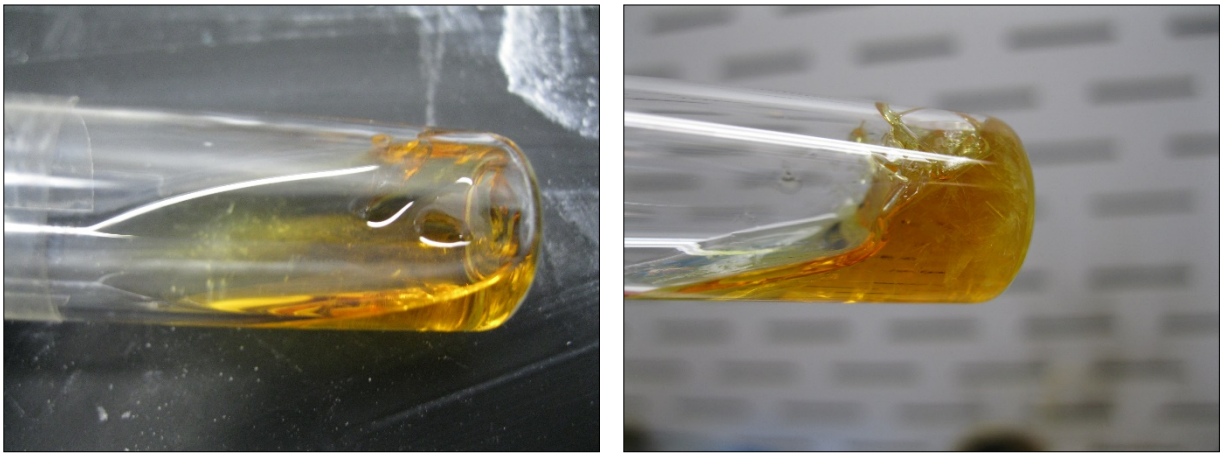

Figure 81. BCEE reacted with DEA and isopropanol (left) after 24 hours and (right) after 6 days. Platelet crystals were observed floating after 24 hours, and had grown to a substantial portion of the entire volume after 6 days.

Diethylamine has not been independently effective at fully neutralizing the surrogate. It was investigated as a solubility enhancing agent for reaction with Li_3N, and other additives. Pressed pellets of Li_3N were submersed in a mixture of BCEE and equimolar DEA/IPA. After an initial reaction period where small bubbles (presumably ammonia) were generated, the pellet developed a layer of LiOH. Further dissolution was not observed, and likely obstructed by the LiOH layer (Figure 82).

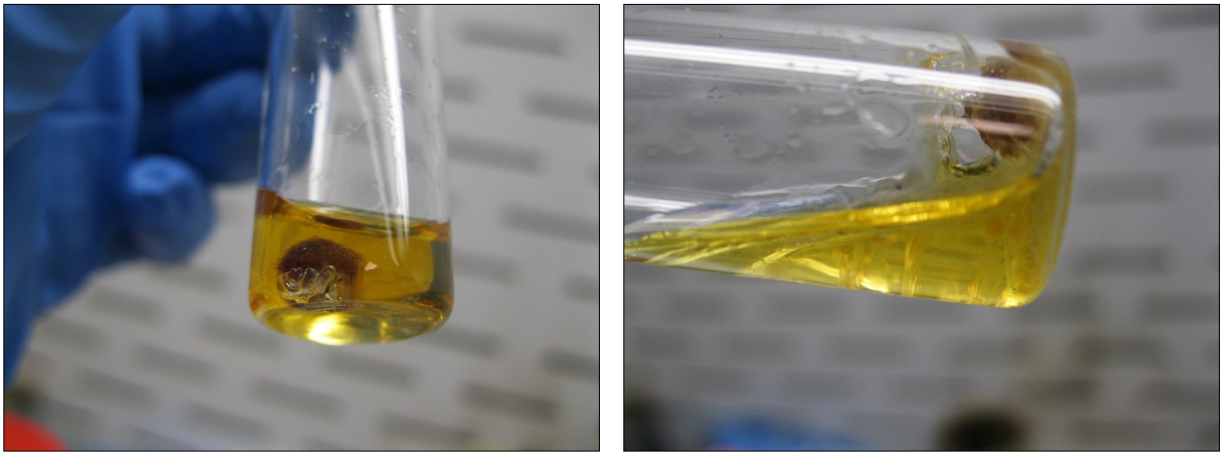

Figure 82. Li_3N pressed pellet after 24 hours (left) and 6 days (right) exposure to DEA/IPA solution.

Fumed silica was also added to DEA as a means to better homogenize and stabilize the mixture with BCEE. An apparently completely solidified product was obtained. Residual BCEE was extracted by adding hexane to the post-reaction product and recovering a light-yellow solution.

Additional efforts to improve the dispersion of reactive chemistry into the surrogate included a solution of ferric chloride in ethanol. A two-phase separation was initially observed, but the solution homogenized easily with moderate agitation. Other metal salt or oxide additives, such as $MgCO_3$, may be a useful HCl scavenger and are under ongoing investigation.

A compatibility test between BCEE and $MgCO_3$ as a loose powder (unpressed, not fabricated as part of the pellet) was allowed to rest for several days. No obvious reaction occurred. Lithium nitride pellets were submerged in the vial with saturated potassium carbonate solution as the reaction initiating water source. A two-phase region developed as the water displaced BCEE. The pellets floated at the brine/surrogate interface. A very faint wispy stream of white precipitate evolved. After an additional two weeks, the pellets had been fully consumed. A companion study was conducted under similar conditions with the addition of diethylamine to the initial reaction mixture. The liquid solidified over night without addition of Li_3N, Figure 83 (left). After resting for five days, the entire bulk material turned an opaque peach color, Figure 83 (right).

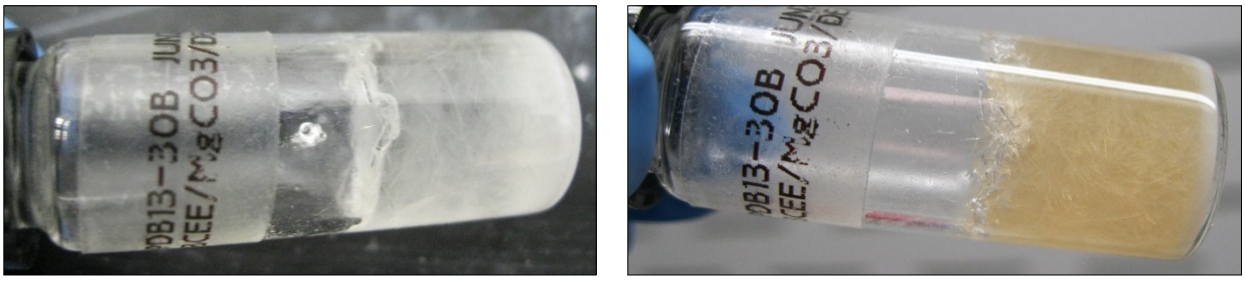

Figure 83. BCEE reacted with $MgCO_3$ and diethylamine after 18 hours (left) and 5 days (right).

Pellets were subsequently fabricated using $MgCO_3$ and Li_3N. The solids were mixed together prior to pressing in a die press. Prepared pellets were added to 1 mL BCEE and 1 mL isopropanol. Dehalogenation of the surrogate would produce hydrochloric acid, which could subsequently react with $MgCO_3$ in order to consume HCl, shift equilibrium, and potentially generate a catalytically active $Mg(OH)_2$ product. Evolution of CO_2 gas should aid mixing, akin to ammonia production from Li_3N. The reaction was conducted in alcohol instead of water to limit aqueous side reactions. Two separate batches of Li_3N were used, one having been air exposed during storage. The aged material reacted slowly (Figure 84 left), while the fresher sample (Figure 84 right) reacted within minutes. Extent of reaction propagation remains a concern, as some material remained unreacted (red layer at bottom of vial, Figure 84 right).

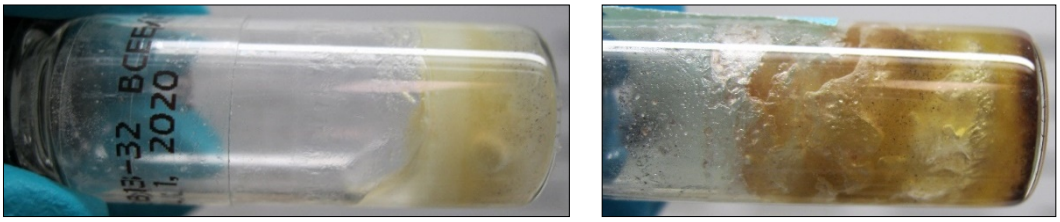

Figure 84. Comparison of aged (left) and new (right) lithium nitride reactivity.

Stoichiometric ratios of $MgCO_3$ and Li_3N were evaluated. Equal mass trials were prepared in which the Li_3N:$MgCO_3$ molar ratio was 1:0, 1:1, or 1:2. A total of 0.49 g material was added to 1 ml BCEE, with the relative molar composition of each powder scaled accordingly. Water was added to each reaction on the basis of 3 equivalents of Li_3N. Due to the low volume of water, reactions were not complete. The 1:1 molar ratio appeared solid but was a viscous slurry; it did appear to fully react as no Li_3N was visible.

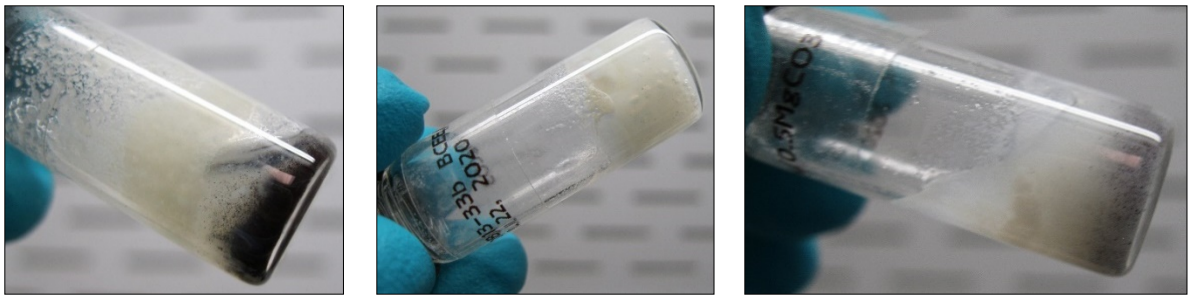

Figure 85. Reactions of BCEE, Li_3N, $MgCO_3$, and water. Li_3N:$MgCO_3$ molar ratio was 1:0 (left), 1:1 (middle), or 1:2 (right).

Larger mass scale-up reactions did not produce well-homogenized results.

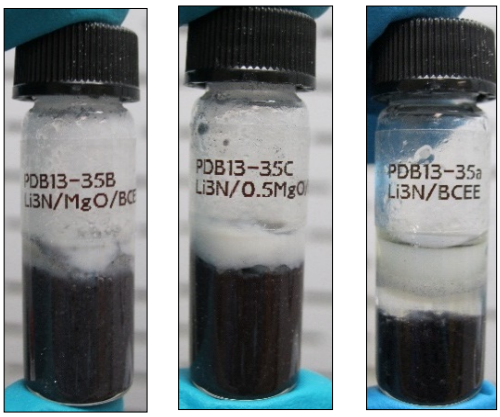

Figure 86. Scaled up reactions of BCEE, Li_3N, $MgCO_3$, and water. Li_3N:$MgCO_3$ molar ratio was 1:0 (left), 1:1 (middle), or 1:2 (right).

Fabrication of pellet proceeded without solid additives. Exploratory efforts found that a wax binder was not needed in order to produce a dense, robust pellet under atmospheric conditions. Similar results could not be achieved in an inert glovebox. Demonstration pellets could also not be fabricated under inert atmosphere. Water vapor was estimated to produce some binding effect for the powder. Substitute organic binders were evaluated. Diethylamine (DEA) was considered as a dual function binder and reagent. Pellets could be produced when sample powder was wetted with DEA under benchtop conditions. A small amount of liquid was expelled when the wetted powder was pressed. Pressed pellets were minimally reactive when tested with BCEE and saturated potassium hydroxide solution. A surface layer evolved over time, and the aqueous phase developed a yellow tint, Figure 87.

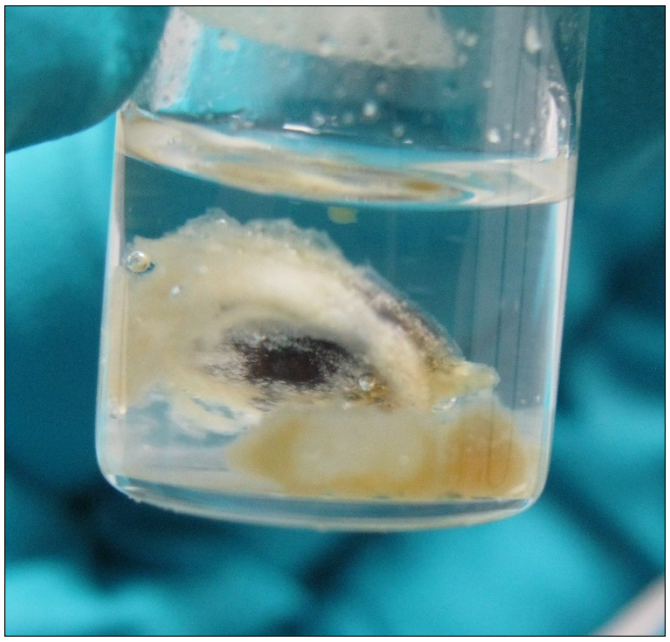

Figure 87. Demonstration of a Li_3N/DEA pressed pellet.

Wax dissolved in hexane was tested as a substitute binder. However, despite dissolving the wax into solvent, it could not be uniformly dispersed through the powder. Fabricated pellets had inconsistent amounts of wax left after immersion in water, Figure 88.

Figure 88. Li_3N/Wax pellet not fully dissolved.

Neat solvents (hexane and 2,3,5-trimethylpentane) were explored next. Similar results were achieved as with the DEA. Excess liquid was expelled from the press. When immersed in water, the pellets were slow to react. Diffusion of the non-polar solvent out of the pellet was observed. Since the solvents were not miscible with water, it was estimated that the solvent could prevent water from reaching the surface of the pellet. Non-polar organic binders were thus determined to be incompatible with the eventual use of the pellets. Water-miscible organic solvents, such as polyethylene glycol, were briefly considered. A demonstration test with Li_3N and 400 MW polyethylene glycol mixed overnight initially was unreactive but had begun to evolve gas by the following morning.

Ambient air pellet fabrication was determined to be the most effective means to produce Li_3N pellets. Fabrication in an inert (no oxygen or water vapor) atmosphere was not feasible without a binder. Since no suitable organic binder could be found, ambient moisture was determined to be suitable. The bulk storage container was maintained in an inert environment, and small aliquots were withdrawn, pressed into pellets, and then returned to the glovebox for inert storage conditions.

The extent of reaction in contact with brine (NaCl or KCl solutions) was evaluated with pellets fabricated in air. A drop of fluorescein dye was added to the brine to enable visual differentiation of the aqueous phase and organic surrogate (DPCP). The brine, prepared from the headspace of NaCl in water, was not dense enough to sink through the surrogate. After five days, the entire volume solidified (Figure 89). A follow-on test was conducted using KCl brine with fluorescein dye applied directly to the surface of an immersed pellet. No immediate reaction was observed, although the surrogate (BCEE) began to turn cloudy after about 10-15 minutes. After four days, the pellet remained intact, but had noticeable residue remaining on the surface (Figure 90).

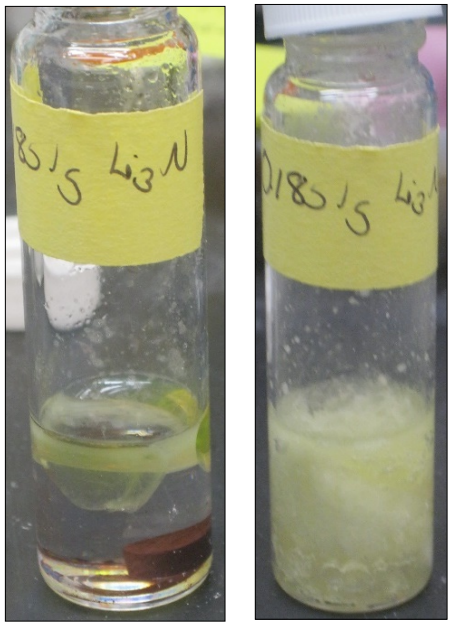

Figure 89 Brine sample as-prepared (left) and aged five days (right).

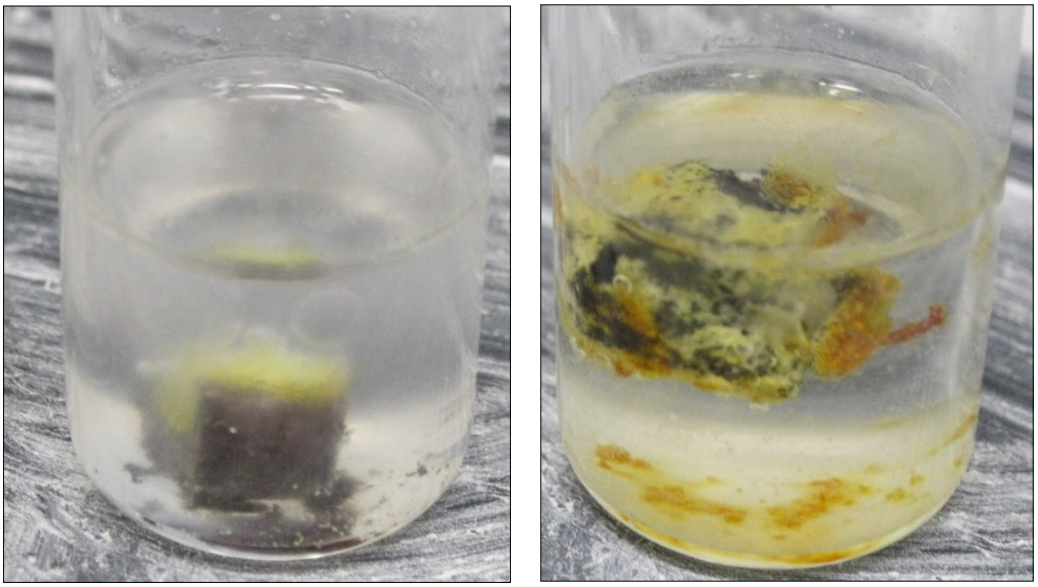

Figure 90 KCl brine with fluorescein dye applied directly to surface of a submerged pellet. Minimal reaction after four days.

The decomposition of Li_3N wetted with surrogate before contact with water was substantially slower than the decomposition of pellets added directly to pure water. The effect of pellet morphology and agitation was investigated to determine if mixing or diffusion was the cause. Replicate vials of Li_3N powder and DPCP, one stirred and one left quiescent, were tested with dyed KCl brine. The brine was added dropwise to each vial, whether stirred or not. Minimal reaction was observed in either vial. The brine remained near the surface of both vials (Figure 91). Some viscous behavior was noted in both vials, although no visible exothermic reaction occurred.

Figure 91 Quiescent (Brine 1, left) and stirred (Brine 2, right) reactions of DPCP and Li_3N powder with dyed KCl brine.

The decomposition product of Li_3N pellets was collected and analyzed via XRD to determine phase composition. In addition to the expected LiOH, Li_2CO_3 and LiO were identified as possible components (Figure 93). The presence of Li_2CO_3 may be due to reaction with atmospheric CO_2:

$$2LiOH + CO_2 \rightarrow Li_2CO_3 + H_2O$$

The presence of a variety of salts may impact hydrolysis of the surrogates. Hydrolysis tests of DPCP in various salt solutions were conducted. Solid NaCl in DPCP was unreactive; but a mixture of 0.27 g NaCl in 1 mL DPCP and 1 mL DI H_2O slowly solidified (≈1/2 by volume) after three weeks. A replicate trial using reduced water conditions (0.24 g NaCl, 0.1 mL DI H_2O, 1 mL DPCP) resulted in an opaque slurry (Figure 92) which eventually completely dried after three weeks.

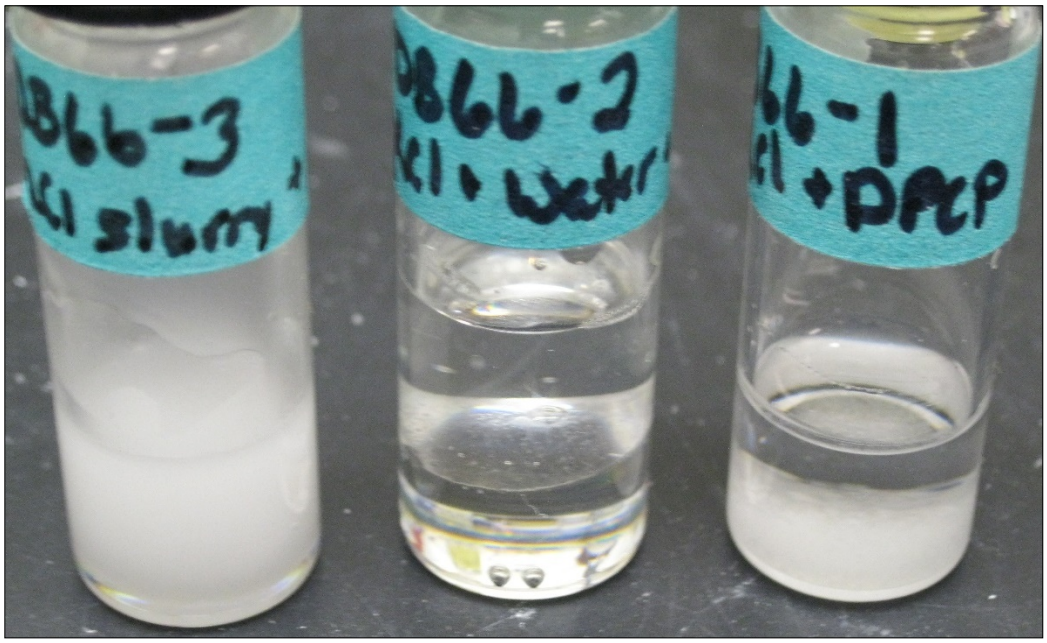

Figure 92 Sodium chloride brine hydrolysis tests with DPCP.

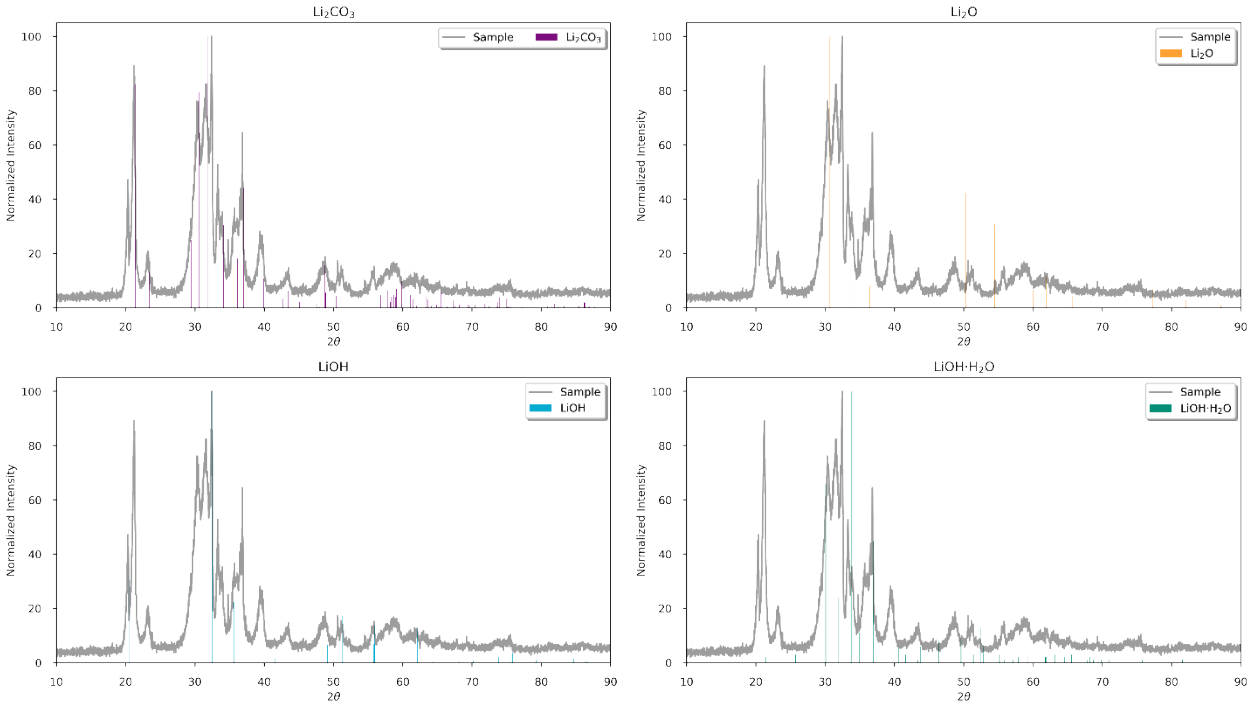

Figure 93 XRD plot of decomposed Li3N residue. Plausible matches to LiOH, Li_2CO_3, weak match to Li_2O.

Similar tests were conducted with sodium citrate, resulting in a viscous, partially crystallized mixture. After three weeks, no free liquid remained in the vial (Figure 94).

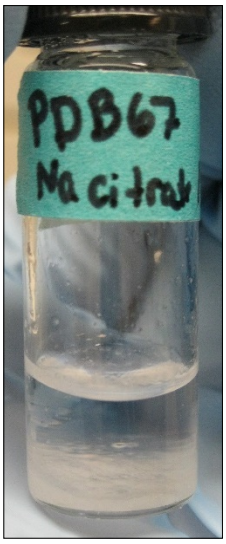

Figure 94 Sodium citrate hydrolysis test with DPCP.

Saturated NaOH and KOH tests were conducted with DPCP. After four days, the vial was entirely solidified, and needle-shaped crystals were growing from the solid surface (Figure 95). Presence of salt products was evaluated to not be an interference with Li_3N decomposing the surrogates. Inhibition of the Li_3N reaction with water was proposed as a possible cause of inconsistent reaction rates.

Figure 95 Fully solidified DPCP after four days exposure to a deliquescent slurry of NaOH flakes.

Accumulation of a surface layer of LiOH (or Li_2CO_3) was hypothesized as an inhibitory mechanism to the reaction of Li_3N with organic surrogates. A side reaction between carbonic acid from ambient CO_2 and water vapor was considered as a possible source of lithium carbonate noted in the decomposition product (see Figure 93).

$$2Li_3N + H_2CO_3 \rightarrow Li_2CO_3 + NH_3$$

Various carboxylic acids were tested to decompose produced lithium carbonate on the pellet. Surface adsorbed carbonic acid was considered unavoidable, and may lead to decreased overall reactivity of aged pellets. Citric acid was added to a test pellet of Li_3N in triethyl citrate as a complimentary organic phase. The pellet reacted vigorously to applied drops of acid solution and did not develop a grey surface coating. Additional solution continued to cause a fresh reaction. A second test adding neat citric acid solution to a Li_3N pellet resulted in a brief exothermic reaction, but did not continue as more liquid was added. After five days, the fluid had gelled, and a small amount of Li_3N solid appeared to be entrained at the surface in froth.

The physical configuration of the Li_3N pellet was considered as a possible contributing factor to the overall reaction rate. Delithiation of lithium nitride may have an intermediate energy barrier that can be more easily overcome when densely packed in a pellet. If the first delithiation step is much faster than the remaining two, a brief initiation followed by much slower kinetics could result in incomplete reactions. A dense pellet would provide more energy in a smaller volume, increasing the likelihood that subsequent reactions would progress:

$$Li_3N + H_2O \rightarrow Li_2HN + LiOH$$

$$Li_2HN + H_2O \rightarrow LiH_2N + LiOH$$

$$LiH_2N + H_2O \rightarrow H_3N + LiOH$$

A kinetics test was conducted with Li_3N powder uniformly stirred in hexane while water was added dropwise. The entire volume of dispersed powder reacted rapidly. Reaction kinetics are therefore unlikely to be impacted by pellet density.

Oleic acid was evaluated as an oily carboxylic acid to introduce reactive functional groups to the pellet while avoiding the miscibility problems associated with water. A pellet immersed in oleic acid with water added to the immediate surface reacted slowly. After twenty minutes, the surface of the pellet developed a grey layer. After two days, the liquid had reacted to form a fluffy white solid. Similar results were observed when reacting Li_3N pellets in oleic acid with acetone and isobutanol as oxygen-containing functional groups. Neat Li_3N powder was mixed with oleic acid in DPCP to test slow degradation activity. No immediate exothermic reaction was observed, but the previously colorless solution developed an amber tint after one week. The use of oleic acid as a Li_3N activator was further tested by immersing a pressed pellet in oleic acid, then adding to DPCP. No observable change occurred.

A validation experiment was conducted to corroborate findings at CBC in which Li_3N pellets reacted in water above the liquid layer of agent. Despite the reaction occurring out of direct contact with the agent, or in a position for the produced ammonia to diffuse through the agent, solidification of the agent was observed. A benchtop experiment to replicate these results was conducted by placing an organic simulant in a vial, covering with water, and then adding a Li_3N pellet. Initial tests were conducted with triethylcitrate as a physical analog to limit the possible unpredictable violent reaction with chemically representative surrogates. Various ratios of water to surrogate were tested while maintaining pellet mass at about 0.3 g in each trial. The pellet reaction time was proportional to the volume of water. In excess water (20 mL TEC, 10 mL H_2O), the pellet reacted rapidly and evolved a vapor plume that turned a witness pH strip blue. The plume is indicative of ammonia formation, and the pellet fully dissolved within a few minutes. A temperature change was evident, and some diffusion of aqueous solution into the organic layer was observed. Smaller volumes of water (25 mL TEC, 5 mL H_2O) resulted in incomplete reactions. At a minimum quantity of (30 mL TEC, 2 mL H_2O), the pellet was initially exothermic, but stopped reacting quickly. Despite the presence of water, the remaining Li_3N did not react. It was postulated that equilibrium conditions of the aqueous phase limited the further production of LiOH. It is likely that excess accumulation of LiOH, rather than insufficient water, is responsible for incomplete reactions observed at CBC. In practice, adding excess water dilutes the LiOH concentration sufficiently to allow the Li_3N decomposition to proceed. Adding other solvents that can dissolve LiOH and improve miscibility with organic liquids would be favorable. Battery electrolytes, such as propylene carbonate, are one possible option. Another may be Cyrene™, a cycloether used as a greener alternative to DMF (Figure 96).

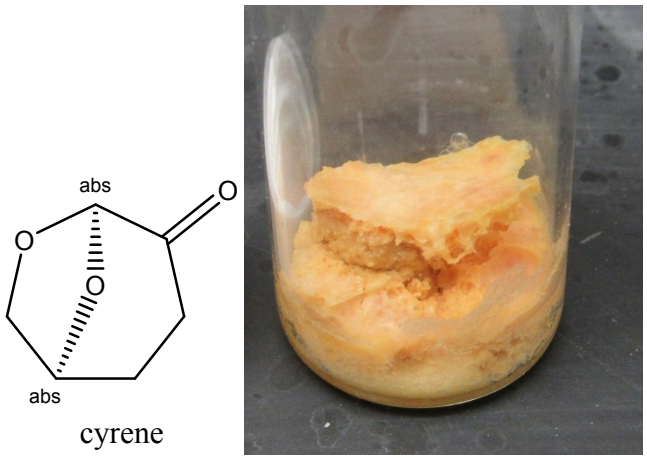

Figure 96 Line structure of Cyrene solvent and reaction product of Li_3N, water, and Cyrene.

Additionally, the conversion of LiOH to Li_2CO_3 may consume lithium ions and alter the equilibrium conditions. Formation of a white insoluble solid has previously (Figure 93) been identified as a mixture of LiOH and Li_2CO_3. The material was subsequently washed and the soluble material was decanted from the insoluble white solid. The soluble fraction was dried and re-analyzed, but found to contain the same composition as before (Figure 97). Since Li_2CO_3 is poorly soluble, it was conjectured that the soluble fraction was initially LiOH rich, but as the solution dried and exchanged CO_2 with the atmosphere, the LiOH reacted to form Li_2CO_3. The produced solid could not be subsequently redissovled in water. Formation of a white solid precipitate on Li_3N pellets is thus likely to be Li_2CO_3. Prolonged air exchange with LiOH-containing aqueous solution is likely to sequester Li ions. While this would shift equilibrium

conditions to enable the Li_3N pellet to fully react, the poor solubility of Li_2CO_3 is likely to form a shell around the pellet.

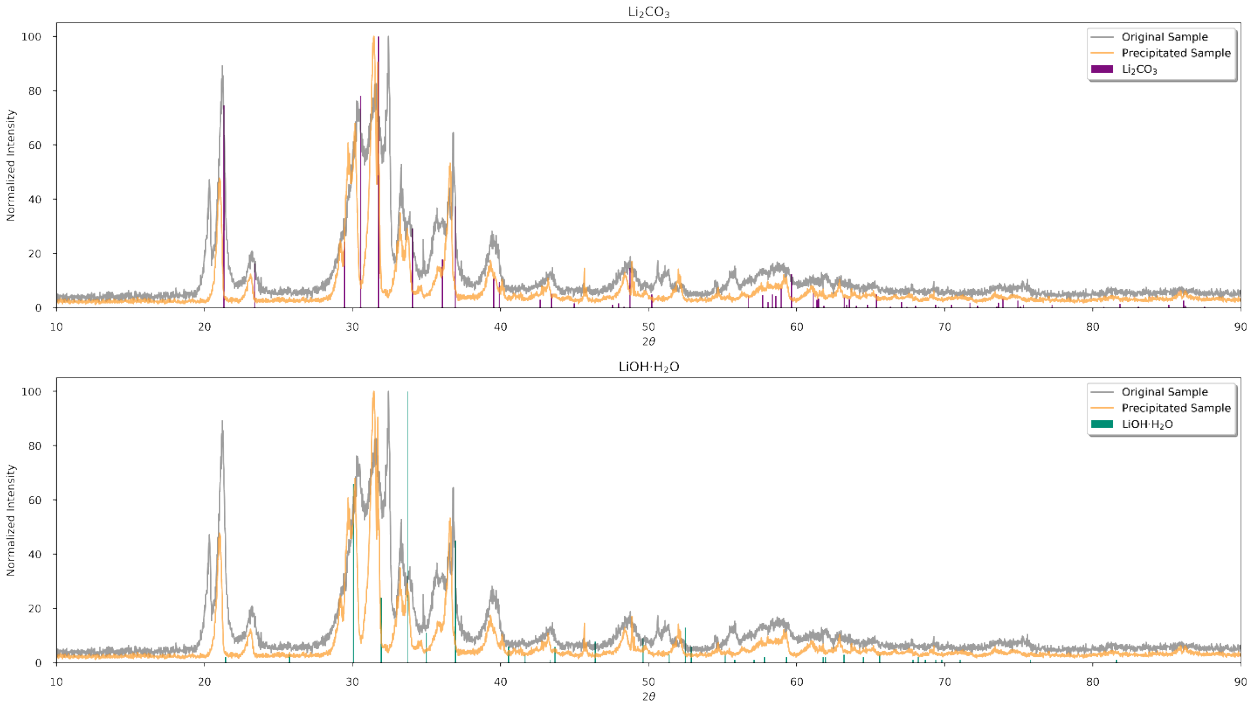

Figure 97 XRD scan of reprecipitated Li_3N decomposition product. The precipitated sample contains Li_2CO_3, which likely formed while drying.

Subtask 6.3.2.3: Test effectiveness at CBC

Reactions of several tablets with GB were studied. The main goal was to monitor the breakup of the reagent pellet in GB, so the ratio of reagent to GB was kept lower than previous studies. (Previous studies seemed to show extra residual unreacted Li_3N on the bottom of the reaction vials.)

All the Li_3N tablets stayed very calm, even after the water was added. The Li_3N pellets that were tested were F09-135H (3%), F09-153H (3%), and F09-138F (2%). In all cases, the pellets did not completely break up in the GB solution, but after 8 days of reaction time, the residual amount of GB was less than 5%. The mixture was not completely solidified, but this may be due to the ratio of reagent to GB being lower (about 5%) than previous studies.

More tablets will be tested that do not contain any wax binder as it was determined Li_3N at Sandia tablets could be fabricated without binder.

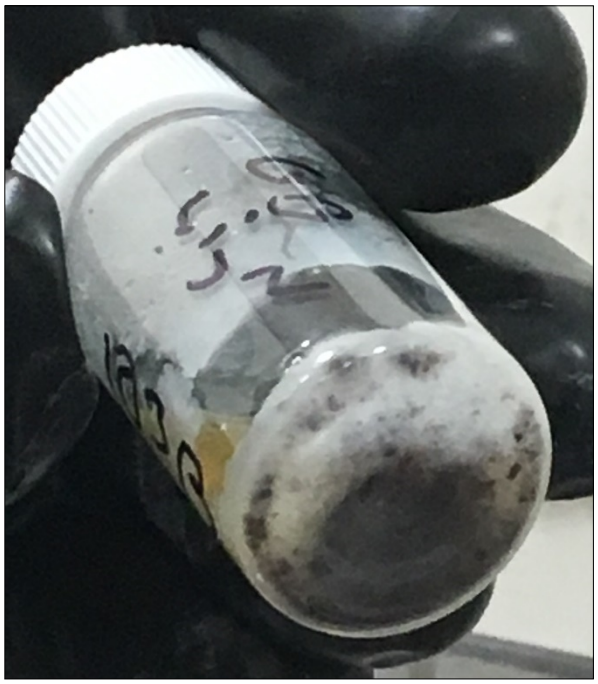

Figure 98. Sample of 6 mL of GB with pellet F09-153H and 0.3 mL H_2O. The pellet is still visibly intact on the bottom of the vial.

Reaction studies were also done with HD and the Li_3N pellets F09-153, F09-138C, and F09-135E. The pellets did not break up in the HD, and they were still visibly intact. As expected from previous studies, no reaction was observed with $Li_3N + H_2O$.

Figure 99. 4.0 mL of HD with pellet F09-138C and 0.4 mL H_2O. The intact pellet can be seen at the bottom of the vial.

Task 7: Ab initio Modeling

Subtask 7.1: Solvation properties (UFR1)

Ab initio molecular dynamics (AIMD) simulation was used as a "gold standard" to benchmark classical force field molecular dynamics (FFMD) for modeling local structures of CAs and simulants. Figure 100 shows two classes of CAs and simulants explored: organophosphorus (OP) and organochlorines (OC). Radial distribution functions (RDFs) were used to investigate the molecular liquid structures of these compounds and to compare the FFMD structure with AIMD.

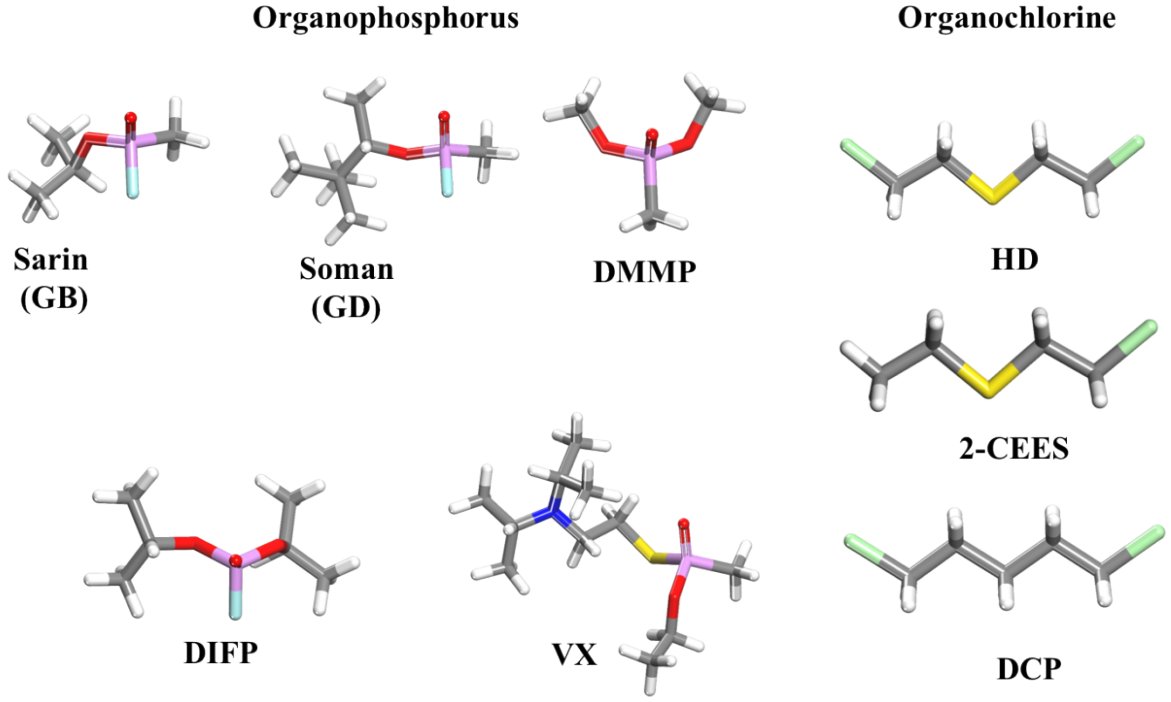

Figure 100. Optimized structures of selected agents and simulants for two classes of agents: organophosphorus and organochlorine. All structures were optimized at the B3LYP/6-311+g(d,p) level of theory. Atom colors are O (red), H (white), N (blue), S (yellow), P (pink), C (grey), F (teal) and Cl (green).

An off-the-shelf force field molecular dynamics (FFMD) package was used with the generalized Amber force field (GAFF) and compared with results from AIMD simulations. To assess the quality of the GAFF parameters, we compared simulated physical and thermochemical properties with experimental results (Table 14).

The computed densities from our FFMD modeling follow a similar trend as experimental measurements, with VX exhibiting the lowest density (1.01 g/cm^3) and DMMP the highest density (1.15 g/cm^3) among the OP compounds. Likewise, calculated densities for OCs follow a similar trend as experimental data, with HD having the lowest density (1.27 g/cm^3) and DCP the highest density (1.11 g/cm^3). Simulation results for the OC densities fall within an acceptable range of ≈ 4 % of the experimental values. For OP densities, simulation results fall between 2.7 to 6.6 % of experimental values. Overall, simulations with GAFF force fields produce reasonable densities compared with experimental values.

Table 14. CA and simulant densities from force field molecular dynamics (FFMD/GAFF) and experiment (Expt.)

CA	FFMD (GAFF)	Expt. g/cm^3	CA	FFMD (GAFF)	Expt. g/cm^3
Sarin	1.118 ± 2.7%	1.088[a]	HD	1.23± 3.2%	1.27[e]
Soman	1.053 ± 2.9%	1.022[a]	DCP	1.064 ± 3.8%	1.106[f]
DMMP	1.178 ± 2.3%	1.151[b]	2-CEES	1.029 ± 3.8%	1.07[g]
DIFP	1.128 ± 6.6%	1.055[c]			
VX	1.032 ± 2.3%	1.008[d]			

a. Langford, R. E. Introduction to Weapons of Mass Destruction-Radiological, Chemical and Biological; John Wiley & Sons: Hoboken, NJ, 2004.

b. G.M. Kosolapoff, *J. Chem. Soc.*,1954, 3222.

c. The Merck Index: An Encyclopedia of Chemicals, Drugs, and Biologicals Merck Index, 11th ed.; Budavari, S., Ed.; Merck & Co.: Rahway, NJ, 1989; p 814.

d. N.B. Munro et al. *Environ. Health Perspect.,* 1999, 933-974.

Enthalpies of vaporization (ΔH_{vap}) were calculated and compared with experiment to validate the FFMD force field (GAFF) (Table 15). Calculated ΔH_{vap} for OPs and OCs follow a similar trend as the experimental values. Overall, the ΔH_{vap} for both classes of CAs and simulants yield reasonable ΔH_{vap} values.

Table 15. Calculated enthalpies of vaporization from AIMD and FFMD simulations compared with experimental results.

OP	FFMD kJ/mol	AIMD kJ/mol	Expt. kJ/mol	OC	FFMD kJ/mol	AIMD kJ/mol	Expt. kJ/mol
Sarin	44.3	56.3	46.9	HD	52.7	63.5	59.8
Soman	52.7	65.4	55.2	DCP	48.5	50.4	50.7
DMMP	50.7	58.0	52.25	2-CEES	41.6	48.2	44.4
DIFP	59.1	59.3	-				
VX	83.3	96.2	80.32*				

Figure 101 shows current RDF plots for OPs based on P-P atom distances on neighboring molecules, and Figure 102 shows running coordination numbers. The AIMD simulation box sizes were kept small for computational efficiency, but still large enough to completely include the first coordination structure (demarcated by the first minimum in the RDF). Some box sizes were large enough to include part of the second coordinating shell of solvent molecules. The results indicate an overall reasonable representation of liquid structures for OPs. FFMD (blue line) results indicate that larger asymmetric alkyl groups demonstrate a slight off-set in structure compared with AIMD results, but the FFMD simulations still capture the overall RDF profile of liquid structures. Figure 103 shows snapshots from the simulations to illustrate the structure of the first coordination shell.

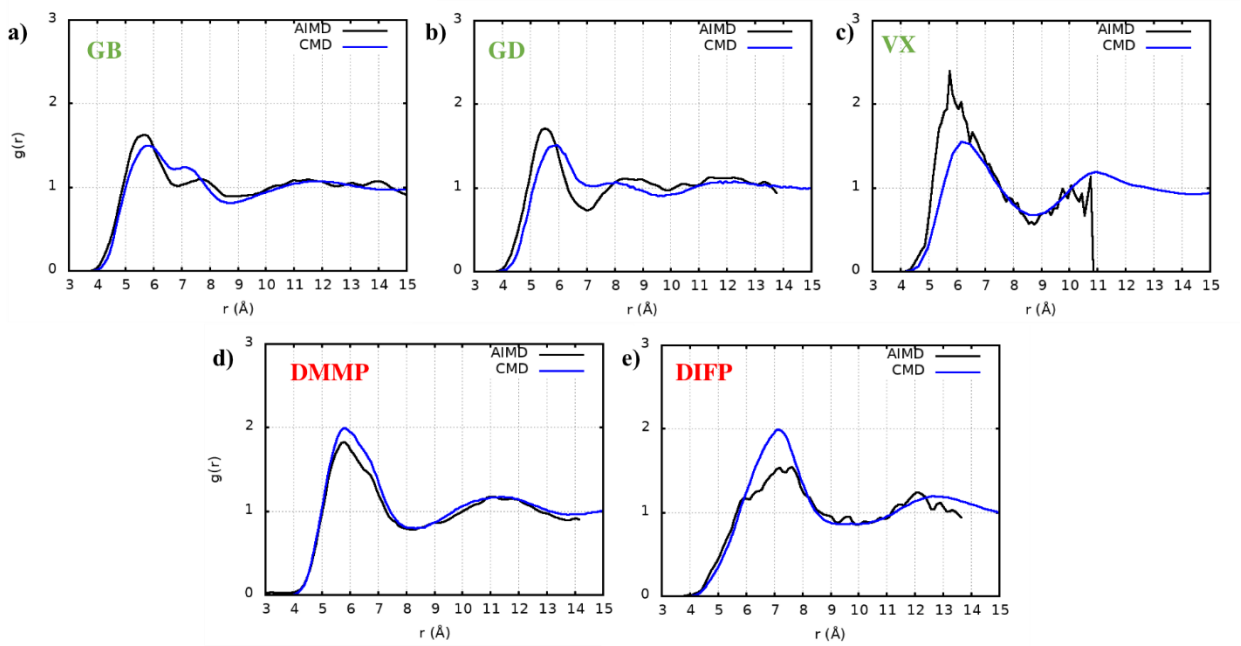

Figure 101. Computed radial distribution functions (RDFs) based on P-P atom distances from AIMD (black curves) and FFMD (blue curves) simulations. Dark green labels represent CAs, and red labels correspond to simulants.

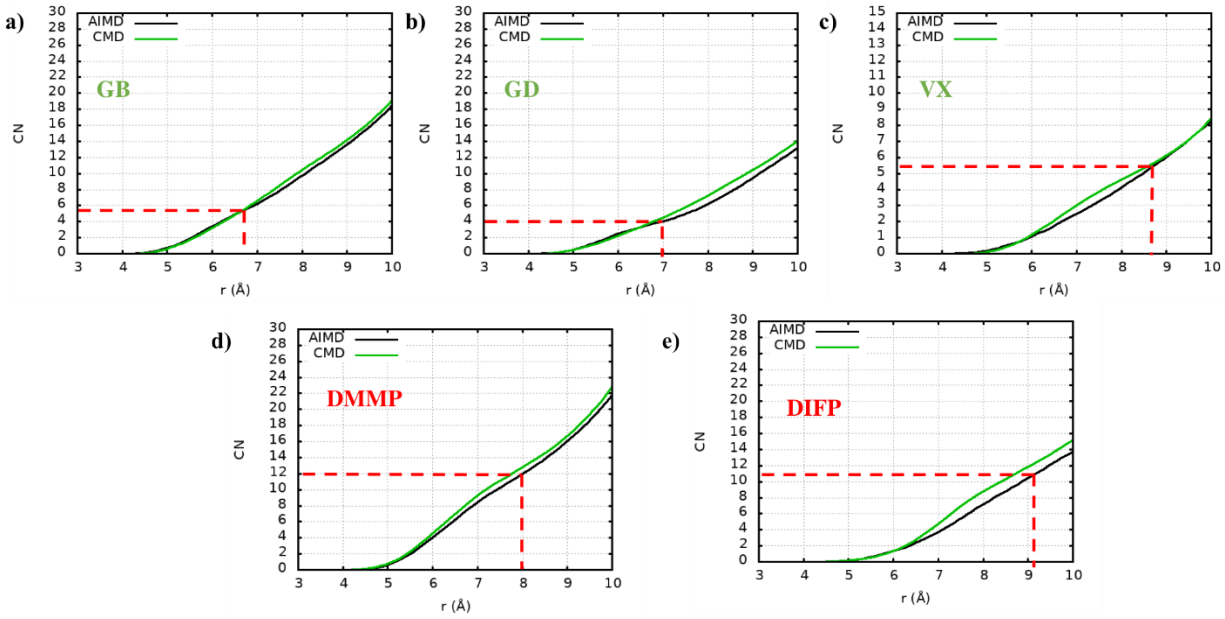

Figure 102. Running coordination numbers for OPs. The black curve represents results from AIMD, while the green curve is for FFMD. The red dashed line is the coordination number within the first coordination sphere from AIMD simulations.

Inspection of the running coordination plots provided further insights into how the compounds pack into their first coordination volumes. As observed in Figure 102 a/b, the asymmetric GB and GD compounds contain larger alkyl groups compared with the other OP compounds, and give lower coordination numbers within the first solvation volume. Additionally, the symmetric DMMP and DIFP molecules follow a similar trend, where DIFP contains bigger alkyl groups and yields a smaller coordination number than DMMP. In general, an overall influence of alkyl group size on the number of coordinating molecules is observed in the running coordination plots.

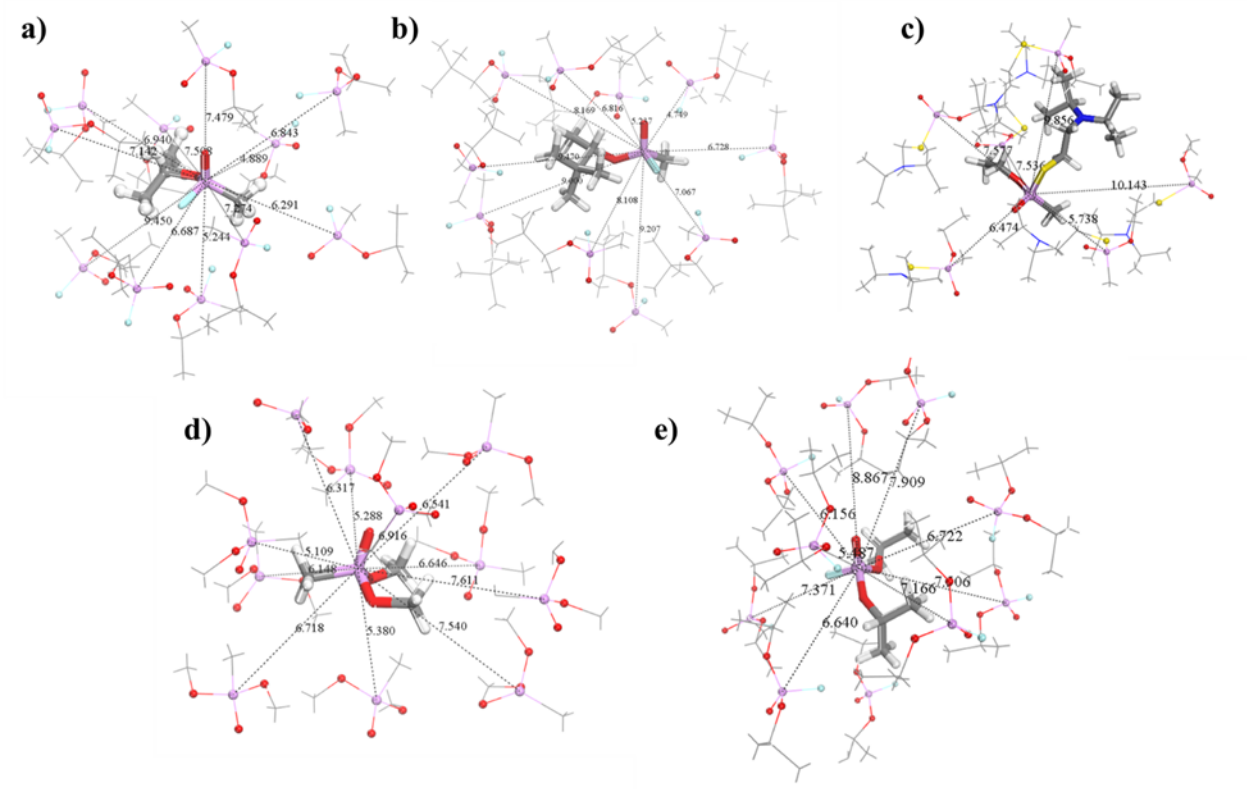

Figure 103. Snapshots of first coordinating solvation shell for a) GB, b), GD c), VX d) DMMP, and e) DIFP. Black lines give distances between phosphates on one OP molecule and its surrounding neighbors within the first coordinating solvation volume.

Trends in solvation structure of OPs can be visualized from snapshots taken from AIMD simulations (Figure 103). The influence of the alkyl group size is observed in the plots. Figure 103-a/b illustrate how GB's propyl group and GD's dimethylbutane groups influence the surrounding environment of coordinating molecules. GB has two molecules separated by the propyl group with distances between 6.9 and 9 A. Likewise, GD exhibits a longer distance of P-P distances between 8 to 9 A. This is consistent with the RDFs for GB and GD present in Figure 101.

Similarly, the liquid structure of OC compounds was explored by comparing RDFs based on S-S distances (HD and CEES) and center C-C distance (DCP), as shown in Figure 104. Short-ranged interactions of OCs are nicely captured with FFMD. For HD and 2-CEES, the AIMD simulation box sizes are large enough to capture most of the second solvation volume. The second peaks in the RDF from FFMD are offset relative to the AIMD structures.

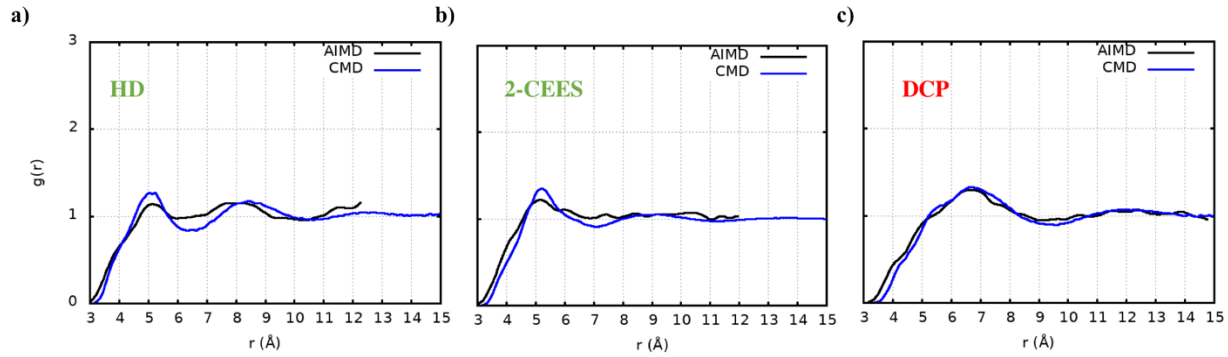

Figure 104. Comparisons of RDF plots for OCs from AIMD (black line) and CMD (blue line). HD and 2-CEES plots are based on the S-S atom distance, while DCP uses center C-C atom distances. Green labels correspond to CAs, red labels correspond to simulants.

The packing of OCs in their liquid environment can be further explored by inspecting running coordination numbers, shown in Figure 105. HD has the smallest coordination number within its first coordination sphere, follow by 2-CEES, and DCP. Overall, DCP gives the best RDF fit and running coordination number fit to its AIMD simulation. Comparing DCP RDF with its coordination number, it is clear DCP has the most surrounding molecules given its wider first peak width. Substituting a center atom from a carbon to a sulfur influences the coordinating environment, illustrated by HD and 2-CEES. The substituted sulfur creates more complexity in the local solvation structure.

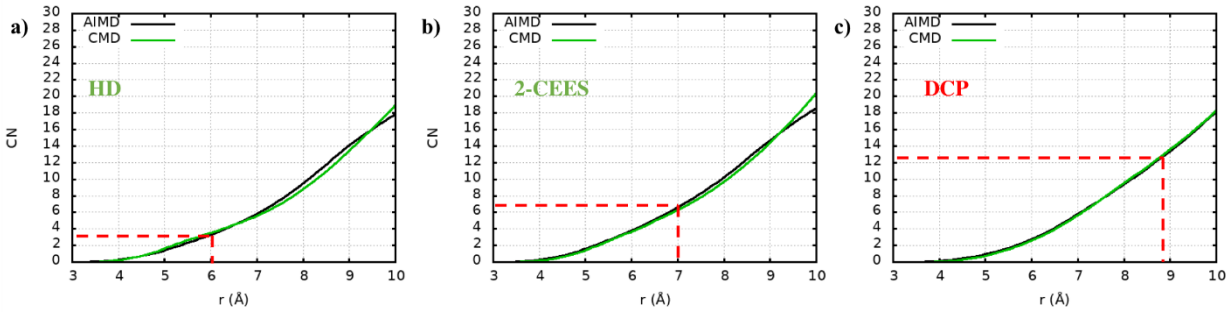

Figure 105. Plots of running coordination number for OCs. The black curve represents results from AIMD, while the green curve is for FFMD. The red dashed line is the coordination number within the first coordination sphere for AIMD simulations.

Snapshots of OCs give a visual inspection of the coordinating environment, shown in Figure 106. The broad first peak for liquid DCP creates a uniform distribution of molecules within its first coordination sphere. However, comparing DCP's first peak to HD's, the substituted sulfur creates substructure in the first peak, producing two peaks. This complexity may be due to van der Waals forces and deficiencies in the dihedral terms from GAFF. These parameters influence how molecules interact due to conformational changes and dispersion forces.

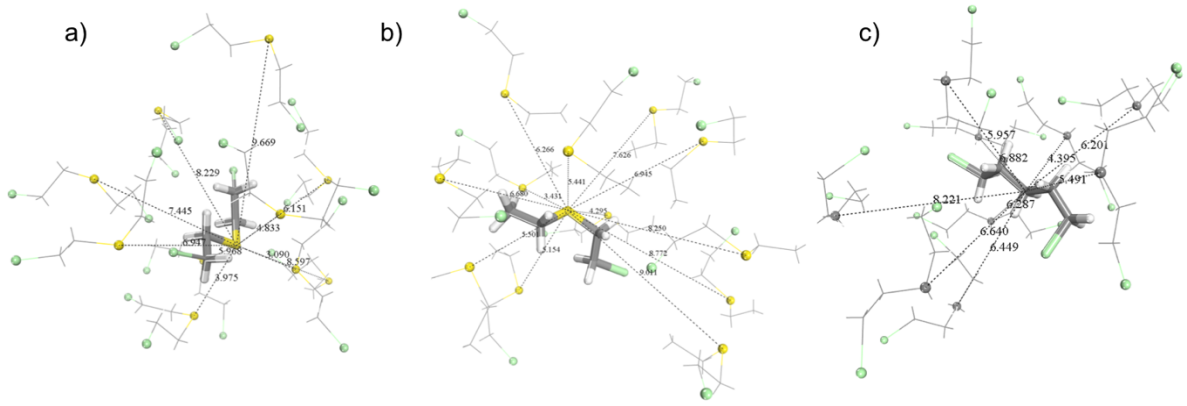

Figure 106. Snapshots of first and second coordinating shells from AIMD for a) HD b) 2-CEES, and c) the first shell for DCP. Black lines give distances of surrounding OPs within the first coordinating solvation volume.

Subtask 7.2: Oligomer reaction mechanism

We explored chemical reactions and dissociation pathways involving VX (Table 16). In the first study, we interrogated the hydrolysis of VX by OH^-. From initial inspection of VX hydrolysis results, we see that cleavage of the P-S bond is favored over dissociation of the P-O (ethoxy) bond.

Table 16. Calculated free energy from two reaction pathways.

Reactants	Products	Free energy (kJ/mol)
$VXEtOH^+ + OH^- \rightarrow$	$VX\_OH\_RS + EtOH$	-126.76
$VX\_RSH^+ + OH^- \rightarrow$	$VX\_OH\_EtO + RSH$	-128.69

We have performed several DFT calculations relevant to VX decontamination from the hydrolysis of OH^- and NH_3. The reaction of VX with NaOH results in two solvolysis reaction pathways: cleavage of P-S and P-O bonds. We explored the different pathways by calculating the free energy of reaction (ΔG_{rxn}) for each elementary step (Table 17). Figure 107 shows the two different pathways involving the P-S and P-O cleavage from OH^-. Our ΔG_{rxn} calculations determined that the initial P-S cleavage has a slight propensity for displacement over P-O cleavage, with -61.14 kcal/mol for P-S compared with -59.27 kcal/mol for P-O. Additionally, the final displacement requires an H_2O molecule to assist in completing the decontamination process. Furthermore, during the reaction we predict that dimerization by the formation of a disulfide bond is possible by the interaction of two DESH molecules.

The decontamination of VX from the reaction with NH_3 was also considered. NH_3 is a by-product from the interaction of Li_3N with H_2O. Figure 108 shows a reaction flow chart for two different pathways: 1) displacement of RS^- and 2) displacement of EtO^-. The initial steps are calculated to have a positive free energy, with the P-S cleavage being less positive than P-O. Table 18 gives the calculated free energies. Although the initial step is thermodynamically less favorable among the other intermediate steps, the overall reactions are negative in free energy change. Furthermore, similar to neutralization of VX with OH^-, the last step requires a H_2O molecule to complete the reaction. Calculations of VX reactions with OH^- and NH_3 Have been performed in the gas phase and with implicit solvent (water).

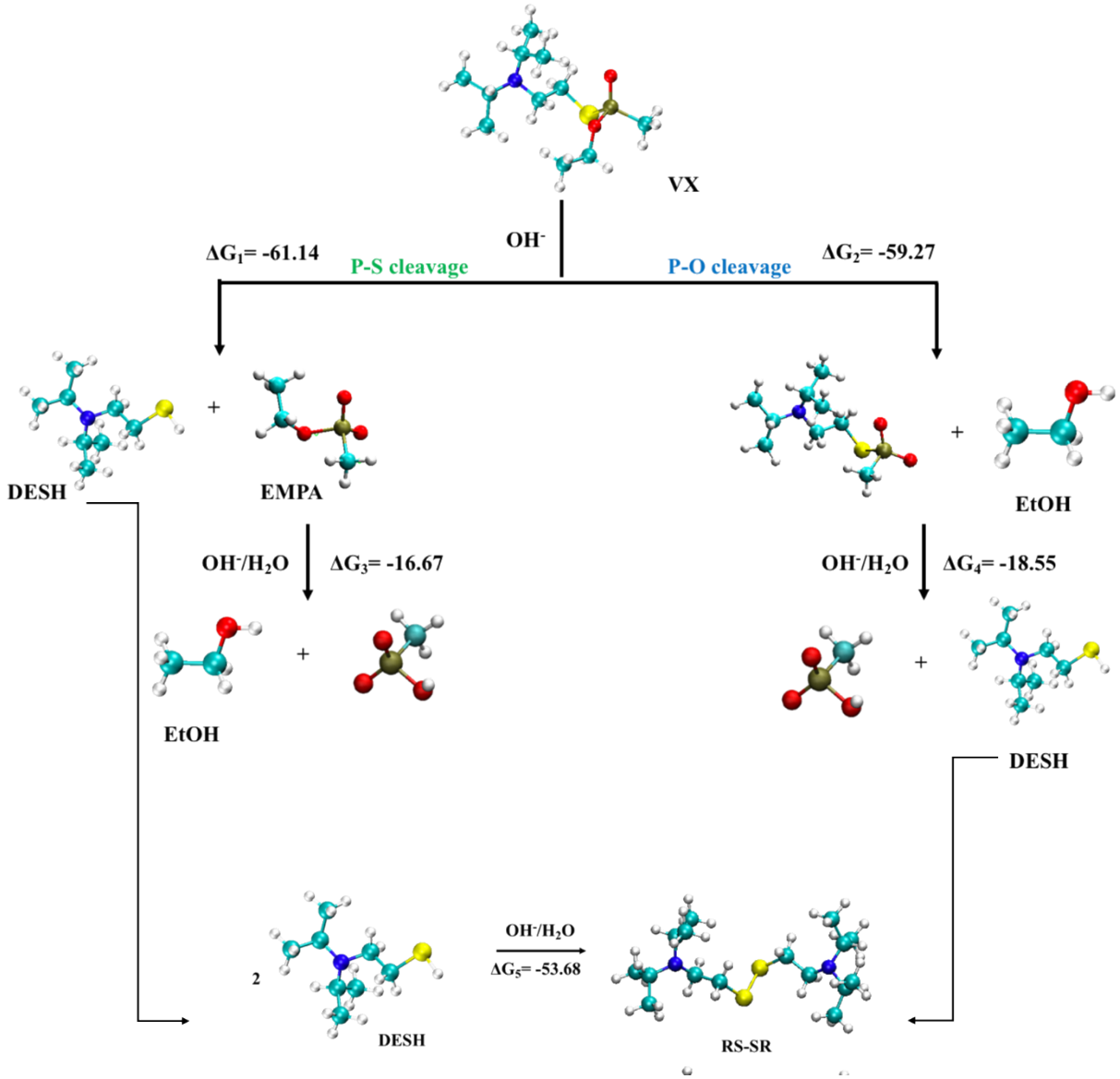

Figure 107. Reaction diagram for the neutralization of VX from the hydrolysis of OH^-, including possible DESH dimerization pathways.

Table 17. Free energies for proposed destruction mechanism of VX with OH^-.

Cleavage	Reactants				Products			ΔG (kcal/mol)
1st P-O	$P(=O)(-OC_2H_5)(-SNC_8H_{18})(-CH_3)]$	+	OH^-	⇋	C_2H_5OH	+	$[P(=O)(O-)(C_8H_{18}NS)(CH_3)]-$	-59.27
2nd P-S	$[P(=O)(O^-)(C8H_{18}NS)\ (CH_3)]^-$	+	H_2O	OH- ⇋	$C_8H_{18}NSH$	+	$[P(=O)(O-)(OH)(CH_3)]-$	-18.55
1st P-S	$[P(=O)(C_2H_5O)(C_8H_{18}NS)\ (CH_3)]$	+	OH^-	⇋	$C_8H_{18}NSH$	+	$[P(=O)(O-)(C_2H_5O)(CH_3)]-$	-61.14
2nd P-O	$[P(=O)(O^-)(C_2H_5O)(CH_3)]^-$	+	H_2O	OH- ⇋	C_2H_5OH	+	$[P(=O)(O-)(OH)(CH_3)]-$	-16.67

Table 18. Free energies for proposed destruction mechanism of VX with NH_3.

Cleavage	Reactants				Products			ΔG (kcal/mol)
1st P-O	$P(=O)(-OC_2H_5)(-SNC_8H_{18})(-CH_3)]$	+	NH_3	⇋	C_2H_5OH	+	$[P(=O)(NH_2)(C_8H_{18}NS)(CH_3)]$	13.98
2nd P-O	$[P(=O)(NH_2)(C_8H_{18}NS)(CH_3)]$	+	OH^-	⇋	NH_3	+	$[P(=O)(O^-)(C_8H_{18}NS)(CH_3)]^-$	-73.25
2nd P-O	$[P(=O)(NH_2)(C_8H_{18}NS)(CH_3)]$	+	OH^-	⇋	DESH	+	$[P(=O)(O^-)(NH_2)(CH_3)]^-$	-41.61
3rd P-O	$[P(=O)(O^-)(C8H_{18}NS)(CH_3)]^-$	+	H_2O	OH- ⇋	DESH	+	$[P(=O)(O^-)(OH)(CH_3)]^-$	-18.55
3rd P-O	$[P(=O)(O^-)(NH_2)(CH_3)]^-$	+	H_2O	OH- ⇋	NH_3	+	$[P(=O)(O^-)(OH)(CH_3)]^-$	-50.19
1st P-S	$P(=O)(-OC_2H_5)(-SNC_8H_{18})(-CH_3)]$	+	NH_3	⇋	DESH	+	$[P(=O)(NH_2)(C_2H_5O)(CH_3)]$	4.15
2nd P-S	$[P(=O)(NH_2)(C_2H_5O)(CH_3)]^-$	+	OH^-	⇋	C_2H_5OH	+	$[P(=O)(O^-)(NH_2)(CH_3)]^-$	-31.79
2nd P-S	$[P(=O)(NH_2)(C_2H_5O)(CH_3)]^-$	+	OH^-	⇋	NH_3	+	$[P(=O)(O^-)(C_2H_5O)(CH_3)]^-$	-65.30
3rd P-S	$[P(=O)(O-)(NH_2)(CH_3)]^-$	+	H_2O	OH- ⇋	NH_3	+	$[P(=O)(O^-)(OH)(CH_3)]^-$	-50.19
3rd P-S	$[P(=O)(O-)(C_2H_5O)(CH_3)]^-$	+	H_2O	OH- ⇋	C_2H_5OH	+	$[P(=O)(O^-)(OH)(CH_3)]^-$	-16.67

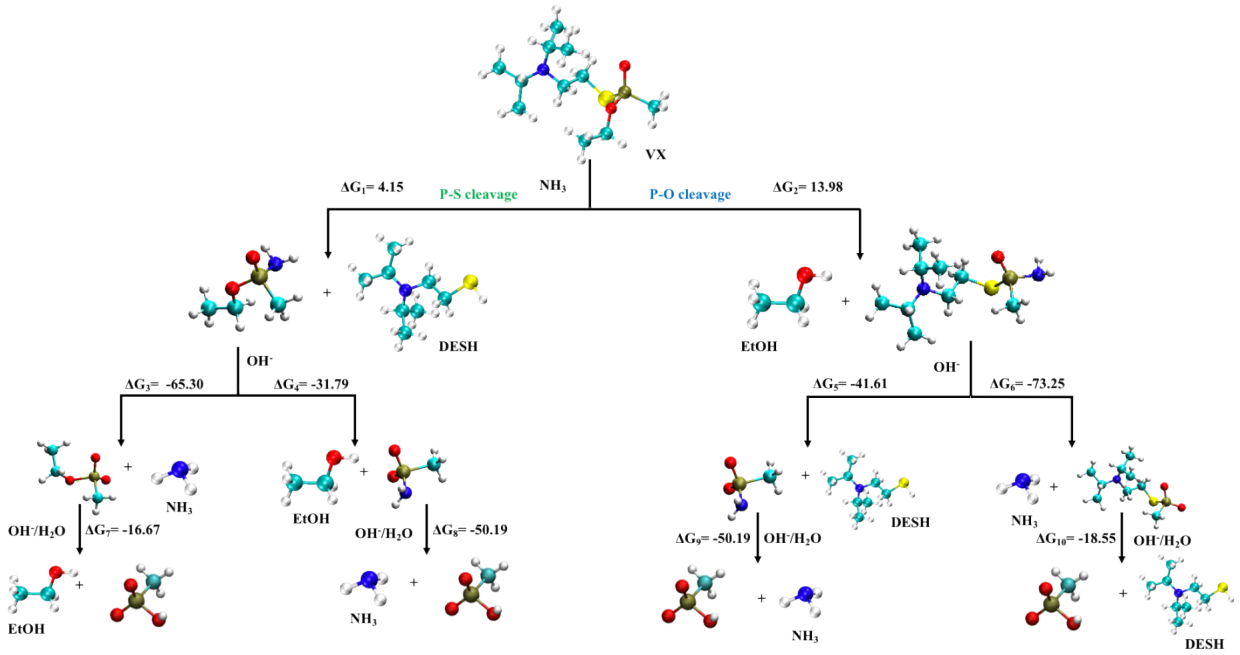

Figure 108. Reaction diagram flow chart for the neutralization of VX with NH_3.

Lastly, we compared the neutralization reaction of GB with OH^- to that of VX. We found that cleavage of the P-F and P-O bonds by OH^- are comparable to one another in free energy, with displacement of $C_3H_7O^-$ slightly more favorable. (Figure 109). The two pathways show a less thermodynamically favorable subsequent displacement (Step 2).

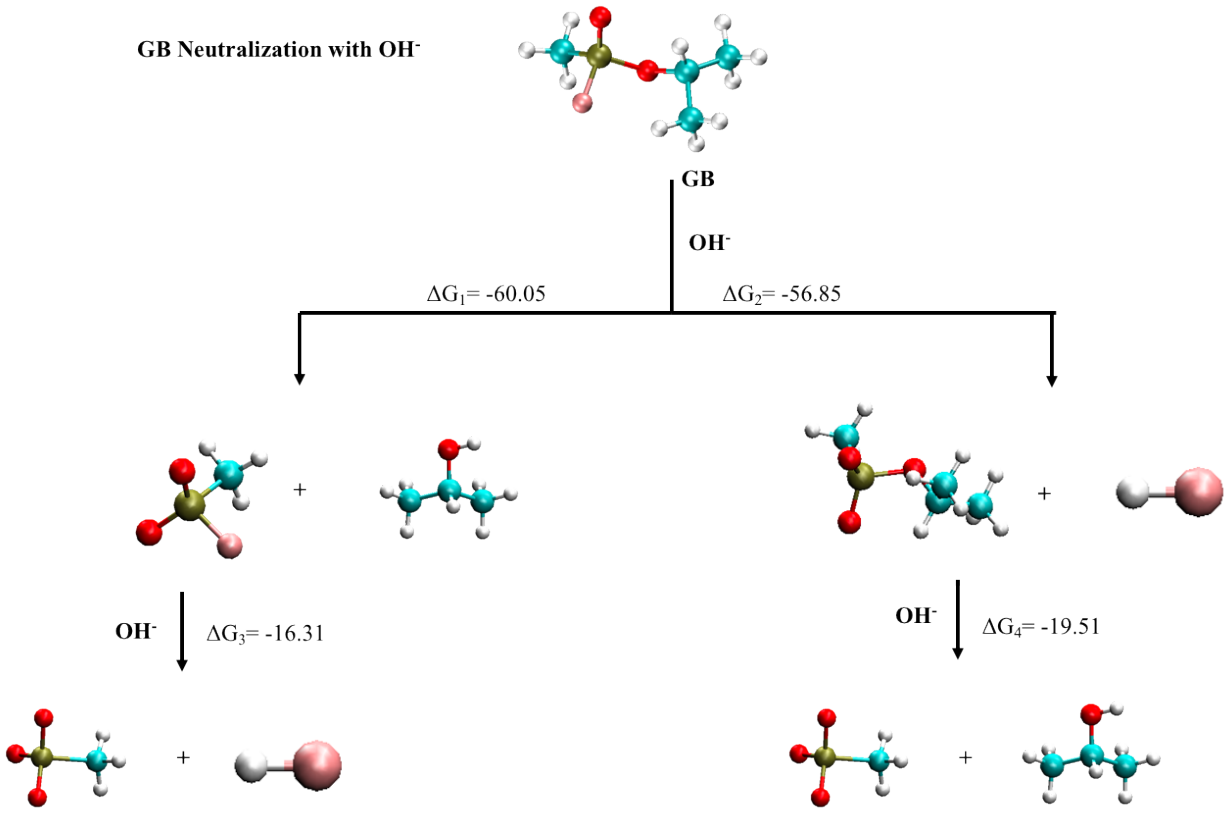

Figure 109. Reaction diagram for the neutralization of GB from the hydrolysis of OH^-.

Complete destruction of VX by alkoxides was studied by DFT methods with gas-phase free energy calculations (Figure 110). The reactions show the products after an addition-elimination reaction, where the incoming nucleophiles displace one of the ligands, the P-S or P-O sites. Among the different alkoxides, the P-S cleavage has shown to be the most favorable for the first step. The first step addition-elimination reaction is mostly favorable with MeO-, follow by PrO-, and then EtO-. Moreover, a second elimination after the first addition-elimination with EtO is not observed.

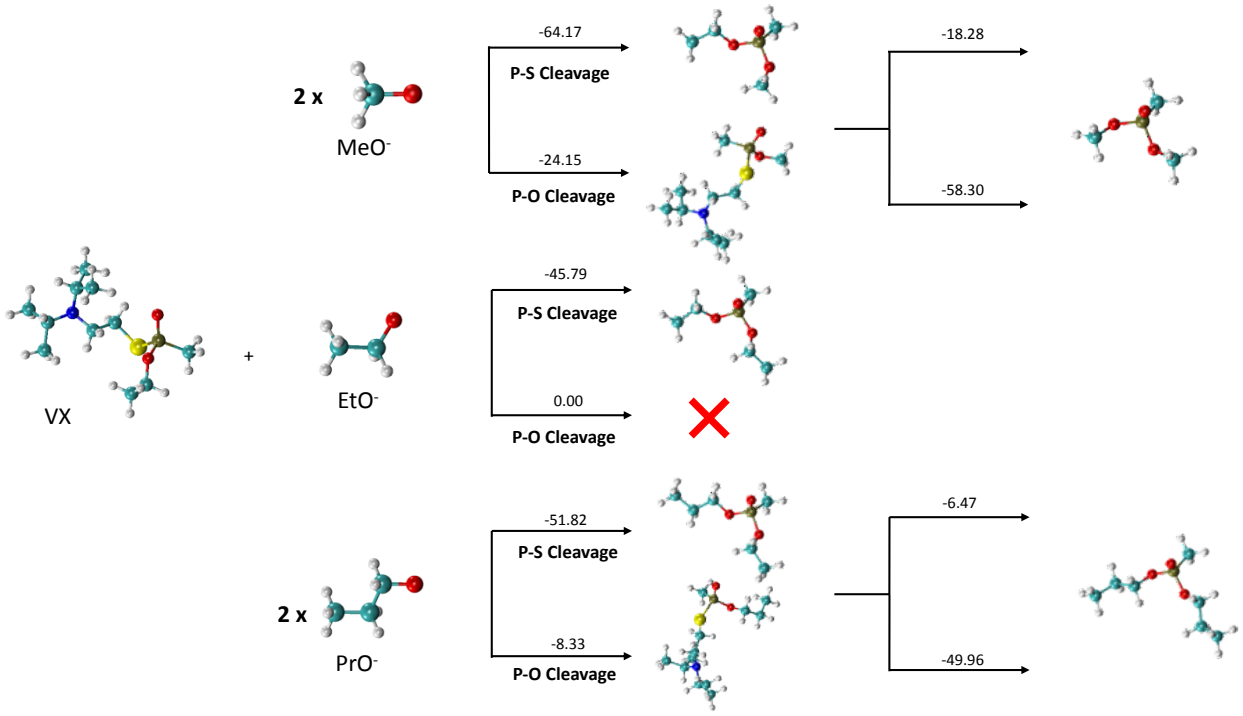

Figure 110. Schematic of the reaction of VX with alkoxides (MeO-, EtO-, and PrO-).

A goal of this subtask is to assist experimental studies with insight into the formation of the intermediates and products in the reaction of HD with different kinds of amines, specifically, unsubstituted amine, ethylamine, and diethylamine. To explore the spontaneity and make comparisons of the reaction pathway intermediates and transition states, we investigated two reaction pathways, S_N2 and E2 (Figure 111).

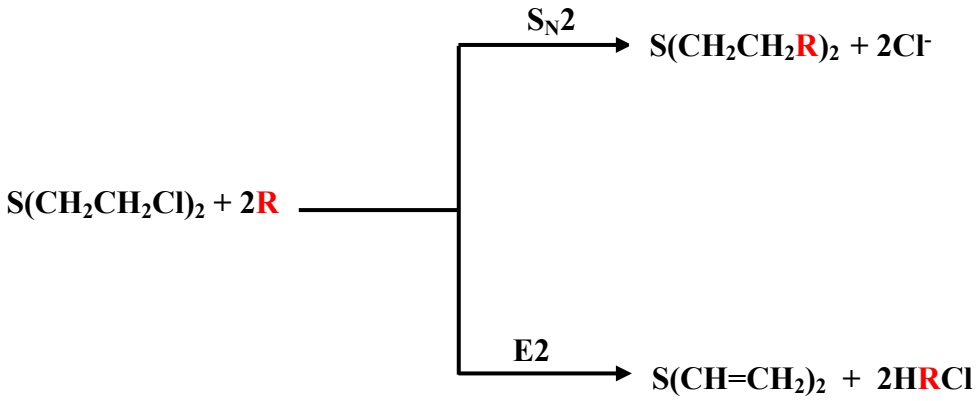

Figure 111. Generalized pathways of S_N2 and E2 for reaction of sulfur mustard with amines.

Calculated reaction energies for HD and BCEE (Figure 112) with various amines were studied to provide theoretical insight to the spontaneity of the reactions. We explored HD pathways of S_N2 and E2 elimination reactions (Figure 113 and Figure 114). Each reaction requires two intermediates and two transition states to form their theoretical products. The S_N2 reaction undergoes two sequential displacement steps that involve the substitution of each chlorine atom with an amine to form either a primary, secondary, or tertiary product (Figure 113 shows tertiary). On the contrary, HD can go through an E2 elimination pathway that involves a sequential twofold hydrogen abstraction that includes the formation of a carbon-carbon pi-bond that, in-turn, kicks-off chlorine atoms to form the twofold unsaturated product (Figure 114). Calculated free energies are shown in Table 19.

Table 19. Transition states, intermediates, and product free energy values (kcal/mol) relative to reactants along E2 and SN2 reaction pathways.*

Dielectric 78 E2/S_N2	TS1	IM1	TS2	Product
HD + NH_3	26.19/24.63	-19.10/-12.63	14.96/17.22	-33.28/-20.61
BCEE + NH_3	31.01/27.22	-15.13/-7.98	15.56/21.40	-30.84/-16.66
HD + $H_2NCH_2CH_3$	23.62/22.17	-18.92/-15.16	10.83/12.45	-33.09/-25.74
BCEE + $H_2NCH_2CH_3$	25.59/27.88	-18.35/-13.15	10.83/14.07	-37.27-25.24
HD + $HN(CH_2CH_3)_2$	22.92/20.79	-25.20/-23.40	3.94/20.73	-45.64/-39.92
BCEE + $HN(CH_2CH_3)_2$	25.88/27.99	-23.40/-13.80	10.40/31.40	-43.14/-25.84
Dielectric 3.6 E2/S_N2				
BCEE + $HN(CH_2CH_3)_2$	34.05/35.22	-2.90/-14.41	29.33/24.84	-4.09/-26.24

* Dielectric refers to the dielectric constant used to represent the solvent (continuum model). A dielectric constant of 78 corresponds to water, 3.6 corresponds to diethylamine.

Given the pathways, (Figure 113 and Figure 114) we explored the free-energy difference (relative to reactants) along the reaction paths with each amine in different solvent environments (water and diethylamine). First, we compared E2 and S_N2 reaction pathways of HD in water (dielectric constant 78, Figure 115). Starting from the reactants to the first transition state (TS1), we immediately noticed significant energy barriers among the E2 and S_N2 reactions between the different amines: TS1 energies are between 22.92 to 26.19 kcal/mol for E2, and 20.79 to 27.99 kcal/mol for S_N2. Diethylamine ($HN(CH_2CH_3)_2$) resulted in the lowest energy barrier for E2, while ethylamine ($H_2N(CH_2CH_3)$) resulted in the lowest barrier for S_N2. After crossing TS1, the reactions fall into a local minimum as an intermediate (IM1), then to the final product via the second transition state (TS2). The S_N2 reaction results in the addition of the amine from the substitution of a chlorine atom. (Figure 113). E2 results in the double bond formation from the first abstraction of a hydrogen (Figure 114). For both E2 and S_N2, $HN(CH_2CH_3)_2$ exhibits the lowest free-energy, -21.28 kcal/mol and -23.40 kcal/mol, respectively. TS2 shows a relatively lower energy barrier for diethylamine along the E2 pathway (3.94 kcal/mol), while a larger barrier exists for the S_N2 pathway (20.73 kcal/mol). After crossing TS2, the reaction falls into a global

minimum for both S_N2 and E2 reactions. Overall, the E2 pathway exhibits the lowest free energy for the formation of the unsubstituted product that ranges between -45.64 to -33.09 kcal/mol. The formation of the tertiary amine exhibits the most stable reaction among the amines. However, the high initial energy barrier required for any of these reactions suggests very slow rates at room temperature.

Likewise, we explored the BCEE reaction pathways in water (dielectric constant 78), see Figure 116. Like HD, BCEE follows a similar trend with few differences among the energy barriers and intermediate states. Along the S_N2 pathway, the different amines experience TS1 energy barriers between 27.22 and 27.99 kcal/mol, while E2 has TS1 barriers between 29.59 and 31.01 kcal/mol. The elimination of the first hydrogen has the largest TS1 (31.01 kcal/mol) for NH_3, while $HN(CH_2CH_3)_2$ has the largest TS1 barrier for S_N2. Upon crossing E2 and S_N2 TS1, a first intermediate (IM1) is achieved. The S_N2 has minimum free energy between -13.85 to -7.98 kcal/mol with $HN(CH_2CH_3)_2$ forming the most stable intermediate. The first carbon-carbon double bond is formed more favorably with diethylamine, but only slightly lower than ethylamine (-13.15 kcal/mol). Additionally, the formation of IM1 (first double bond formation) is more stable with diethylamine. To move from the first minimum to the second transition state (TS2), energy barriers of 14.07 to 31.40 kcal/mol exist along the S_N2 pathway, with ethylamine having the lowest barrier and diethylamine having the largest. However, the E2 pathway exhibits larger barriers ranging between 10.40 to 15.45 kcal/mol, with diethylamine having the lowest barrier. After TS2, the reaction proceeds to formation of the twofold substituted amine product (similar to Figure 114) with twofold substituted tertiary amine having the lowest energy and primary amine with the greater free energy. It should be noted that in all cases diethylamine forms the most stable intermediates and products along both pathways.

Additionally, we explored the E2 and S_N2 pathways of BCEE with $HN(CH_2CH_3)_2$ in a dielectric of 3.6 (dielectric of $HN(CH_2CH_3)_2$), see Figure 117. In general, E2 exhibits the most favorable pathway, while S_N2 is less favorable. For both pathways, the TS1 energy barrier decreases as the solvent dielectric medium increases (*i.e.*, lower TS2 barrier in water compared to diethylamine). For the S_N2 reaction pathway, the products are only slightly favored thermodynamically (-4.09 kcal/mol).

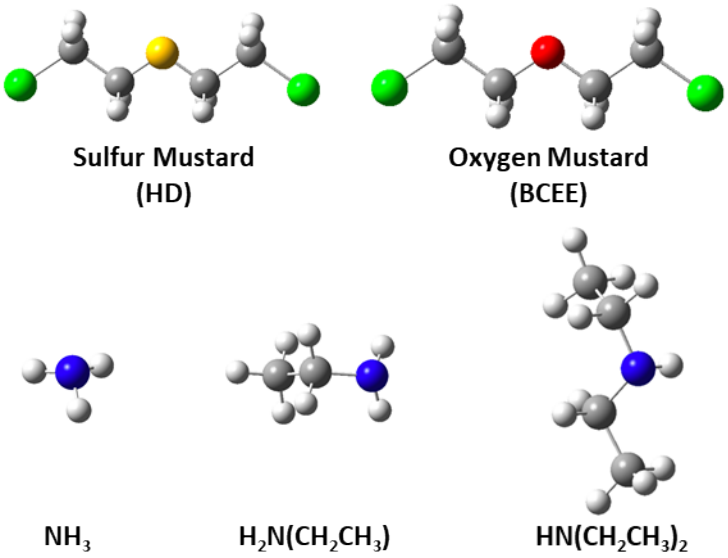

Figure 112. Snapshots of optimized electronic structures of sulfur mustard (HD), surrogate (BCEE), unsubstituted amine (NH_3), ethylamine ($H_2N(CH_2CH_3)$), and diethylamine ($HN(CH_2CH_3)_2$.

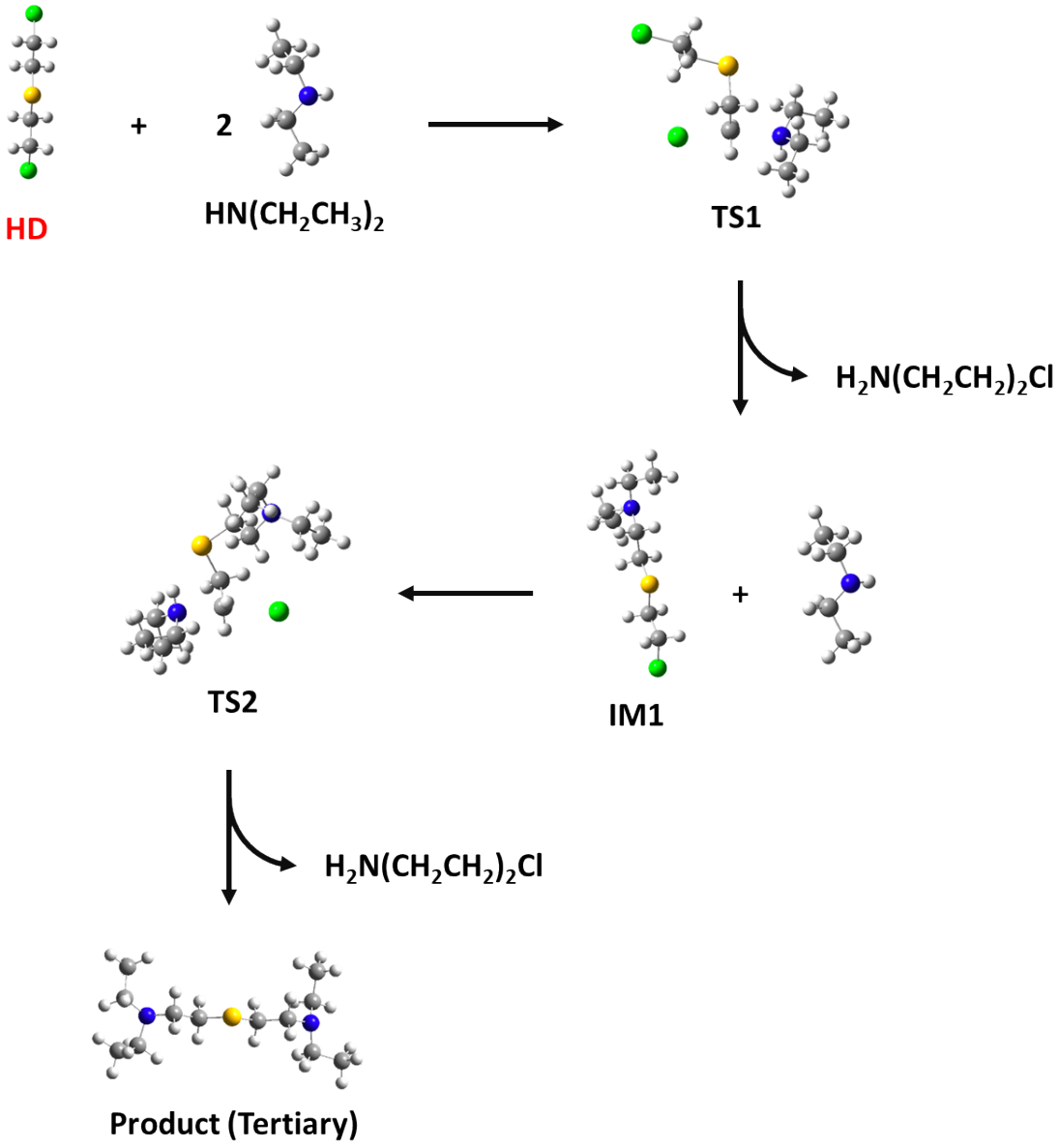

Figure 113. S_N2 reaction pathway for the formation of unsaturated sulfur mustard.

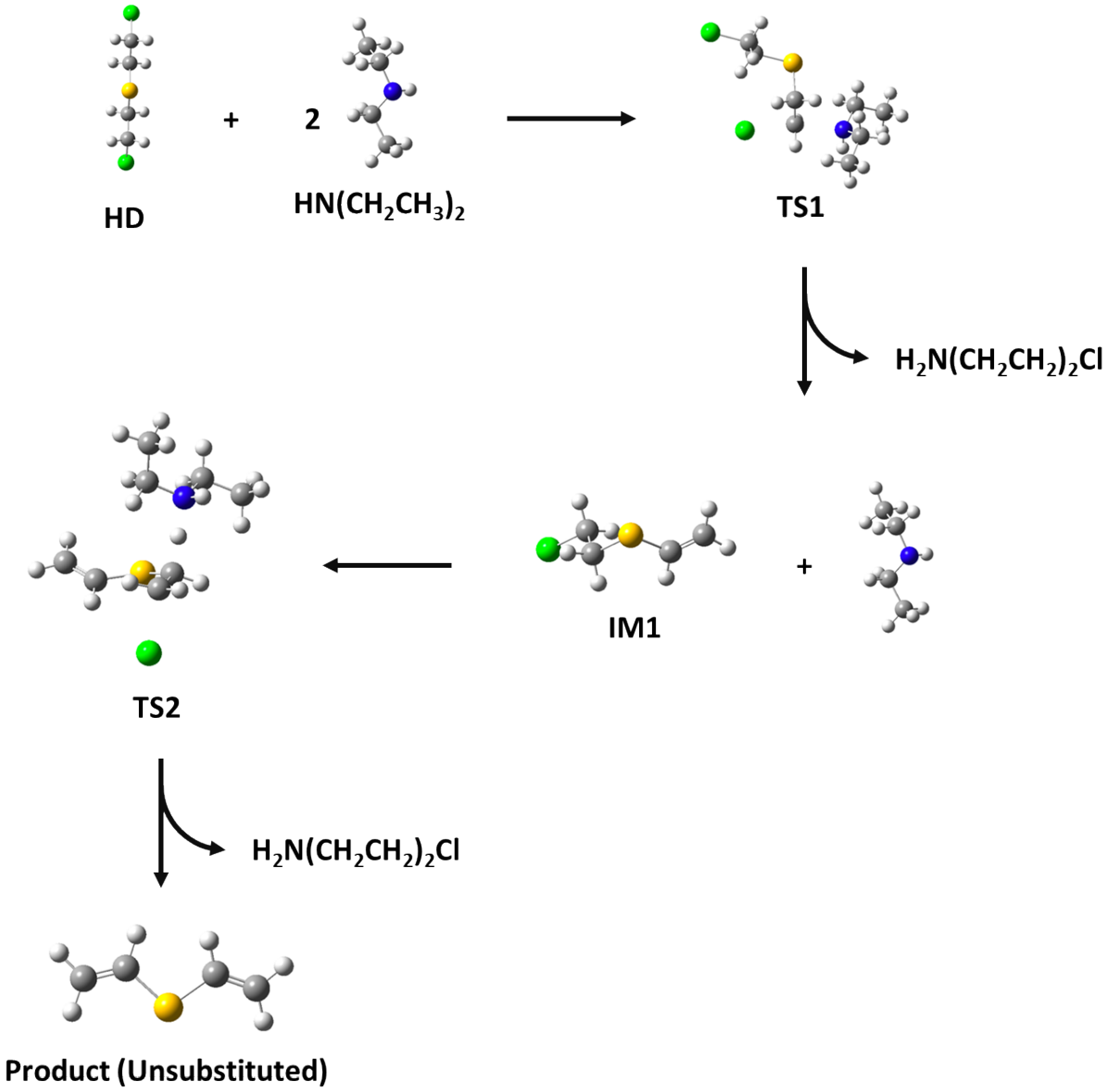

Figure 114. E2 reaction pathway for the formation of unsaturated sulfur mustard.

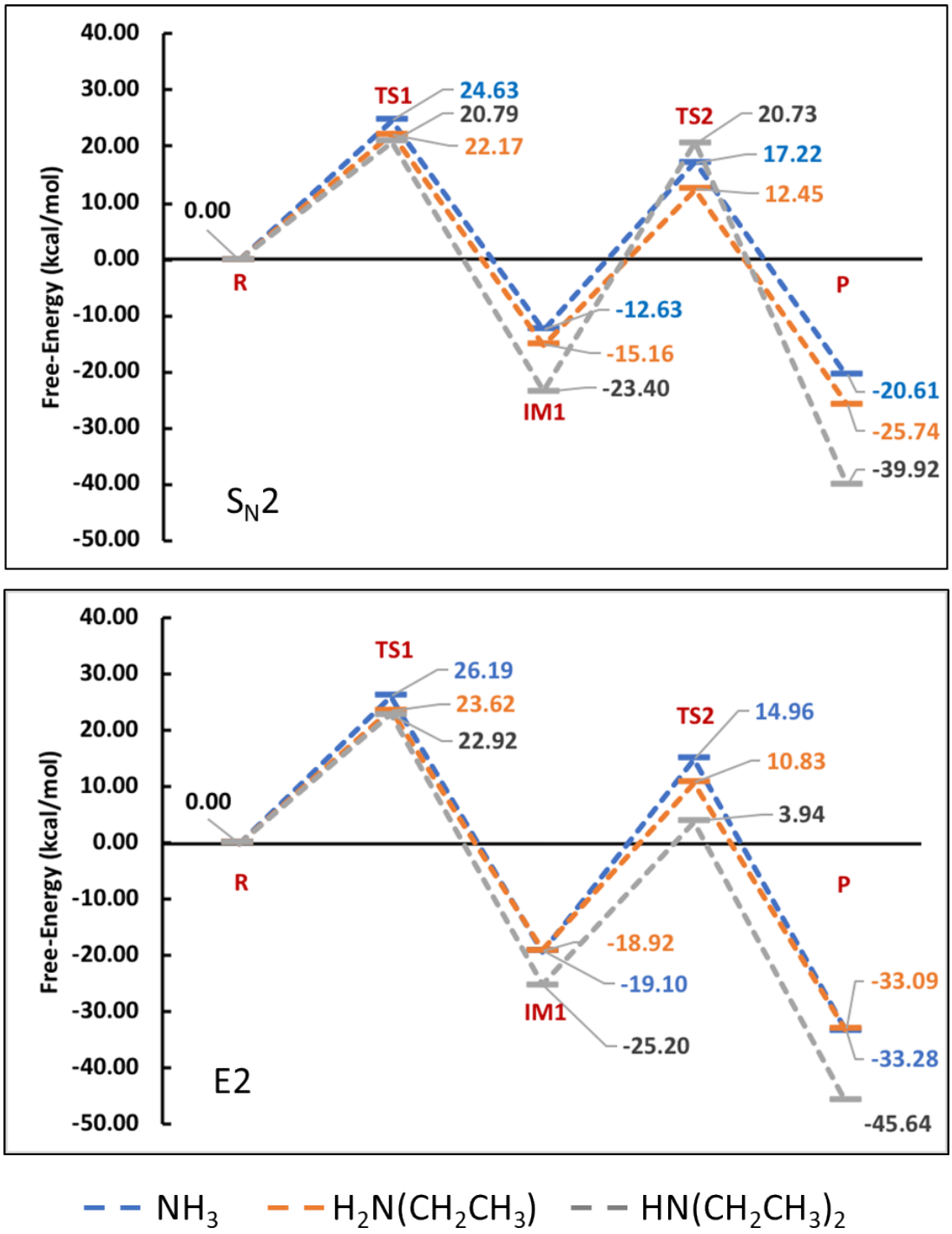

Figure 115. E2 and S_N2 reaction pathways for the decontamination of HD with different amines [NH_3, $H_2N(CH_2CH_3)$, and $HN(CH_2CH_3)_2$] in dielectric of 78.

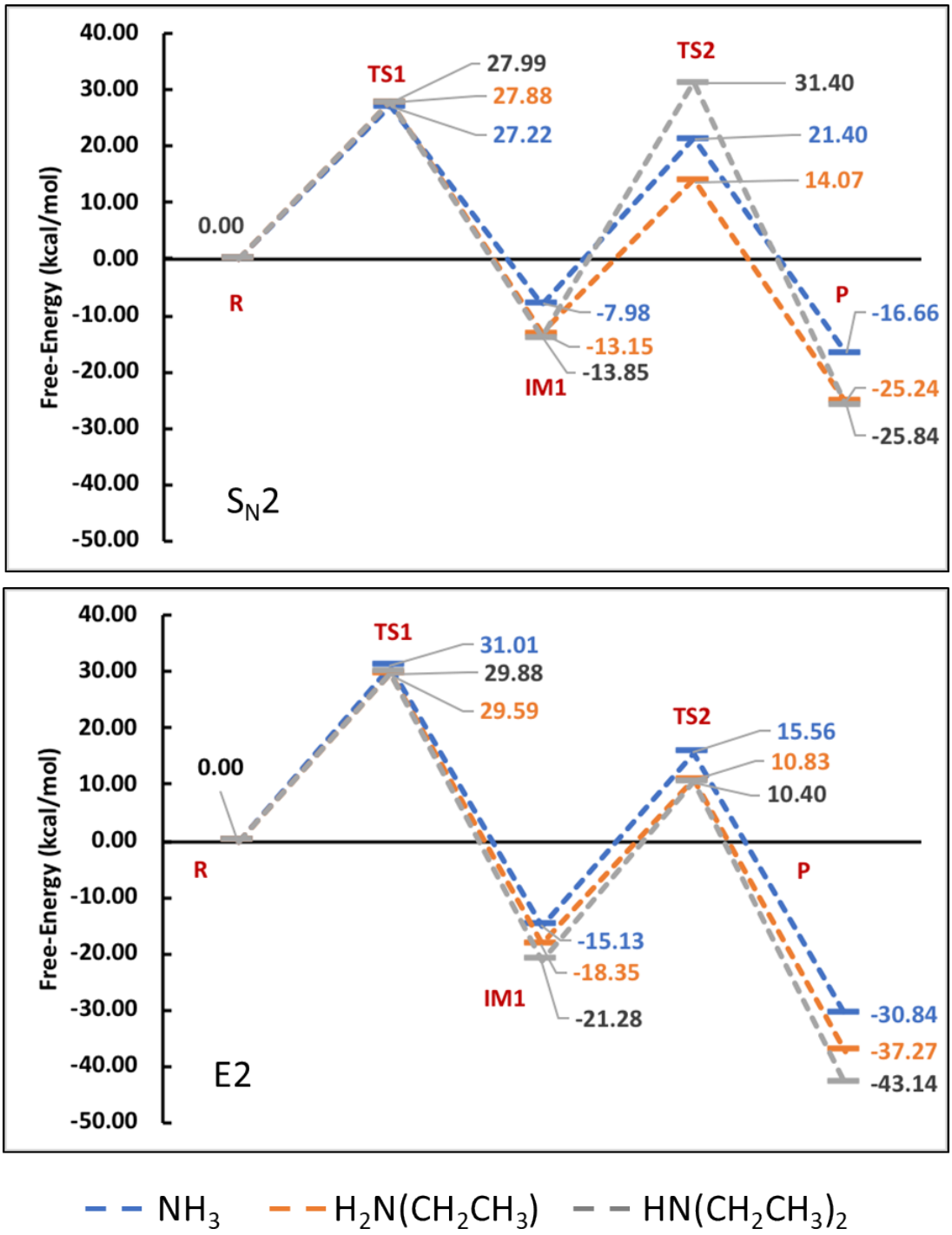

Figure 116. E2 and S_N2 reaction pathways for the decontamination of BCEE with different amines [NH_3, $H_2N(CH_2CH_3)$, and $HN(CH_2CH_3)_2$] in dielectric of 78.

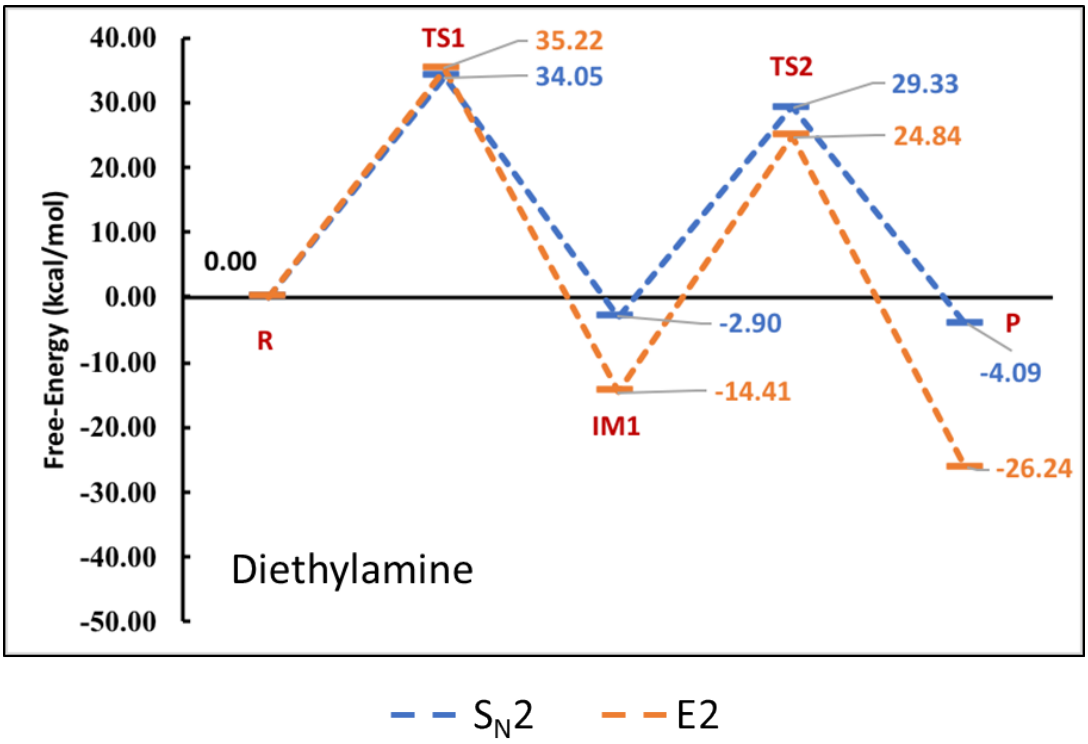

Figure 117. E2 and S_N2 reaction pathway for the decontamination of BCEE with $HN(CH_2CH_3)_2$ in dielectric set to mimic diethylamine (3.6).

We also investigated HD's surrogate, CEES, reacting with different classifications of amines. such as unsubstituted (NH_3), primary $(CH_2CH_2)NH_2$, secondary, and tertiary. Since experimental work has been conducted on CEES with triethyl amine, we aimed to complement those studies. We believe the sulfonium cationic ring is not exclusive to hydrolysis and, therefore, began modeling the reactions with the sulfonium cation to explore the chemical alacrity of the reactions with the different classification of amines and the sulfonium ion, shown in Figure 118.

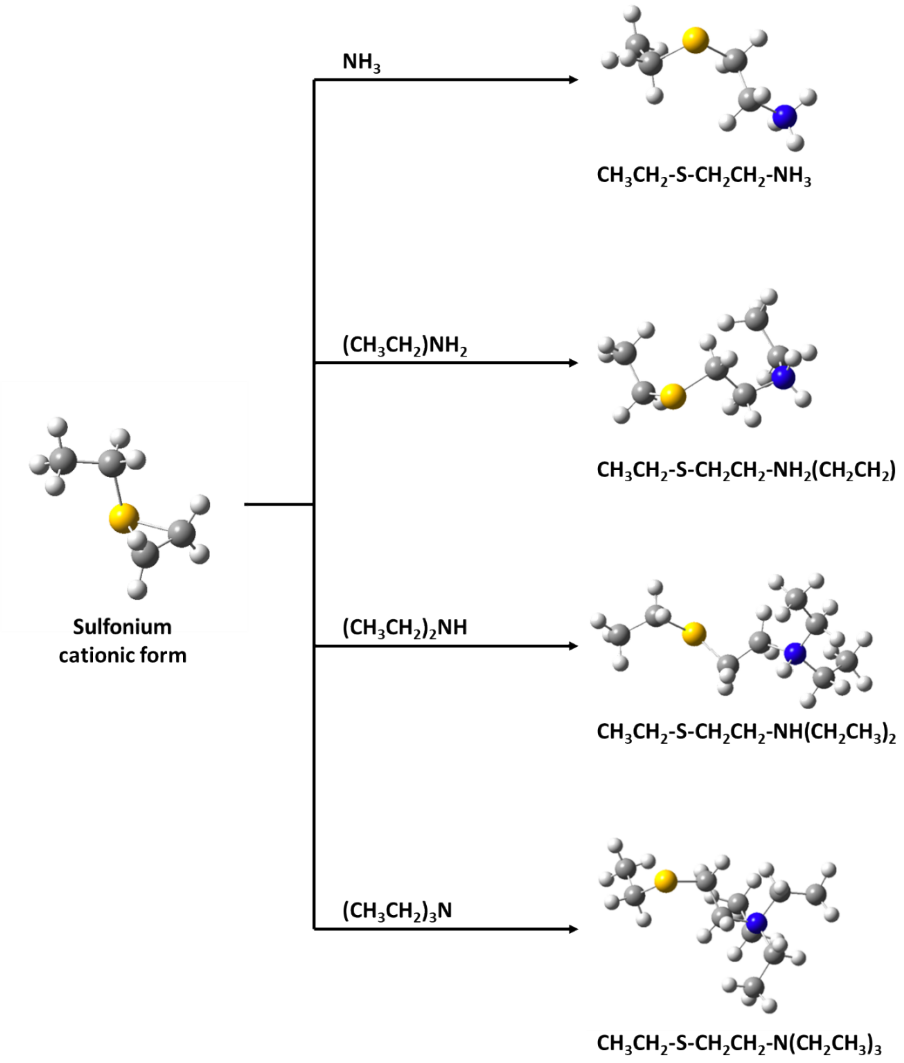

Figure 118. Shows the reactions of CEES with different classifications of amines starting from the sulfonium ring.

Figure 118 shows the intermediate formed for each species contains an overall positive charge. Furthermore, most of the intermediates not only contain positive charge, but also contain a hydrogen that can promote further reactions to the neutral product. However, the reaction of sulfonium ion + triethyl amine ($(CH_2CH_2)_3N$ product lacks the necessary hydrogen for pushing the reaction further and suggests the reaction completes after the first step.

Table 20. Gas phase free energies for CEES reaction with different classification of amines.

Reactants				Products	ΔG (kcal/mol)
$[CEES –Sulf]^+$	+	NH_3	=	$[CH_3CH_2\text{-}S\text{-}CH_2CH_2\text{-}NH_3]^+$	-10.41
$[CEES –Sulf]^+$	+	$(CH_3CH_2)NH_2$	=	$[CH_3CH_2\text{-}S\text{-}CH_2CH_2\text{-}NH_2CH_2CH_3]^+$	-17.81
$[CEES –Sulf]^+$	+	$(CH_3CH_2)_2NH$	=	$[CH_3CH_2\text{-}S\text{-}CH_2CH_2\text{-}NH(CH_2CH_3)_2]^+$	-66.06
$[CEES –Sulf]^+$	+	$(CH_3CH_2)_3N$	=	$[CH_3CH_2\text{-}S\text{-}CH_2CH_2\text{-}N(CH_2CH_3)_3]^+$	-52.71

The first step is a simple addition of a specific amine to the sulfonium cation. Table 20 shows the free energy accompanied with the addition of each amine sulfonium cation. Although all the reactions undergo the addition spontaneously, the unsubstituted NH_3 shows to be the least favorable reaction, while the $(CH_2CH_2)_2NH$ adds to the sulfonium most favorably.

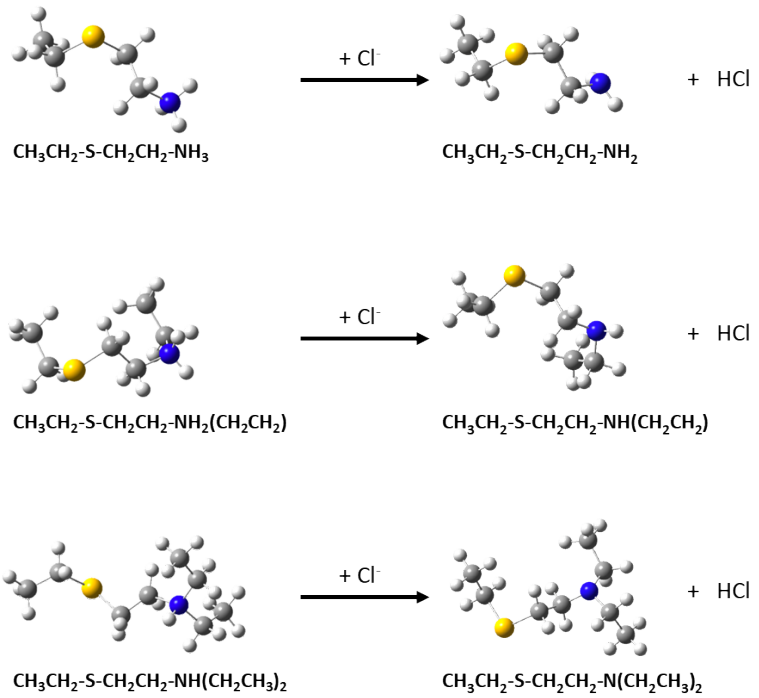

Figure 119. Formation of the neutral products from the deprotonation of N-H.

From our calculations, the most likely event for the reaction to progress forward to the neutral product is from the deprotonation of a N-H by a chloride ion (Cl^-). Figure 119 shows the neutral

products formed after the deprotonation of the amine hydrogen. Table 21 shows gas phase free energy for the spontaneous formation of the neutral products from deprotonation of the N-H from a Cl^-. The calculated free energies convey that, although NH_3 proceeds least favorably in the first addition step, it readily gives up a hydrogen more freely than the other intermediates.

Table 21. Show the second step for the formation of the neutral product.

Reactants				Products			ΔG (kcal/mol)
$[CH_3CH_2\text{-}S\text{-}CH_2CH_2\text{-}NH_3]^+$	+	Cl^-	=	$[CH_3CH_2\text{-}S\text{-}CH_2CH_2\text{-}NH_2]$	+	HCl	-112.64
$[CH_3CH_2\text{-}S\text{-}CH_2CH_2\text{-}NH_2CH_2CH_3]^+$	+	Cl^-	=	$[CH_3CH_2\text{-}S\text{-}CH_2CH_2\text{-}NHCH_2CH_3]$	+	HCl	-104.67
$[CH_3CH_2\text{-}S\text{-}CH_2CH_2\text{-}NH(CH_2CH_3)_2]^+$	+	Cl^-	=	$[CH_3CH_2\text{-}S\text{-}CH_2CH_2\text{-}N(CH_2CH_3)_2]$	+	HCl	-55.87
$[CH_3CH_2\text{-}S\text{-}CH_2CH_2\text{-}N(CH_2CH_3)_3]^+$	+	Cl^-	=	$[CH_3CH_2\text{-}S\text{-}CH_2CH_2\text{-}N(CH_2CH_3)_3]^+Cl^-$		-	

To gain insight into the sulfonium/chloride ion interaction stability due to polarity influence, the ion-pair was studied by investigating the sulfur-chloride (S-Cl-) distance interactions as a function of dielectric constant (Figure 120). Each calculation began with the same initial configuration similar to Structure 1 in Figure 120). At low dielectric or gas phase environment, Cl- attacks the sulfonium ring at the terminal carbon to form a covalent bond, resulting in a linear sulfur mustard. As the dielectric increases, the ion pair between the S/Cl pair become stable. However, as the dielectric increases further, the interaction distance increases, which suggests the sulfonium ion short range interaction begins to weaken. This result is interesting because without explicit water, the short-range interactions are influenced by the dielectric. One can imagine when water is added to the system, the ion-dipole interaction of Cl- and water will play a role. Additionally, it would be interesting to see how aprotic vs. protic solvents influence the S/Cl stability.

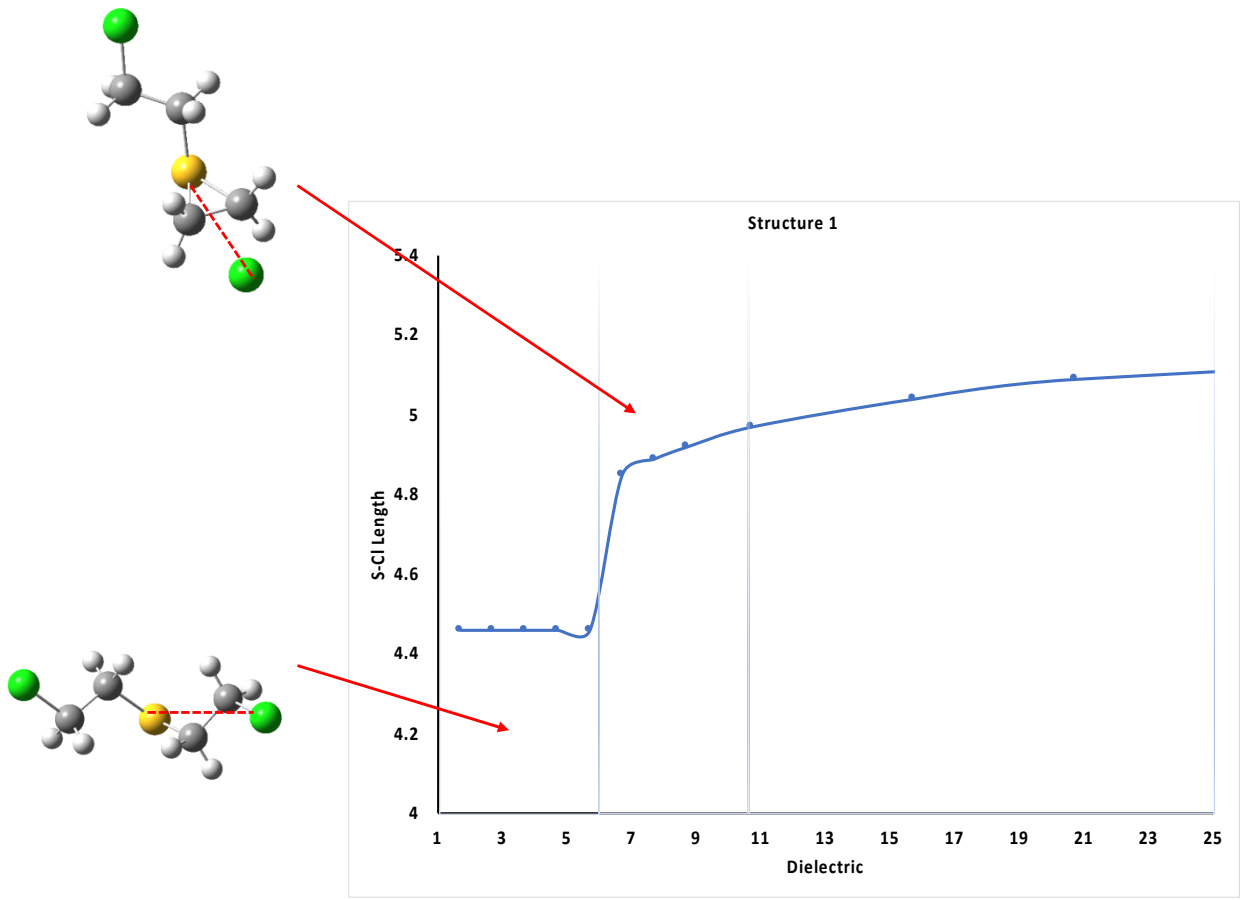

Figure 120. Sulfur/Cl ion interaction distance change as a function of dielectric.

To explore the mode of interaction of the Cl^- anion around the sulfonium cation, Cl^- is placed along the CH2-CH2 bond by the ring and around the sulfur atom (Figure 120)The structures underwent a geometry optimization to obtain an optimal lowest energy configuration. The most stable sulfonium/Cl ion pair interaction is along the sulfonium ring, while the Cl^- positioned aside the sulfur atom yielded second lowest energy, and the Cl^- positioned directly behind the structure interacting with the sulfur atom yielded in the highest mode of interaction. Cl^- seems to be stable in the Structure 1, but more work by charge distribution on the sulfonium ion needs to be done along with Natural Bond Orbital (NBO) analysis to provide more support to the analysis.

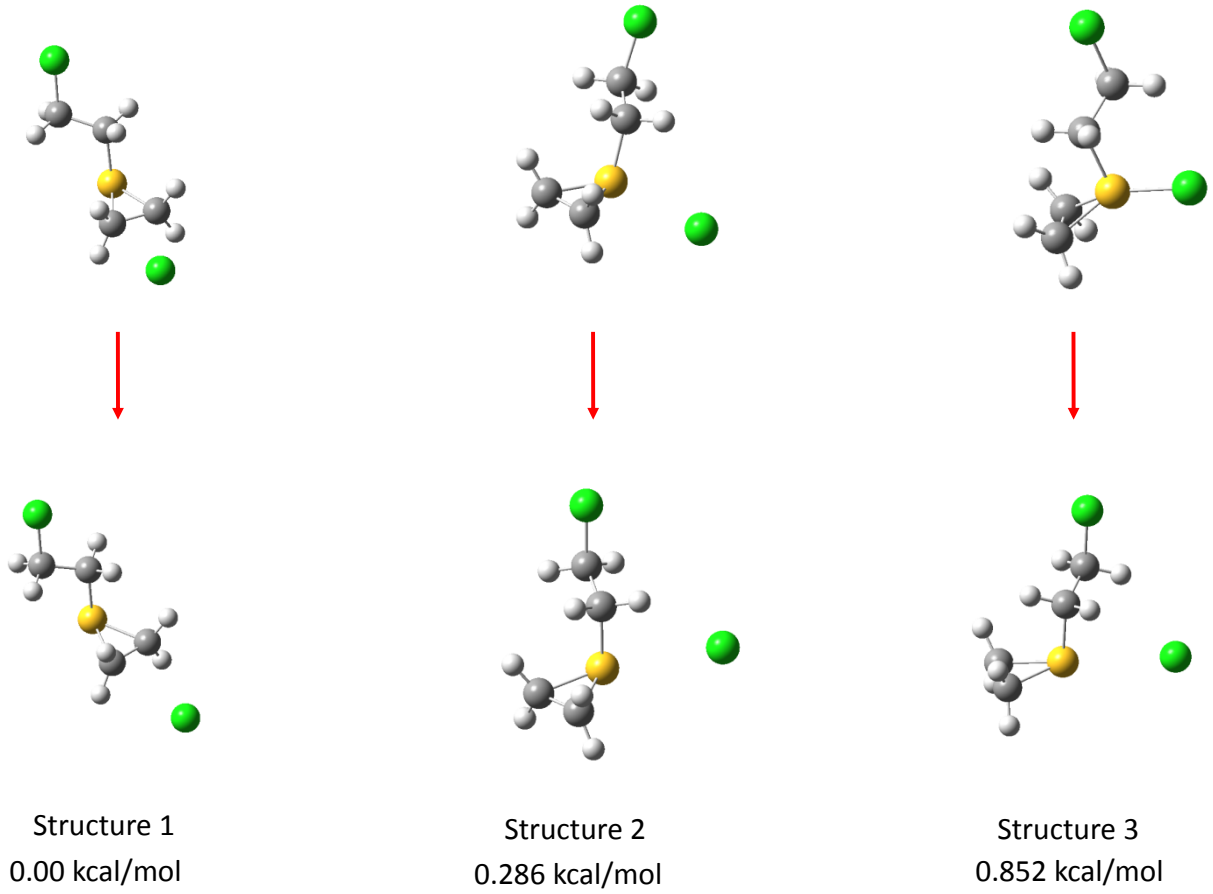

Figure 121. Electronic structure optimization for the sulfonium/Cl ion modes of interaction.

Finally, we explored alternative methods to predict chemical reactions using machine learning (ML) methods. We pursued ML with the short-term goal of predicting physical properties of common agents and simulants, and a long-term goal of predicting chemical reactions. ML models typically require inputs to be of a fixed dimension. Therefore, the first step involves processing the data to extract useful molecular information from chemical structures while transforming them into a fixed dimensional representation. We did this by transforming molecular formulae into extended connectivity fingerprints (ECFP) in the python module RDKIT.[12,13] These ECFPs are fixed length vectors that capture relevant molecular features and substructures using only a smiles string.[14] These molecular fingerprints can be used as input to the ML model by themselves, when no additional information is available, or they can be combined with additional features for optimal performance.

A proof-of-concept deep artificial neural network model was constructed to predict solubility using the open-source ESOL aqueous solubility database.[15] This database contains over 1000 chemical compounds with experimental solubility values and five relevant features for each chemical compound (polar surface area, number of hydrogen bond donors, number of rings, molecular weight, and number of rotatable bonds). Additionally, the database comes with ESOL

solubility predictions which are computed from a linear regression model based on the features listed above. We made three versions of the model, each trained on different input features. The models were trained using 1) only the ECFP, 2) the five expert chosen features, or 3) a combination of the features and the ECFP. The original ESOL model has a mean squared error of 0.83, while our models have mean squared errors of 1.01, 0.67, and 0.47, respectively. This shows that artificial neural networks can achieve high accuracy on property prediction when trained on well selected features combined with ECFPs. Moreover, even without expert chosen features available, the model can make good predictions based on the fingerprints alone. The predicted values from our combined fingerprint and features model is plotted against experimental values in Figure 122a. Green and red points corresponding to data that was used to train and test the model, respectively. Figure 122b shows the performance of our models and the original ESOL model in mean squared error.

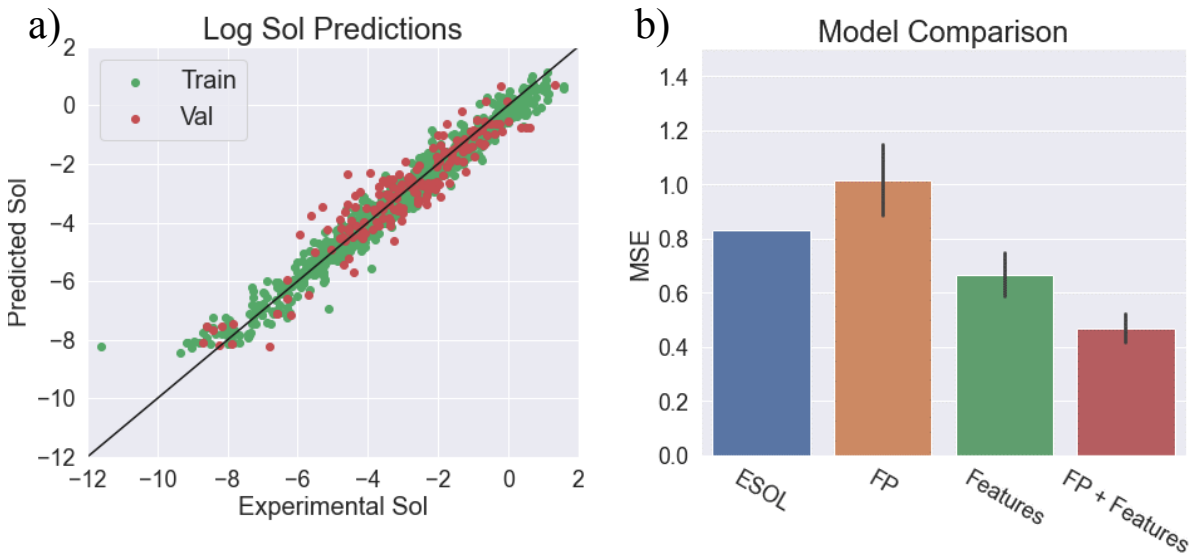

Figure 122. a) Predicted solubility of our fingerprint and features model vs. the experimental values. The black line represents perfect agreement. b) The accuracy of the ESOL model and our models in mean squared error.

There have been numerous published works using artificial neural networks (ANNs) to predict reaction enthalpies; however, many of these methods take optimized geometries as a descriptor (i.e. input to the ANN). Optimized geometries need to be obtained using DFT and, therefore, such methods provide no clear benefit as opposed to using DFT to directly calculate the reaction enthalpy. We have identified an ANN model, BAND NN, that can perform its own ML-based geometry optimization and does not need DFT optimized geometries to make reaction enthalpy predictions.[16] BAND NN was trained on DFT total energy calculations on theoretical molecules containing elements H, C, N, and O. As such, BAND NN can only be used on molecules made up of these elements and of a limited size (≈10 heavy atoms per molecule). Due to this limitation, BAND NN cannot currently be used to calculate reaction enthalpies for CA reactions.

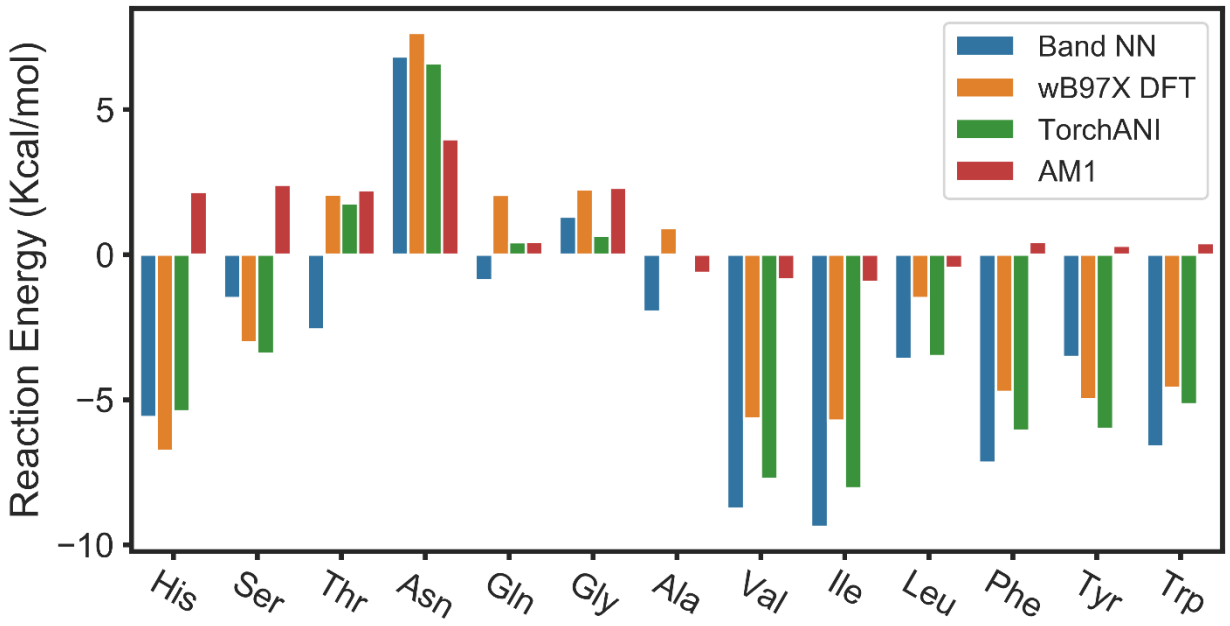

Figure 123. Reaction energy for amino acid to keto acid reactions predicted by BAND NN (Blue) and TorchANI (Green) ANNs, wB97X DFT (Orange), and semiempirical method AM1 (Red). Value predicted by wB97X is considered the target value.

We identified another ANN model, TorchANI,[17] that has numerous advantages over BAND NN. Like BAND NN, TorchANI accepts non-optimized molecular geometries and returns optimized structures and thermochemistry information; however, rather than simply providing reaction energies, TorchANI provides reaction energies, enthalpies, and Gibb's free energies. The addition of Gibb's free energy values will more accurately predict reaction favorability compared with reaction energy values alone. Moreover, TorchANI works for molecules containing elements H, C, N, O, Cl, F, and S. This expanded element compatibility allows for prediction of mustard compounds that was not previously possible with BAND NN. Finally, TorchANI provides thermochemistry values more accurately and consistently than BAND NN. When compared to our DFT standard method (ωB97X) for select organic molecules (amino acids and their derivatives chosen for their elemental compatibility with BAND NN), TorchANI and BAND NN have an average error of ≈1.3kcal/mol and ≈2.3kcal/mol, respectively. Figure 123 shows the net reaction energy for 13 amino acids to keto acid reactions predicted by BAND NN (blue), TorchANI (green), and AM1 (red), a semi-empirical method similar to the ANNs in computational time, compared to the DFT target value (orange). Not only is TorchANI often the closest prediction to DFT out of the three methods, but it also did not make any predictions that had a large error (>3kcal/mol). On the contrary, BAND NN and AM1 both have predictions that had errors in excess of 3kcal/mol (Thr, Val, Ile for BAND NN and numerous for AM1). Although the current BAND NN has a low average error, the appearance of these larger inaccurate predictions creates an increased uncertainty for continued exploration. However, the ≈1.3kcal/mol average error, and consistency, for TorchANI is extremely promising and shows that TorchANI predictions are near DFT accuracy.

Concurrently, a student intern developed a web-based ANN chemical reaction calculation portal for users (experimentalists and modelers) to quickly calculate and/or look up chemical reaction information for specified reactants. Results included products (chemical identification number, formula, structure) and reaction energies, provided from previously submitted calculations or on-the-fly ANN calculations. A graphical user interface based on the React framework was constructed and tested (Figure 124). Work was also done to build a Python-based Flask website to implement the TorchANI model that will perform user-specified ANN chemical reaction calculations. The graphical interface makes it easier and more efficient to perform the calculations.

The web-based portal progressed rapidly and allows for single molecule free energy calculation in addition to reaction calculations (Figure 124 and Figure 125). The web-app is hosted on a Sandia server to allow for easy access among distributed users. A database has been created to store calculations to allow users to revisit calculations run in the past. The NIH cactus server is used to convert SMILES input structures to an input file for easier use. Users can adjust stoichiometric coefficients, molecule symmetry, and molecule geometry for a given input file. Input files which have been optimized using TorchANI are available for download to users following a calculation. A PowerPoint tutorial file has been created to provide users with a guide on how to use the web-app. The project is stored in a shared Sandia hosted gitlab repository accessible to members of the team.

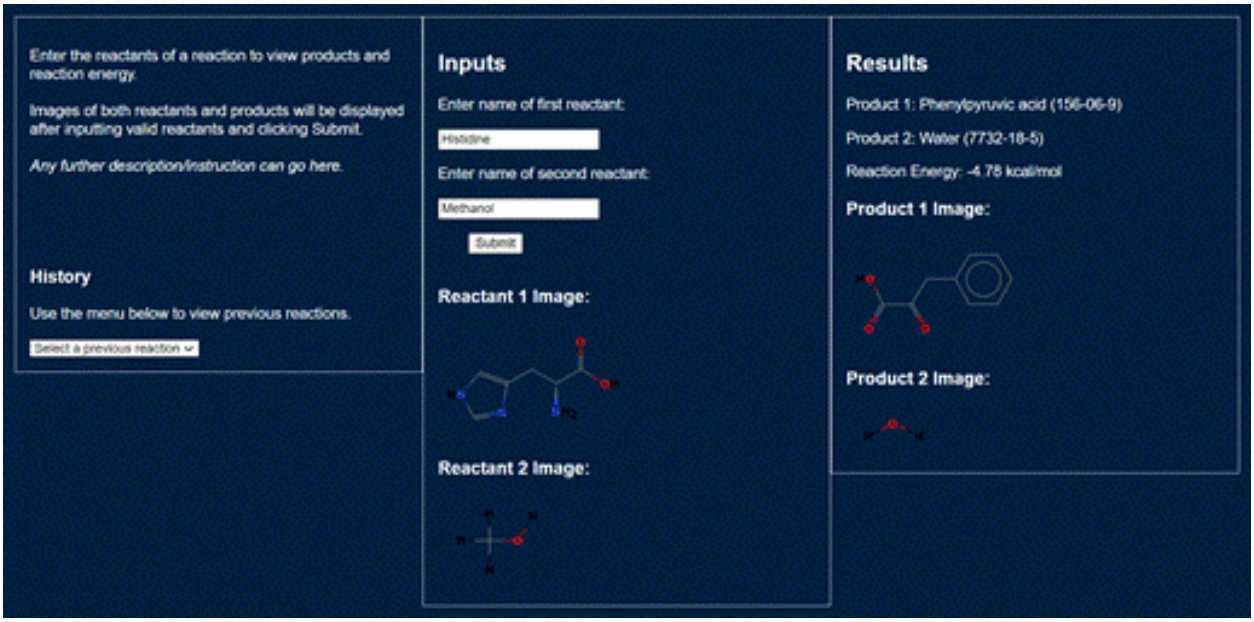

Figure 124. Graphical user interface for ANN chemical reaction calculations.

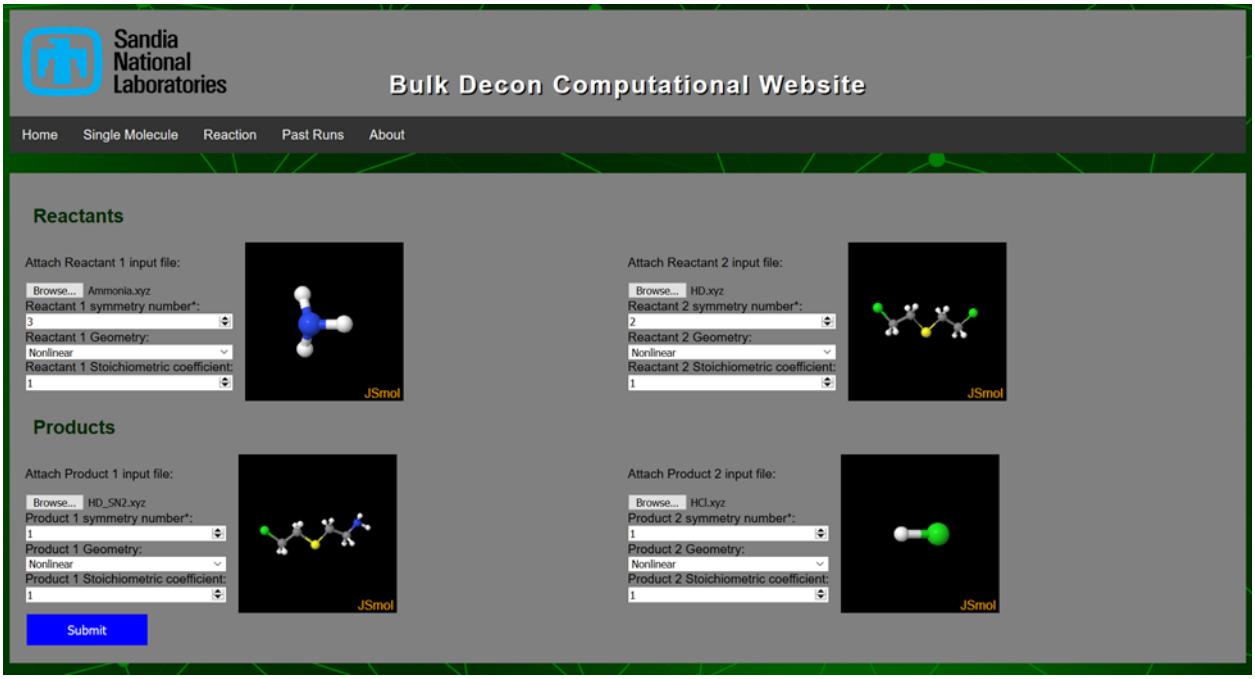

Figure 125. Updated reaction functionality of graphical web interface.

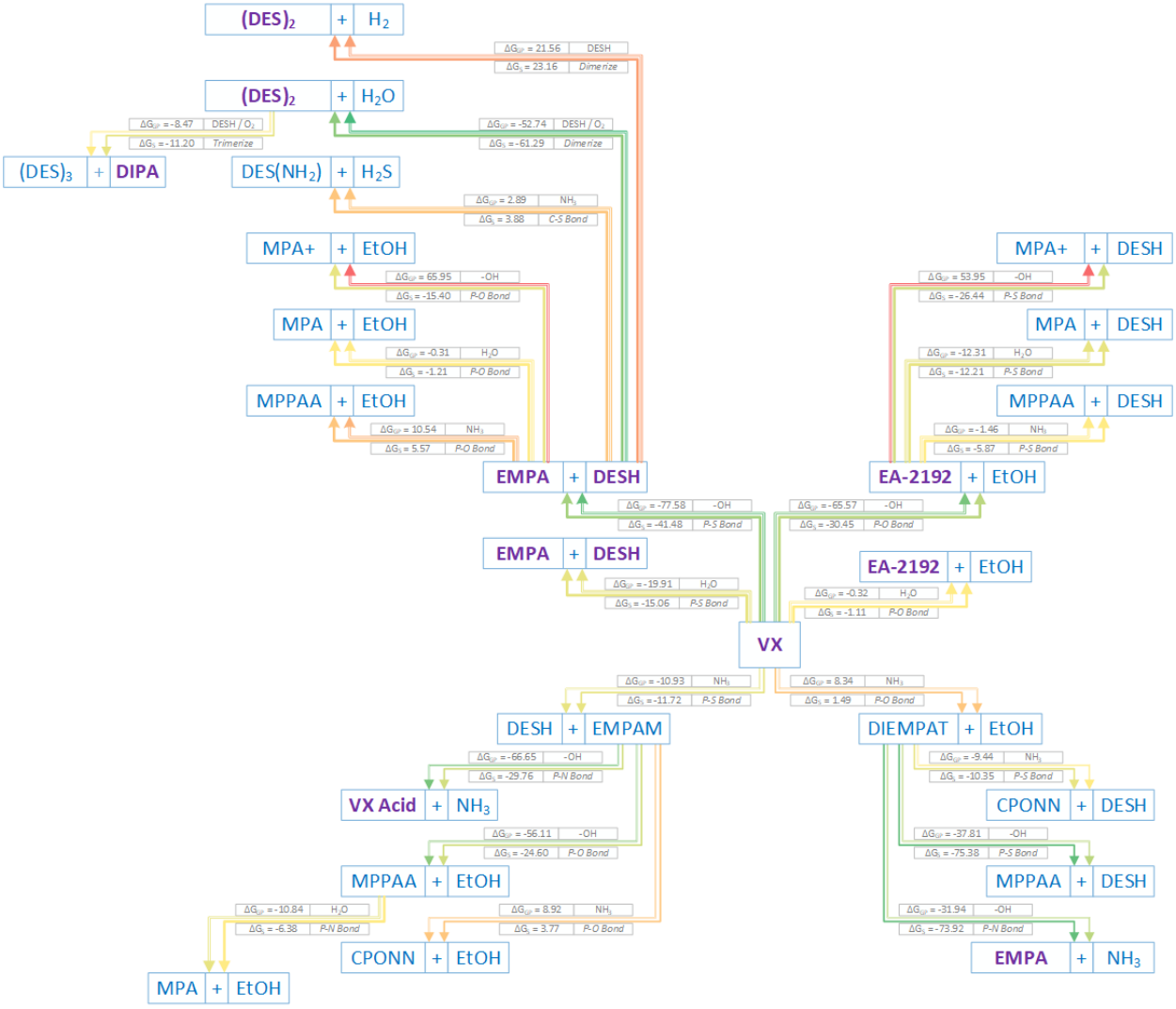

Figure 126. Reaction pathways for the complete degradation of VX in alkaline environment. Reaction free energies were obtained from quantum calculations at the Hartree-Fock (HF) level of theory in gas phase (GP) and solvent (water, S) environments. Compounds in purple indicate species that have been detected experimentally. Reaction arrows are colored according to the reaction free energy values (green: favorable, yellow: slightly favorable or unfavorable, red: unfavorable).

Figure 126 shows expected products and reaction energies for the degradation of VX in alkaline environment. Results are shown for calculations in the gas phase and with implicit solvent (water). Similar reaction energies are obtained from either method. Cleavage of either the P-S or P-O bond by OH- is strongly favored, and confirmed experimentally by the presence of intermediates EMPA DESH, and EA-2192 in the reaction mixture. Subsequent reaction of EA-2192 and EMPA with OH- are generally unfavorable, but the dimerization of DESH to form the VX disulfide is predicted to be favorable. Reaction of VX with NH_3 is either unfavorable or only slightly favorable. Nonetheless, subsequent reactions of intermediates were carried out to

identify potential chain reaction mechanisms in which NH_3 is produced. Figure 128 provides chemical structures for chemical names and abbreviations. Using the Sandia computational model, we can correctly identify the reaction pathways for the degradation of VX using Li_3N pellets.

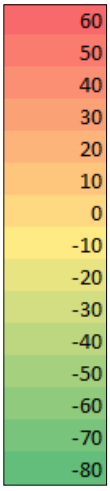

Figure 127. Delta G color scaling for Figure 126. Red (60) denotes unfavorable reactions and Green (-80) represents favorable.

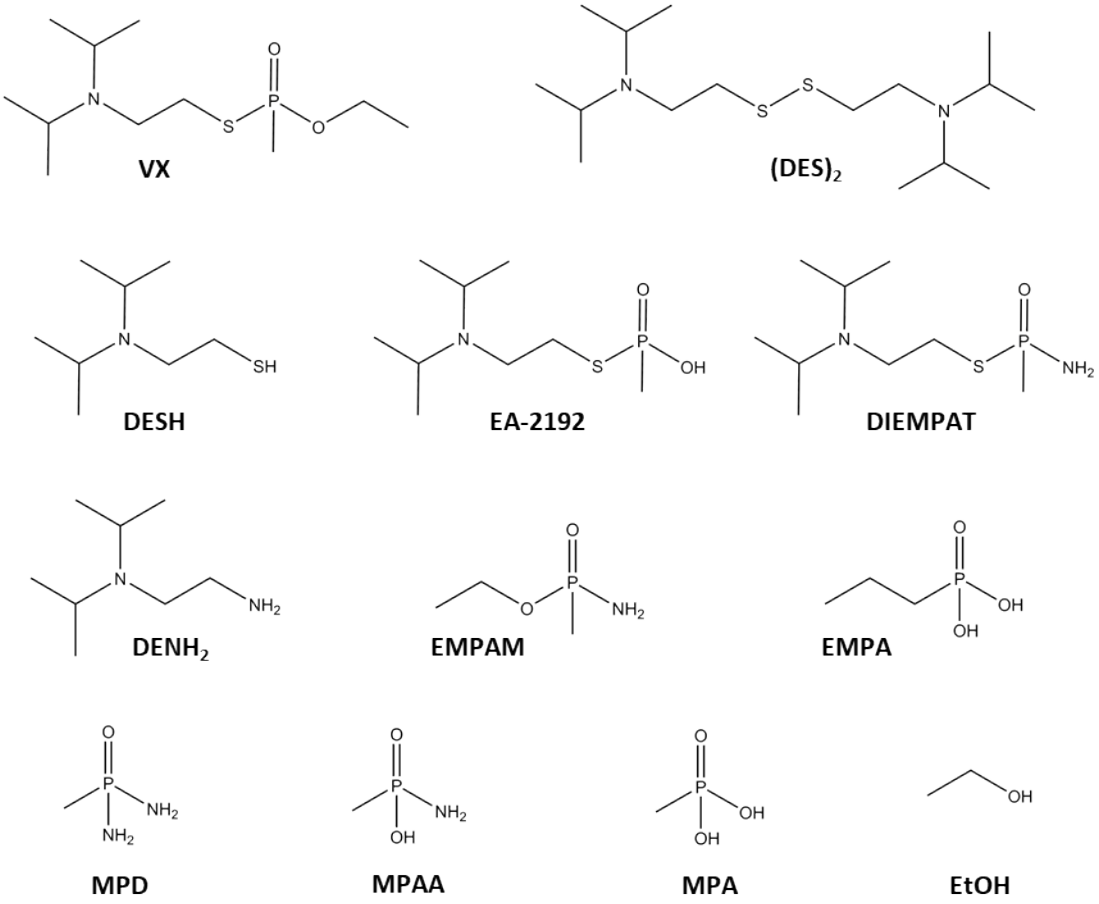

VX = Ethyl ({2-[bis(propan-2-yl)amino]ethyl}sulfanyl)(methyl)phosphinate
EA-2192 = S-(2-(diisopropylamino)ethyl) O-hydrogen methylphosphonothioate
EMPA = ethyl methylphosphonic acid
DESH = Diisopropylamino ethanethiol
EtOH = Ethanol
EMPAM = Ethyl P-methyl phosphonamidate
DIEMPAT = S-(2-(diisopropylamino) ethyl) P-methyl phosphonamidothioate
$(DES)_2$ = VX Disulfide
MPA = Methylphosphonic acid
MPPAA = P-methylphosphonamidic acid
MPD = P-Methylphosphonic diamide
$DENH_2$ = N,N-Diisopropylethylenediamine

Figure 128. Structures for chemical names and abbreviations.

Task 8: Classical Modeling

Subtask 8.1: Identify Parameters and Methodology for GB and VX (UFR1)

Because there are currently no identifiable CMD force field parameters developed for VX, we compared our GAFF model with parameters developed for GB and its simulant (DMMP), shown in Figure 60. The GAFF force field shows much better agreement with AIMD compared to literature parameters (Figure 60).[11]

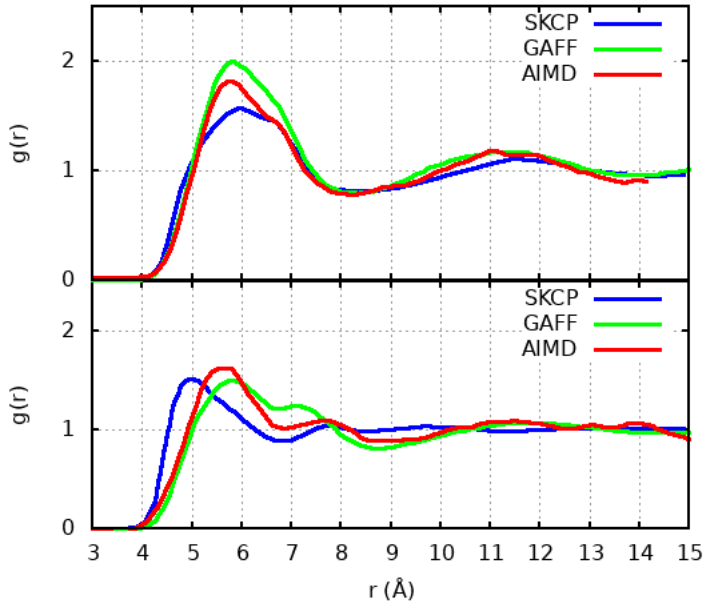

Figure 60. RDF plots from MD simulations comparing DMMP (top) and GB (bottom). Colors correspond to a previously developed force field model (blue line), GAFF force field model (green line), and quantum model with AIMD (red line).

Subtask 8.2: Perform simulations on GB and VX (UFR1/2)

Simulations for GB and VX have been performed and are shown in Figure 107, Figure 108, and Figure 109.

5. Performance Issues/Impacts

a. Inactivation of neat Sulfur Mustard (HD) has been problematic. Nearly all the literature and non-literature reported reactions for HD reactivity do not work when HD is neat (not diluted in solvent). We hypothesize that the reactions do not occur for most of these reagents because of unfavorable solvent affects in the presence of pure HD. The reactions are expected to proceed by formation of a three-member sulfonium ion intermediate, and this ionic intermediate is not stabilized in the nonpolar HD.
b. COVID-19 has caused delays with performing experiments onsite at SNL and CCDC-CBC.

6. Conclusions

a. CAs (GB, GD, VX) and precursors (QL and DF) were reactive with $Li_3N + H_2O$ and could be decontaminated. The reaction mixtures of GB, GD, and VX formed viscous gels that had different physical properties compared to neat agent.
    a. Reactions at small scale (1 and 10 mL) worked better than larger scale (> 50 mL) reactions.
    b. More work needs to be performed to understand the challenges in scaling and identify more effective reaction conditions (e.g., stirring, applied heat, etc) at larger scale reactions.
    c. More work needs to be performed to transition the chemistry to the field.
b. HD was not effectively decontaminated using the $Li_3N + H_2O$ chemistry.
    a. More work needs to be performed to understand the limitations of the chemistry towards HD.
c. Computational modeling can be used to predict reaction products based on Gibbs Free Energy. Results were validated using experimental results for VX.

7. References

1. Iwasaki, T.; Imanishi, R.; Shimizu, R.; Kuniyasu, H.; Terao, J.; Kambe, N., Copper-Catalyzed Alkyl-Alkyl Cross-Coupling Reactions Using Hydrocarbon Additives: Efficiency of Catalyst and Roles of Additives. *J. Org. Chem.* **2014,** *79* (18), 8522-8532.
2. Ethylaluminium sesquichloride. https://en.wikipedia.org/wiki/Ethylaluminium_sesquichloride.
3. DeSain, J. D.; Curtiss, T. J.; Cohen, R. B.; Brady, B. B.; Frolik, S. A. *Testing of LiAlH4 as a Potential Additive to Paraffin Wax Hybrid Rocket Fuel*; AEROSPACE CORP EL SEGUNDO CA: 30 OCT 2007, 2007.
4. Ashby, E. C., A Review of: "Complex Hydrides and Related Reducing Agents in Organic Synthesis, A. Hajos', Elsevier Scientific Publishing Corporation, Amsterdam and New York, 1979, 398 pp., $76.00 (Dfl. 156.00)". *Synthesis and Reactivity in Inorganic and Metal-Organic Chemistry* **1980,** *10* (4), 427-428.
5. Quin, L. D., *A Guide to Organophosphorus Chemistry*. Wiley: 2000.

6. Payne, N. C.; Stephan, D. W., PREPARATION AND P-31 NUCLEAR MAGNETIC-RESONANCE STUDIES OF CHIRAL PHOSPHINES. *Can. J. Chem.-Rev. Can. Chim.* **1980,** *58* (1), 15-21.
7. Safety, E. H. a. Environmental Health and Safety, Ohio State University, Guidelines for pyrophoric materials. https://ehs.osu.edu/sites/default/files/pyrophoric_materials_guidelines.pdf.
8. Mason, P. S. J. *Reactions of Lithium Nitride With Some Unsaturated Organic Compounds*; LSU Historical Dissertations and Theses.: 1963.
9. Chemical Datasheet Lithium Nitride. https://cameochemicals.noaa.gov/chemical/1001.
10. Bevilacqua;, V. L. H.; McGarvey;, D. J.; Creasy;, W. R.; Maguire;, K. J., Reaction Rates of Binary Chemical Weapon Components by ^{31}P NMR. In *Scientific Conference on Chemical and Biological Defense Research*, Hunt Valley, MD, 2004.
11. Vishnyakov, A.; Gor, G. Y.; Lee, M. T.; Neimark, A. V., Molecular Modeling of Organophosphorous Agents and Their Aqueous Solutions. *J Phys. Chem. A* **2011,** *115* (20), 5201-5209.
12. Rogers, D.; Hahn, M., Extended-connectivity fingerprints. *J Chem Inf Model* **2010,** *50* (5), 742-54.
13. RDKit. https://www.rdkit.org/.
14. https://en.wikipedia.org/wiki/Simplified_molecular-input_line-entry_system.
15. Delaney, J. S., ESOL: estimating aqueous solubility directly from molecular structure. *J Chem Inf Comput Sci* **2004,** *44* (3), 1000-5.
16. Laghuvarapu, S.; Pathak, Y.; Priyakumar, U. D., BAND NN: A Deep Learning Framework for Energy Prediction and Geometry Optimization of Organic Small Molecules. *J. Comput. Chem.* **2020,** *41* (8), 790-799.
17. Gao, X.; Ramezanghorbani, F.; Isayev, O.; Smith, J. S.; Roitberg, A. E., Torchani: A Free and Open Source Pytorch-Based Deep Learning Implementation of the Ani Neural Network Potentials. *J Chem Inf Model* **2020**, *60*, 3408-3415.

8. APPPENDIXES/ATTACHMENTS

a. None.